

The IMOS “Radiometry Task Team”

August 2016 - June 2017

David Antoine¹, Thomas Schroeder², Matt Slivkoff¹, Wojciech Klonowski³, Martina Doblin⁴, Jenny Lovell⁵, David Boddle⁶, Brett Baker⁶, Elizabeth Botha², Charlotte Robinson¹, Edward King⁵, Peter Fearn¹, Nick Hardman-Mountford⁷, Rob Johnson⁸, Nagur Cherukuru⁹, Arnold Dekker⁹, Tim Malthus⁹, Ross Mitchell⁹, Peter Thompson⁵, Paul Van Ruth¹⁰

- ¹ Remote Sensing & Satellite Research Group (RSSRG), Department of Physics and Astronomy, Curtin University, Perth, WA 6845
- ² CSIRO Oceans and Atmosphere, Aquatic Remote Sensing, Brisbane, Dutton Park, QLD 4001
- ³ In situ Marine Optics, Bibra Lake, WA 6163
- ⁴ C3 - Climate Change Cluster, University of Technology, Sydney, Broadway, NSW 2007
- ⁵ CSIRO Oceans and Atmosphere, Hobart, TAS 7001
- ⁶ CSIRO Land and Water, Australian Tropical Science and Innovation Precinct, Townsville, QLD 4811
- ⁷ CSIRO Oceans and Atmosphere, Marine Biophysics, Indian Ocean Marine Research Centre, Crawley, WA 6009
- ⁸ Bureau National Operations Centre, Bureau of Meteorology, Hobart, TAS 7001
- ⁹ CSIRO Oceans and Atmosphere, Canberra, ACT 2601
- ¹⁰ South Australian Research and Development Institute - Aquatic Sciences, West Beach, SA 5024



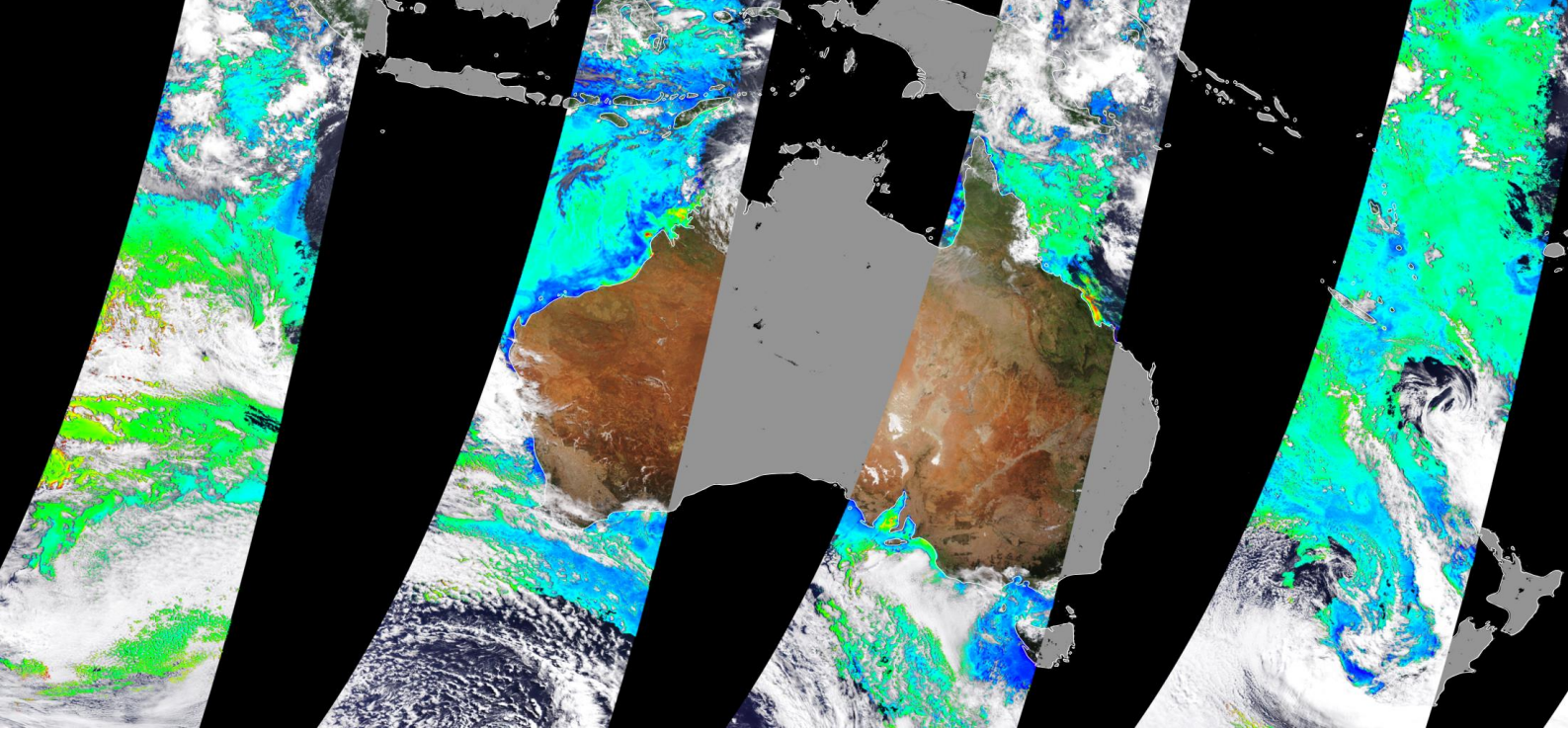
**Final report
30th June 2017**

Blank page

Table of content

1	BACKGROUND	1
2	RATIONALE	1
3	OBJECTIVES.....	2
4	OVERALL SCHEDULE OF THE ACTIVITY, COMMUNICATIONS, USE OF FUNDS	2
4.1	SCHEDULE.....	2
4.2	COMMUNICATIONS	3
4.2.1	<i>Annual IOCCG committee meeting, Perth, February 2017.....</i>	3
4.2.2	<i>IMOS annual planning meeting, Perth, February 2017</i>	3
4.2.3	<i>"FRM4SOC" workshop, ESA-ESRIN, Frascati, Italy, February 2017.....</i>	4
4.2.4	<i>Sentinel 3 validation team, ESA-ESRIN, Italy, February 2017</i>	4
4.2.5	<i>IOCS meeting, Lisbon, Portugal, May 2017</i>	4
4.2.6	<i>AMSA conference, Darwin, Australia, July 2017.....</i>	4
4.2.7	<i>Marine Matters, IMOS bulletin.....</i>	4
4.2.8	<i>Web stories.....</i>	4
4.3	USE OF FUNDS	4
5	MAIN FINDINGS FROM THE LABORATORY AND FIELD EXPERIMENTS	6
5.1	ABOUT OUR COMMUNITY.....	6
5.2	ABOUT INSTRUMENT CHARACTERISATION AND CALIBRATION	6
5.3	ABOUT FIELD DEPLOYMENT PROCEDURES	7
5.4	ABOUT DATA PROCESSING METHODS.....	7
5.5	ABOUT SATELLITE VALIDATION OPERATIONS	8
6	WHERE TO FROM HERE? SOME RECOMMENDATIONS ON THE WAY FORWARD.....	9
6.1	ACTIONS / RECOMMENDATIONS DIRECTLY ISSUED FROM THE RTT WORK	9
6.1.1	<i>Keeping the momentum; do we need these experiments at regular intervals?</i>	9
6.1.2	<i>Reprocessing of historical data?</i>	9
6.1.3	<i>Community assets, are they sufficient? Where should we invest/disinvest?</i>	9
6.1.4	<i>Community practices for field measurements.....</i>	10
6.1.5	<i>The future of the Lucinda Jetty Coastal Observatory (LJCO)</i>	11
6.1.6	<i>The future of en-route radiometry measurements.....</i>	12
6.2	MID- TO LONG-TERM DEVELOPMENTS AROUND RADIOMETRY MEASUREMENTS.....	13
6.2.1	<i>Radiometry measurements on research voyages.....</i>	13
6.2.2	<i>Blue-water cal/val site off WA.....</i>	13
6.2.3	<i>Radiometry from Bio-Argo and other autonomous platforms</i>	14
6.2.4	<i>Uncertainty budgets</i>	14
6.2.5	<i>Instrumentation development.....</i>	15
6.2.6	<i>Improving the uptake of data by the IMOS nodes and the overall Australian science community</i>	15
6.2.7	<i>International engagement.....</i>	16
7	SUMMARY OF RECOMMENDATIONS, ASSOCIATED NEEDS, AND LIKELY IMPACT IF IMPLEMENTED	17
8	REFERENCES	22
9	ACRONYMS.....	24
10	APPENDIX 1. ERROR SOURCES IN ABOVE-WATER RADIOMETRY	25
11	APPENDIX 2: REPORT OF THE LABORATORY CHARACTERISATION AND CALIBRATION EXPERIMENTS.....	26
12	APPENDIX 3: REPORT OF THE FIELD EXPERIMENT AT THE LJCO	49
13	APPENDIX 4: PARTICIPANTS LISTS.....	92
14	APPENDIX 5. WHAT'S "SYSTEM VICARIOUS CALIBRATION" (SVC), AND THE NEED FOR IT	93

Blank page



Normalized water-leaving radiance at 443 nm from several overpasses of the ESA's Sentinel-3-OLCI sensor, covering Australia's surrounding seas
© ESA/EUMETSAT, NOAA OCview

Preamble

The long-term vision that has underlain the proposal to IMOS for the “Radiometry Task Team” (RTT), whose work is summarised in this report, is as follows.

We think that the Australian research community involved into ocean colour and bio-optics science has the potential to become a major player in the Southern hemisphere in the coming years. We want to play this role by providing crucial validation data to the upcoming global satellite missions (Sentinels in particular), by delivering satellite products tailored to the needs of Australian researchers, institutions and users, and by improving practices and knowledge of our community in the domain of fieldwork in optics.

The Australian Government has now an agreement with the European Commission (EC), signed by Geosciences Australia (GA) on hosting the collaborative Ground Segment for the Sentinel system. This agreement was, amongst other reasons, reached on the understanding that Australia would deliver world-class calibration –validation data back to the EC, the European Space Agency (ESA) and the European Organisation for the Exploitation of Meteorological Satellites (EUMETSAT).

This will be feasible by building on the investments of the past 10 years, by taking advantage of the next slice of NCRIS funding to leverage co-contributions, and also by reorganizing significantly our assets and activities. International engagement will also be key to success here, for instance through the validation teams of global mission, the IOCCG, the building of international research proposals.

We hope that the present report shows how the RTT has achieved a first step in that direction and, above all, has allowed a community plan to be put together for the coming years.

Blank page

1 Background

Given Australia's vast ocean territory, satellite measurements form an important means by which to establish baselines and assess spatial and temporal patterns of change in coastal and offshore ecosystems. The technique considered here is ocean colour radiometry (OCR; Acronyms in section 0), provided now for about 20 years by dedicated OCR satellite missions, from NASA and ESA in particular.

These OCR missions have the capacity to deliver publicly available data at spatial resolution from 250m to 1km on daily time-steps, and have been used to describe large to meso-scale patterns in ocean properties for the last several decades. A recent example relevant to the Australia Integrated Marine Observing System (IMOS) is the analysis of the spatial and temporal variability of the Leeuwin Current from MODIS observations (Huang and Feng, 2015). IMOS currently serves such products to the Australian research community, with an emphasis on tailored continental-scale products, which are not necessarily available from the space agencies owning the satellite missions. A phytoplankton chlorophyll product adapted to the southern ocean is for instance proposed by the IMOS Satellite Remote Sensing Facility (SRS), following the work by Johnson et al. (2013). The Marine Water Quality Dashboard (<http://www.bom.gov.au/marinewaterquality/>) operated by the Australian Bureau of Meteorology (BoM) for the Great Barrier Reef (GBR) is an example of an operational system that relies on OCR.

Algorithms used to derive ocean properties from remote sensing reflectance have largely been developed using in situ data collected in locations distant from Australia (large northern hemisphere bias). Validation of some satellite products for regional application has already demonstrated that global algorithms are not sufficient to accurately describe some local ocean properties – e.g. in east Australian coastal waters, satellites generally over-estimate Chl-a, due to confusion with coloured dissolved organic matter (CDOM) and the organic component of non-algal particles (NAP) (Qin et al., 2007; Everett and Dobbin 2015). Moreover, in Australian turbid tropical waters with very high NAP concentrations, discriminating Chl-a requires a highly accurate radiometric signal (Qin et al., 2007; Brando et al., 2012). In Tasmanian waters with very high CDOM, discriminating Chl-a from CDOM also requires highly accurate radiometry and suitable inversion algorithms (Schroeder et al., 2008). Given the key role played by the Southern Ocean in climate, and the known shortcomings of existing OCR algorithms in that domain (e.g., Johnson et al., 2013), improved bio-optical modelling, driven by in situ observations of Apparent Optical Properties (AOPs), will be critical to maximising the value of satellite observations.

Biogeochemical (BGC) modelling is one important use of IMOS data, in particular via the Blue Water & Climate node activities (<http://imos.org.au/nodes/bluewaterclimate/>) (Steven et al., 2014). An important avenue of research in the BGC modelling community has focused on improving the modelling of the underwater light field (Baird et al., 2014). Indeed, doing a better job of propagating solar energy in the water column has two main impacts. On the one hand, a more realistic heat deposition as a function of depth in the water column leads to a better modelling of the mixed-layer dynamics. On the other hand, a better calculation of the amount and spectral composition of irradiance at various depths provides more accurate photon counts for photosynthesis quantification. Techniques exist now to accurately model underwater light propagation in a way that is not particularly demanding in terms of computational time (Mobley et al., 2015). The parameters that drive light propagation and use in the water column are absorption and scattering. As such, the IMOS bio-optical data set is critically important for BGC modelling of Australian waters.

To address these needs, researchers are using alternative approaches that involve measuring the inherent and apparent optical properties (IOPs and AOPs) of the upper ocean, alongside ocean biogeochemical properties, to develop regionally specific satellite algorithms (Blondeau-Patissier et al., 2009, Schroeder et al., 2012). As a complement to satellite observations, submersible optical sensors that measure Chl-a and CDOM fluorescence, optical backscatter and radiometry at depth are being deployed on ocean observing platforms worldwide to estimate the concentration and productivity of subsurface phytoplankton. Yet despite our increased vertical view of the ocean, there are still substantial challenges in using optical properties to estimate primary productivity (PP) and other biogeochemical properties in coastal water.

2 Rationale

In the coming 5 years, the IMOS remote sensing facility will progressively incorporate data from the VIIRS (NOAA), and is proposing to deliver data from the Copernicus Sentinel missions (ESA), in order to serve the Australian community with data for the long term. This diversification is essential as MODIS, on which we have relied since 2002 (and solely since 2010) is already operating long past its planned mission lifetime, with sensor degradation indicating that it is very close to the end of its operational life. Future NASA satellite missions are in planning but will focus on novel, experimental Earth observing concepts rather than

maintaining current ocean colour observing capabilities; thus it is necessary for operational ocean colour products from other agencies to be made accessible by the ocean colour community. In this process of adaptation, the IMOS bio-optics community must evaluate whether the data they generate for calibration/validation operations (hereafter “cal/val”) of ocean colour sensors are relevant.

Many remote sensing algorithms are presented as being global, yet are only validated locally, usually in northern hemisphere locations centred on US and European research institutes. Thus, local validation of algorithms used in Australian waters is critical for ensuring their suitability locally. It is essential when comparing global or regional algorithms that the underpinning radiometric satellite derived datasets are of the highest ascertainable quality so that in algorithm comparisons it is only the algorithm that has effect on the outcomes and not radiometric differences in the measurements used for validation. These same radiometric and in situ biogeochemical data can also be used in developing new locally applicable algorithms, which in turn require appropriate cal/val data.

Critical to improving the accuracy and application of satellite derived products is the calibration of the satellite radiometry signal using in-water and above water radiometry to correct for satellite sensor drift, atmospheric aerosols and satellite geometries; and to better connect water leaving radiance to the unique optical and biogeochemical properties of Australian waters.

Measurements of the required radiometric quantities, from which AOPs are derived, are performed by IMOS from a variety of platforms (ships and fixed stations) and using different instruments (essentially the DALECs on the AIMS vessel, Solander, and the SeaPrism at the Lucinda Jetty Coastal Observatory, LJCO). Ensuring consistency of these different measurements is essential, but a systematic comparison has not been undertaken. Normalizing protocols helps also in sharing data by improving consistency among measurements and therefore the confidence that we put in the derived data.

The IMOS “Radiometry Task Team” (RTT) was proposed in 2016 to address these issues.

3 Objectives

The objective of the task team was to perform activities that can ultimately improve usability (and re-usability) of IMOS radiometric data sets for research purposes as well as for validation of satellite ocean colour products. Improving usability essentially means improving the quality of the data sets, and improving re-usability means that data collection and processing protocols, as well as uncertainties, are well described. For example, the various instruments used to collect IMOS ocean radiometry are ostensibly measuring the same parameters, but each produces data that are specific to that instrument and processing methodology. For instance, the DALEC radiometer is a 3-sensor hyperspectral instrument used from ships, and the LJCO collects radiometric data from other types of radiometers on a fixed platform, such as the multiband SeaPrism instrument. Furthermore, there are at least two other types of radiometers used in the wider Australian bio-optical community, thus, in the absence of any inter-comparison there is no way to evaluate whether these data sets are mutually consistent.

Appendix 1 provides a list of factors possibly impacting the accuracy of the radiometry products and the quantities derived from them, such as the remote sensing reflectance. A number of these factors were addressed in the work reported here.

These activities are upstream of any research endeavour that is based on using field radiometry or satellite observations.

A further objective was to develop a plan for the evolution of radiometry measurements in IMOS for the next decade as there are imminent developments in further sophistication of optical instrumentation that Australia will need to adopt.

These objectives were addressed through the following actions:

1. Evaluate the degree of consistency among existing field-platform and sea-going radiometers used in the IMOS and the wider Australian bio-optical community, through dedicated laboratory and field experiments.
2. If needed, propose actions to improve consistency among these instruments and the way they are deployed (protocols) and the way data are processed.
3. Develop a plan for the evolution of IMOS radiometry measurements for the next decade.

4 Overall schedule of the activity, communications, use of funds

4.1 Schedule

The overall schedule of the activity is presented in Table 1.

	2016	2017
--	------	------

	July	Aug	Sep	Oct	Nov	Dec	Jan	Feb	Mar	Apr	May	June
Laboratory characterizations and calibrations												
Lab work												
Data processing												
Report writing												
Field inter-comparison at LJCO												
Field work												
Data processing												
Report writing												
Project meetings, presentation, and final reporting												
Project meetings					*	*						*
Talks & Posters									***		*	* ¹
Web stories										**		
Final report												

Table 1: overall schedule of the activities performed by the IMOS “Radiometry Task Team”

The work undertaken comprised:

- Laboratory calibration and characterisation of field-platform and sea-going radiometers used by the Australian community
- Deployment of these radiometers in a field inter-comparison exercise at the Lucinda Jetty Coastal Observatory (LJCO)
- Processing and interpreting data from these two activities, and discussions about what we learnt and how we move forward.

The main findings are summarised in section 5, and the associated recommendations and future possible developments are discussed in section 6. Then section 7 is a summary of recommendations.

The meetings listed in Table 1 were:

- Numerous discussions during the LJCO experiment (7th – 11th November 2016)
- A WebEx discussion on 1st December 2016
- A Teleconference on 3rd February 2017
- A face-to-face meeting at the UWA IOMRC, the morning before the IMOS Annual planning meeting (14th February 2017)
- Two WebEx discussions on the 8th and 28th June 2017 (final report preparation).

Otherwise, the project has been managed through frequent email communication.

4.2 Communications

The work of the IMOS RTT has been presented at several occasions during the course of the work, in particular by taking advantage of already-planned participation of members of the RTT to international meetings.

4.2.1 Annual IOCCG committee meeting, Perth, February 2017

The RTT activities were included in the overview talk that Nick Hardman-Mountford delivered at the 22nd annual IOCCG committee meeting in Perth:

Hardman-Mountford, N. Australian ocean colour activities. 22nd annual IOCCG committee meeting, Perth, 7-9 February 2017.

4.2.2 IMOS annual planning meeting, Perth, February 2017

A status report of the activity was presented at the annual IMOS planning meeting, as part of the project deliverables (talk):

¹ AMSA conference, Darwin, actually in July 2017 (3rd to 6th)

Antoine D., T. Schroeder, E. Botha, N. Cherukuru, A. Dekker, M. Doblin, P. Fearn, N. Hardman-Mountford, R. Johnson, E. King, W. Klonowski, J. Lovell, T. Malthus, C. Robinson, M. Slivkoff, P. Thompson, P. Van Ruth, Update on the Australian Integrated Marine Observing System (IMOS) radiometry task team. Australia Integrated Marine Observing System (IMOS) Annual Planning Meeting, 14–16 February 2017, Perth.

4.2.3 “FRM4SOC” workshop, ESA-ESRIN, Frascati, Italy, February 2017

The activity was presented (talk) at the occasion of a workshop organised by ESA, as an opportunity to further establish the connection between the OCR Australian community and the international community working on similar subjects:

Antoine D., T. Schroeder, E. Botha, N. Cherukuru, A. Dekker, M. Doblin, P. Fearn, N. Hardman-Mountford, R. Johnson, E. King, W. Klonowski, J. Lovell, T. Malthus, C. Robinson, M. Slivkoff, P. Thompson, P. Van Ruth, The Australian Integrated Marine Observing System (IMOS) radiometry task team: a community effort towards improved field ocean colour measurements. ESA workshop on options for future European satellite OCR vicarious adjustment infrastructure for the Sentinel-3 OLCI and Sentinel-2 MSI series, 21 – 23 Feb. 2017 ESA/ESRIN, Frascati, Italy.

4.2.4 Sentinel 3 validation team, ESA-ESRIN, Italy, February 2017

The activity was presented by T. Schroeder (talk) at the occasion of a meeting of the ESA Sentinel-3 Validation Team:

Schroeder T., Evaluation of Sentinel-3 OLCI Level 2 products in Australian waters, Sentinel-3 Validation Team Meeting, 15–17 February 2017, ESA ESRIN, Frascati, Italy

4.2.5 IOCS meeting, Lisbon, Portugal, May 2017

The participation of D. Antoine to the 2017 IOCS meeting was another opportunity to present our activities to a larger international community (Poster):

Antoine D., T. Schroeder, E. Botha, N. Cherukuru, A. Dekker, M. Doblin, P. Fearn, N. Hardman-Mountford, R. Johnson, E. King, W. Klonowski, J. Lovell, T. Malthus, C. Robinson, M. Slivkoff, P. Thompson, P. Van Ruth, The Australian Integrated Marine Observing System (IMOS) radiometry task team: a community effort towards improved field ocean colour measurements. International Ocean Colour Science Meeting 2017, Lisbon, Portugal, 15–18 May 2017.

4.2.6 AMSA conference, Darwin, Australia, July 2017

The RTT activity will also be presented at the 2017 AMSA conference in Darwin (“PEP talk”), as part of the project deliverables:

Antoine D., T. Schroeder, E. Botha, N. Cherukuru, A. Dekker, M. Doblin, P. Fearn, N. Hardman-Mountford, R. Johnson, E. King, W. Klonowski, J. Lovell, T. Malthus, C. Robinson, M. Slivkoff, P. Thompson, P. Van Ruth, The Australian Integrated Marine Observing System (IMOS) radiometry task team: a community effort towards improved field ocean colour measurements. Australian Marine Sciences Association annual conference, 3–6 July 2017, Darwin.

4.2.7 Marine Matters, IMOS bulletin

An article was published in the IMOS bulletin “Marine matters”:

Slivkoff, M., D. Antoine, and the RTT team, “IMOS Task Team goes troppo to solve radiometry challenges”, Marine Matters, issue 27, June 2017.

4.2.8 Web stories

Web stories have been also posted on:

http://imos.org.au/newsitem.html?&no_cache=1&tx_ttnews%5Btt_news%5D=616&cHash=dacfec2c1e35f422b86a9c13fb7d678c

and

<https://frm4soc.org/index.php/the-australian-integrated-marine-observing-systems-radiometry-task-team/>

4.3 Use of funds

The funding for the activity of the IMOS RTT was of \$100,420. It was used as follows:

- \$25,920 to support CSIRO staff
- \$15,000 to the laboratory experiment (work by *Insitu Marine Optics*)
- \$50,000 to salary support for Matt Slivkoff at Curtin University (0.38 FTE)
- \$9,500 to travel support to the experiment at LJCO and associated consumables

Other cash and in-kind contributions were:

- Curtin : salary + on-costs for D. Antoine, 0.1FTE for one year: \$24,390
- CSIRO : Salaries \$17,200 co-investment with additional in-kind from IMOS Ocean Colour
- UTS : \$5,700; \$1,175 cash, remainder in-kind
- BoM : Salary + on-costs for R. Johnson, ended up being review of documents only: ~\$300

5 Main findings from the laboratory and field experiments

The aims of the laboratory experiment were:

- To consistently calibrate all radiometers to be subsequently used in the field for this experiment, so that differences due to inconsistent calibrations do not confuse the comparison of results
- To perform characterisation experiments in order to better understand how these instruments respond to environmental conditions and to various levels of radiance or irradiance
- To provide some training to non-specialist members of the RTT about the radiometric calibration process to build national capacity

The aims of the field experiments at LJCO were:

- To bring together the community for an inter-comparison of radiometry measurements at a well-characterized site, i.e., the Lucinda Jetty Coastal Observatory (LJCO)
- Use that opportunity to further build capacity by training the community in best practice for deployment of, and data processing from, radiometers.

The detailed reports of these two activities are provided as appendices 2 and 3 of this final summary report, while we provide a summary of the main findings and observations in the subsequent sections.

5.1 About our community

It was definitely of significant benefit to bring together the Australian research community working on OCR-related topics in order to start building capability (see list of participants to the lab and field experiments in Appendix 4). As reminded in the introduction, field radiometry is definitely a difficult endeavour. This community spans physicists, mathematicians, biologists, ecosystem scientists, involved in, e.g., algorithm development, instrument development, remote sensing (RS) applications, modelling, but all with a common need to understand the potential and limitations of RS and marine optics.

Only two groups have significant expertise on those topics, namely the Curtin RSSRG and the CSIRO O&A group in Brisbane and Canberra. Other research groups (e.g., UTS, SARDI) use (or plan to use) sea-going radiometers, yet they do not necessarily have the focus on calibration and characterization of these types of instruments, although they do acknowledge such activities are important to collect accurate data.

Alignment of field practice, together with common language for calibration and metadata, are critical community characteristics that facilitate re-use of bio-optical radiometric measurements. This in turn enables the assembly of larger merged national data sets that can support a larger downstream research community.

The RTT work was also an opportunity to appreciate that the Australian “bio-optical” community is not that large, so that collaborative actions could be rather easily developed.

5.2 About instrument characterisation and calibration

- The Australian OCR community use a range of field instruments that have differing characteristics, although most of them rely on the same basic sensor technology, i.e., Zeiss spectrometers. The way the instruments are designed, deployed, and the way the data are processed to generate the quantities of interest is where the differences come from.
- Temperature effects on instruments (spectrometers delivering hyperspectral measurements) must be characterised in the laboratory and taken into account when processing data collected in the field, especially when the temperature at which the instruments operate is significantly warmer or cooler than the typical room temperature during laboratory calibrations. Sensors can deviate by as much as 0.56%/°C, (wavelength dependent) so temperature can easily introduce greater than 5% errors in radiometric measurements for the typical temperature differences encountered between initial factory calibrations and above water deployment temperatures. Some sensors, such as the TriOS RAMSES do not record internal temperature, so the accuracy of these instruments is limited in these types of applications unless a warmer calibration is applied. For sensors that do record internal temperature, post-processing schemes can be applied to improve accuracy throughout the temperature ranges encountered during deployment.
- The behaviour of instruments with respect to changing integration time at a given level of radiation or varying radiation levels for a given integration time should be fully characterised in order to define the “comfort zone” of instruments, i.e., the domain where they linearly respond to radiation levels and, possibly, to introduce non-linearity corrections if the instruments are to be operated in their non-linear domain.
- Non-IMOS instruments did not behave significantly differently from IMOS instruments (after all these instruments went through a unified calibration at IMO). See Figures 17 to 28 in the annexed report of the field experiment at LJCO.
- The DALEC cosine response could be improved if measurements are to be performed at low sun elevation angles.

- The RAMSES tested did not have internal temperature sensors, so users cannot apply temperature-specific corrections to them (meaning up to 10% uncertainties simply due to the difference between measuring temperature and calibration temperature)
- The HyperOCR spectra frequently have what the manufacturer describes as spectral “glitches”, which need to be filtered out during post-processing. This means “raw” data from HyperOCR are actually pre-filtered to remove outliers.
- A pixel shift correction is required to rectify an incorrect wavelength assignment in the IMOS DAEC.
- Two UTS RAMSES irradiance spectrometers were measuring 20% lower in the blue, compared to the factory calibration performed 5 years previously. This demonstrates the need for regular radiometric calibration.
- The wavelength calibration of all 3 Curtin DAEC spectrometers was shown to have drifted in time from the original calibration, and this directly impacts on the radiometric calibration. It is recommended that wavelength calibration be routinely performed during radiometric calibrations.
- The irradiance of two different FEL calibration lamps of varying ages and burn times agreed to within 2% of each other (compared with a 3rd reference lamp), indicating they are an appropriate calibration reference standard.
- The SeaPRISM calibration was found in excellent agreement with the NASA performed calibration within $\pm 1\%$ for visible wavelengths and $\pm 1.5\%$ for NIR wavelengths.

5.3 About field deployment procedures

- Properly placing instruments so that they are not (or minimally) perturbed by the superstructure hosting them is always a challenge, even at a site like the jetty based LJCO which does not suffer from needing to operate with a sea-going ship infrastructure.
- When a reference sensor is used to measure the downward solar irradiance, its location should be selected with great care so that shading or reflection from the vessel (more generally the platform) does not compromise the measurements.
- Where possible additional dark count measurements should be taken (by completely covering the sensor heads). With spectrometer-based instruments, these measurements are normally not used in the data processing because the instruments are equipped with internal shutters that provide the dark current measurements. However, the “caps ON” measurements are still useful to monitor instrument behaviour specifically at variable temperature conditions.
- Above-water measurements are the most commonly carried out in the Australian community, whether it is from LJCO (the case here) or ship of opportunity or during dedicated research voyages. Albeit simple to put in practice, which is likely why they are popular, they actually require great care for the data to be of high quality. When carried out from a ship, the ship speed, the ship superstructure shape and colour, the ship orientation with respect to the sun, the location of instruments, the recording of wave characteristics, are important factors that will eventually define data quality.

5.4 About data processing methods

- Radiance sensor fields of view and integration times vary amongst sensors, and the sea-surface is a temporally variable target, so direct comparison of radiance coming from the sea (L_{sea}) from different instruments at their native integration settings does not necessarily make sense. In this scenario, processing steps are needed to derive the water-leaving radiance (i.e., the total radiance recorded by the instrument corrected from the reflection of skylight), and it is only at that step that meaningful comparison can be made.
- Measurements of the above-water downward irradiance, E_s , can be checked against theoretical clear-sky computations including an uncertainty budget to provide a reference measurement of irradiance free of instrumental errors. These theoretical computations can be performed with high accuracy when combined with measurement of actual conditions (wind speed, atmospheric pressure, aerosol optical thickness, and ozone vertical column density).
- Solar zenith angle is a key parameter to be accounted for in data QC, because environmental perturbations and uncertainties in a number of processing steps increase as it increases.
- Sensor internal temperature affects radiometric accuracy, so must be measured during deployment and then considered when post-processing any radiometric data. Currently, none of the instrument manufacturer’s post-processing software or factory calibrations consider internal temperature. Furthermore, the RAMSES spectrometer does not collect internal temperature, making improvements in post-processing RAMSES data difficult.
- Due to the diversity of users, native instrument file formats and resultant workflow (including embedded corrections), new manufacturer-emulated calibration files based on the lab characterisation needed to be

created in order to utilise native software to apply the new calibration coefficients. This is not ideal but unavoidable.

- Ideally, raw instrument data would be collected and then re-formatted and stored in a standardised human-readable data format, after which temperature correction, dark offsets and radiometric calibration coefficients can be applied. The output of this processing would then also be stored in a standardised human-readable data format such as the one used in this project, thereby greatly assisting the comparison and subsequent uptake of information.

5.5 About satellite validation operations

The international OCR community actually never managed to establish clear requirements for the accuracy or uncertainty of marine reflectances in coastal waters. There is a quasi-single requirement for clear, open-ocean, waters, which is “5% uncertainty in the blue part of the e.m. spectrum for oligotrophic waters” (Gordon and Clark, 1981; Antoine et al., 1999), and is largely based on deriving geophysical products using band ratio techniques. It is, therefore, somewhat difficult to claim whether a given measurement site or data set is qualified to produce validation data for satellite-derived R_{rs} in coastal (turbid) waters. Different applications using a variety of products and algorithms for their specific objectives might end up with different requirements.

What can be done, however, is to assign an uncertainty estimate to the R_{rs} values derived from field measurements, so that it can be subsequently assessed against requirements, assuming that such requirements would be derived at some point.

Deriving relevant uncertainty budgets for field measurements of radiometric quantity is currently an area of international research. To our knowledge, radiometric quantities or derived products such as R_{rs} from popular databases (e.g., SeaBASS, MERMAID) do not yet include such uncertainties.

Deriving uncertainty budgets will require more work than that done during the field experiment at LJCO.

6 Where to from here? Some recommendations on the way forward

The two sub-sections below (6.1 and 6.2) correspond to actions/recommendations that:

- Directly come from the work performed in the laboratory and in the field during the course of the RTT work and are fully relevant to IMOS
- Come from more general discussions that took place among the RTT members or that took place for some time in the larger bio-optics community in Australia. Those ones go beyond IMOS only, yet are definitely relevant to IMOS as well.

The recommendations outlined in these 2 sections are subsequently summarized in Section 7.

6.1 Actions / recommendations directly issued from the RTT work

6.1.1 Keeping the momentum; do we need these experiments at regular intervals?

As said in section 5.1, bringing together the members of the Australian community whom carry out activities involving field radiometry was definitely useful, not only because such occasions are rare and this community needs increased communication, but also because this community is highly heterogeneous in terms of science goals, instrumentation used, and level of understanding about what makes measurements of radiometry in the ocean of good quality.

What came out from this exercise is that the BGC community still needs education/training on optics. The fieldwork at LJCO was an excellent learning exercise for those participating. The reason why the training is important is that we want qualified people to make radiometric measurements alongside BGC measurements and increase our opportunities to validate OC products. This will increase credibility of OC products and thus uptake by the user community.

Other reasons that justify repeating such exercises include checking instrument drift, and also maintaining consistency to facilitate data reuse. Promulgating a data interchange format and helping groups to implement it would also help.

Periodic radiometric calibration is needed (annually at least) for IMOS and other radiometers, and spectrometer wavelength calibrations should be verified during each radiometric calibration.

This would also provide continued opportunities for to bring less experienced users to the same level of experience, and to fully understand all instruments in use.

Therefore, there would definitely be value in conducting regularly similar exercises than the ones described in this report. What this 12-month RTT activity has shown, however, is that the amount of work needed and associated resources (funding and staff) are significant.

Recommendation 1: Undertake similar experiments to the ones described in this report every other year. Some core activities would be the same for each of these experiments, and additional more-focused activities would be included depending on the community needs and resources. Ideally, we could include below-water radiometry if supported by enough interest and instruments. It might actually also be feasible to carry out core laboratory calibration activities annually.

6.1.2 Reprocessing of historical data?

The logic here is: how can we do better with the data we collected prior to the RTT, considering what we observed during the RTT work?

Actions that could be taken include the reprocessing of historical data by accounting for (when feasible) the temperature during data collection, and also accounting for the wavelength shift that was observed, and the addition of some well-defined quality control steps.

Recommendation 2: establish a list of data sets that could be reprocessed, and implement the necessary changes (for instance to include temperature dependencies). Finalise the radiometric file format used in the RTT Field comparison work to allow all users easy access to radiometry in various levels of processing.

Recommendation 3: agree on instrument-specific data processing codes that the community could use in order to improve consistency of end products.

6.1.3 Community assets, are they sufficient? Where should we invest/disinvest?

As said above, the pool of instruments (radiometers) used by the Australian community is made of several types of instruments, which have various degrees of characterisation, and varying frequencies of calibration.

Some of them, e.g., the Curtin DALEC, are prototypes that never really underwent full radiometric characterization². Similarly, commercial instruments rarely undergo more than a basic characterization, which is then applied to all instruments produced in the same series (“class-specific” parameters instead of “instrument-specific” parameters). Basically, most manufacturers undertake just enough radiometric characterisation to determine they are fit for commercial sale. Some of them can carry out more sophisticated rounds of characterization, but the cost is generally prohibitive and usually requires participation and/or co-investment from external groups. Another approach for manufacturers is to collaborate closely with research institutions, yet the latter have to be supported in such activities.

Otherwise, most instruments in the Australian community are aging as well and no replacements are foreseen for the moment.

The former Bio-optical Working Group (BWG) suggested that radiometric measurements should be aligned with biogeochemical (BGC) measurements wherever possible. Radiometry is currently performed at LJCO, and BGC measurements are currently performed at the National Reference Sites (NRS). Our experience in the RTT suggests that bringing BGC measurements to a single radiometric site has a better likelihood of best quality radiometric data than bringing radiometry to numerous BGC sites. Another option for IMOS investment is to bring radiometers on targeted voyages where many in situ measurements are made (see later on, **Recommendation 15**). This would provide increased spatial coverage of radiometric measurements in targeted regions where in situ measurements have been prioritised. This was the rationale behind the DALEC installation on the AIMS vessel (discussed below).

Another asset of our community are the calibration facilities. At least four can be identified here: the Curtin facility, the IMO facility (used for this RTT work), and the two national facilities managed by CSIRO (Perth and Canberra; the latter being transferred to Brisbane). Here the question is whether these facilities are equipped appropriately and involve staff with the appropriate expertise to carry out comprehensive characterisation and calibration of sea-going radiometers. What is the status of their equipment, such as NIST-calibrated FEL lamps, Spectralon™ plaques or integrating spheres? There would certainly be value in these facilities to interact and compare their assets (e.g., lamps).

The question is what role these different facilities can have in helping the Australian bio-optics community to get its instruments at the best possible level. This will no doubt involve the acquisition of additional equipment in order to perform more comprehensive characterisation measurements. It is worth noting that instruments can be operated during many years when they are properly maintained and their calibration regularly verified, allowing for greater return from investments in instrumentation.

Recommendation 4: Maintain an inventory of radiometric instruments in use in the Australian community, along with their calibration history (traceability and repeatability), and with a plan for future maintenance, refurbishment and modernisation when needed. Consult with the group before replacing / upgrading instruments. Existing IMOS assets need to be looked after to extend their life as long as possible.

Recommendation 5: work with the Australian Satellite Calibration Working Group (ASCWG) to evaluate the status of the existing radiometric calibration facilities and how they can be used by our community (see Malthus et al., 2015) and whether they need upgrades to fulfil this role.

6.1.4 Community practices for field measurements

Published protocols should be brought to the attention of the Australian bio-optical community so that the recommended best practices are known.

Literature exists that can be used as guidelines on best practices for different radiometer types, e.g., Mobley (1999), Hooker and Morel (2003), Hooker and Zibordi (2005), Hooker (2014).

The IOCCG is in the process of establishing revised protocols from those that were initially published by NASA in the frame of the SeaWiFS and MODIS missions. Instead of being frozen document, the idea is to have on-line living documents that can be updated on a regular basis.

Recommendation 6: pool together documentation on protocols for easy access by the Australian bio-optics community.

² Which normally includes, non exhaustively: detector(s) linearity, dynamic range, SNR, temporal stability, spectral calibration, stray light when appropriate, cosine response for irradiance sensors, immersion coefficients, residual sensitivity to polarisation.

Recommendation 7: Organize training exercises/workshops on various aspects of collecting and processing radiometric quantities.

6.1.5 *The future of the Lucinda Jetty Coastal Observatory (LJCO)*

Ocean Colour remote sensing provides information on the fundamental radiometric quantity, the water-leaving radiance or reflectance, which is subsequently used in many ocean colour algorithms to infer inherent optical properties such as absorption and scattering and concentrations of key water constituents. Higher-level products, such as primary productivity as one example, can then be derived from the inherent optical properties and biogeochemical concentrations, thus allowing the remote sensing community to establish the link between the observed satellite radiometry and biogeochemical processes which are of interest to the community, such as coastal dynamics, flood plumes, changes in eutrophication due to land use or carbon cycling and fixation - only to name a few examples.

Because of these important linkages with our Earth's climate system (e.g carbon fluxes) and ocean biology (e.g. primary productivity), the Global Climate Observing System (GCOS) has listed Ocean Colour (Radiometry) as an Essential Climate Variable (ECV). It is therefore of utmost importance to monitor the accuracy of the satellite-derived radiometric products through accurate in situ radiometric observations. In this way, satellite-based radiometric measurements such as reflectance can be established as a reliable long-term data record.

The Lucinda Jetty Coastal Observatory was established to support validation of satellite ocean colour radiometry and to help advance the understanding and link between the radiometry and the inherent optical properties to support the study of biogeochemical processes and modelling. The site is currently the only fixed-platform in Australia that does sustained observations of this nature and the only southern-hemisphere ocean colour validation platform within NASA's global network of sun-photometers (AERONET-OC). Thus it is nationally and internationally significant and was a key bargaining aspect in convincing the European Commission to enter into the Copernicus-Sentinel Data Hub agreement.

Specifically the unprecedented amount of data from the Copernicus Sentinel series will provide Australia with finer spatial and spectral resolution ocean colour observations that offer new national opportunities for coastal bio-geochemical process studies and remote sensing both relying on coastal optical observations. The Jetty is a near-ideal platform for collecting these observations and testing instrumentation alongside the well-characterized and maintained AERONET-OC radiometer. The site is highly cost-effective when compared to any other methods of collecting such a systematic optical dataset as there are no ship costs involved. The platform can also support regular instrument inter-calibration and training exercises.

Since reinstatement in 2013 the site is operating continuously producing the relevant above and in-water optical time-series and has just reached the status of having sufficient sustained long-term measurements to start investigating trends. Australia needs at least one coastal and one blue-water cal/val site as proposed in our recommendations. One cannot replace the other and each has a unique role.

More concurrent above and in-water optical measurements such as performed at Lucinda are needed in other locations around Australia to adequately characterise coastal waters at continental scale. These recommendations are in-line with recommendations supported by all major space agencies at the 2017 International Ocean Colour Science meeting to develop more sites in coastal and estuarine waters such as LJCO as ~60 to 80 % of the global population lives on or near the coast.



Sentinel2-MSI true colour image taken above the Lucinda Jetty Coastal Observatory (LJCO). The observatory is located at the end of a 6-km long jetty, which appears clearly as a white strip in the image. The spatial resolution of this image is 60m. © ESA, Copernicus Australia

Recommendation 8: Continued support to maintain LJCO as AERONET-OC site and invest in new sensor technology if recommended by AERONET.

Recommendation 9: Enhance the multi-spectral AERONET-OC acquisitions with hyperspectral radiometry for on-going instrument inter-comparison and quality control of radiometric measurements.

Recommendation 10: Reinstate a reduced number of core in-water optical measurements and regular water quality sampling to support ocean colour algorithm development and validation as well as BGC modelling. This would include: in-water measurements of temperature, salinity, spectral total absorption and attenuation as well as spectral backscattering in addition to regular water sampling to determine the concentrations of chlorophyll-a and total suspended matter and the absorption of particulate and dissolved organic matter from laboratory analysis.

Recommendation 11: Consider LJCO as a platform for regular inter-comparison exercises and testing of new instrumentation including practical training exercises.

Recommendation 12: Work towards characterization and correction of the superstructure shading effects at LJCO to provide improved uncertainty estimates of the radiometric data.

6.1.6 The future of en-route radiometry measurements

En-route measurements have the advantage of covering different water masses in shorter time periods and, therefore, have the potential to increase the spatial footprint for ocean colour validation compared to point measurements taken during research voyages or from fixed platforms such as LJCO or (potentially) moorings.

Under IMOS, en-route radiometric measurements are performed with the DALEC, which is deployed in collaboration with AIMS on the RV Solander during selected voyages mainly covering the northern tropical waters of Western Australia and the Northern Territory. Recently, Brando et al., 2016, have demonstrated the potential of these measurements for satellite ocean colour validation, provided that the instrument is well maintained when deployed on the ship and that all necessary metadata are properly recorded (geometry of measurements, sea and sky state).

Existing non-IMOS data should be catalogued and made available so that further exploitation can be envisaged.

Other routes could be envisaged (e.g., the SOTS mooring refurbishments), yet requirements for installation on the ship and proper measurements might significantly differ when it comes to collecting data in the Southern Ocean.

Recommendation 13: En-route DALEC deployments under IMOS should be maintained to increase the spatial footprint for satellite ocean colour validation. Existing data sets should be made available as reflectance products for further use.

Recommendation 14: The IMOS DALEC instruments used for en-route measurements should be inter-compared with the SeaPRISM at LJCO on annual basis.

6.2 Mid- to long-term developments around radiometry measurements

6.2.1 Radiometry measurements on research voyages

Collecting radiometry measurements should be part of the core activities during research voyages whose objectives revolve around ocean biogeochemistry, carbon cycle, primary productivity and carbon export. The amount and spectral composition of the incoming solar radiation that then propagates down the water column is indeed a key energy input in the ecosystem, and should be known when dealing with science questions in these domains. It is not just a quantity of interest for optical oceanographers only.

Options here include en-route measurements (see section below) or dedicated deployments of in-water profiling instruments, both requiring staff properly trained to perform this sort of measurement. Enough time has to be included in the daily schedule of operations to accommodate these measurements, and flexibility has to be possible as well because good radiometry data cannot be obtained in all sorts of atmosphere and ocean conditions, and in any ship behaviour (speed, position w.r.t. the sun).

The adapted instruments obviously need to be available, which is not easy to achieve with a limited instrument pool in the Australian community, combined with staff and funding availability.

Therefore, the community might consider collectively maintaining at least one profiling radiometer, which could be used to piggy-back on research voyages, either long ones (e.g., several weeks on the MNF) or shorter ones such as 1-week research cruises off the coast. Advanced planning would be necessary to achieve this, as well as dedicated funding for an annual calibration and servicing (minimum) plus basic data quality control and processing (so staff time).

Recommendation 15: purchasing and maintaining a minimum of one profiling radiometer system and use it on research voyages following a plan to be updated twice a year. Identifying one technical staff as being responsible of its deployment, maintenance and of the data processing.

6.2.2 Blue-water cal/val site off WA

Australia also needs a blue water calibration/validation site so that Australia can provide relevant data back to international space agencies for both coastal and ocean waters. A “blue-water” calibration/validation site off Perth, WA, has been proposed to IMOS in June 2016 as one option for growth of IMOS. The rationale for developing such a site is the following:

- “System Vicarious Calibration” (SVC; see appendix 5) is a mandatory step in the generation of high-quality geophysical products from satellite ocean colour radiometry (OCR). Currently only two sites exist: MOBY (US NASA, off Hawaii; PI Ken Voss, U. Miami) and BOUSSOLE (Europe, ESA, Mediterranean Sea; PI D. Antoine, Curtin Uni. / CNRS). Recommendation by the international community is to ensure at least a few sites are available and consistent.

- There is no SVC site in the Southern hemisphere, which is an issue in terms of the sites in the northern hemisphere not covering all geometries of the satellite observations. In addition, there is a clear difference in atmosphere properties (clarity) between the two hemispheres, and this has an impact on the SVC process.
- Expertise exists in WA in particular and Australia in general that can be used to develop such a site
- The geophysical conditions are close to ideal for a SVC site, i.e., clear atmosphere (low aerosol and ozone contents, low humidity), low cloudiness, rather stable oligo- to meso-trophic conditions (Zibordi and Mélin, 2017).
- There is already some existing logistics thanks to the monthly sampling at the Rottnest IMOS NRS.
- The establishment of the Australian Copernicus data hub has been possible in particular because Australia has put forward a record of historical activities in the calibration/validation domain, so that pursuing this goal with the development on new infrastructure is likely needed to maintain this role.

There are a number of hurdles to pass, however, for this site to become a reality. A first question is whether the NASA PACE mission is going to move forward after publication of the 2018 Presidential budget in the US. Officially, PACE continues but is on the list of possible candidates for cancellation. The “MOBY-NET” concept is fully linked to PACE, and may disappear if PACE is cancelled. If PACE eventually proceeds, NASA funding is in principle dimensioned so as to produce two full MOBY systems for being used at the original MOBY site in Hawaii, and one system for use on another site. We would likely have to compete with other proposals to host this system. Apart from this, some practicalities related to the deployment of such buoys would have to be solved, e.g., can we find a ship adapted to deployments?

Recommendation 16: further evaluate the feasibility of a globally-relevant blue water site off Perth, WA, in terms of deployment conditions, availability of adapted vessels for deployment and recovery of the mooring, and possible funding sources.

6.2.3 Radiometry from Bio-Argo and other autonomous platforms

Multi-spectral radiometers have also been integrated and deployed on autonomous platforms by the Australian bio-optical community. Initial results from deployments on biogeochemical profiling floats (Bio-Argo) have shown that these autonomous deployments can be used for validation of ocean colour radiometry as well as chlorophyll-a products (Wojtasiewicz et al., submitted). The advantage of these platforms is that they can make many more measurements and at lower cost than from ship-based sampling, substantially increasing the number of measurements coincident with satellite overpasses (match-ups) that can be used for validation.

Equivalent sensors have also been deployed on gliders although the quality of glider-based radiometry for this application has yet to be assessed as the measurements occur at variable depths below the surface.

Continued evaluation of these autonomous platforms for undertaking ocean colour validation studies will be important to ensure Australia use ocean colour satellite data in the most cost-effective ways. Finding ways to work with manufacturers to ensure that these autonomous radiometers can be locally calibrated for consistency with other systems in use would be one area for immediate improvement.

Recommendation 17: Evaluate cost-effective approaches for local calibration of radiometers integrated on autonomous platforms.

Recommendation 18: Evaluate and assess the quality of radiometry and optical measurements from the IMOS gliders

6.2.4 Uncertainty budgets

Although any measurement of a physical quantity should come with an uncertainty related to the technique used to measure it and the conditions into which it was measured (and other elements depending on what is at stake), it is actually seldom the case that such a number is provided. When it comes to using the measurement as a “truth” in the process of validation other measurements, uncertainties become of the utmost importance.

By their very nature, radiometry measurements depend more significantly than many others on the conditions under which they are performed. Because they are passive measurements of the ambient light field, any perturbation of this field will affect the process. That is what makes these measurements difficult to perform properly. Perturbations can originate from, non exhaustively: instabilities of the sun illumination (measurements should normally be performed under stable illumination), degree of diffuseness of the incoming light, state of the air-water interface, shading from the platform under use (whatever it is a ship or a fixed platform), self-shading by the instrument itself, geometry of the measurement (e.g., pointing angles for above-water radiometry), degree of polarisation of the measured radiation.

Data collection protocols are designed either to completely avoid such perturbations (e.g., deploying free-fall systems way off the ship so as to avoid shade) or to minimize them (building small instruments so as to minimize self-shading).

Additional uncertainties come into play when processing the data, yet this is less radiometry-specific than the above environment perturbations.

As said in section 5.5, deriving relevant uncertainty budgets for field measurements of radiometric quantity is currently an area of international research. It needs first identifying all sources of uncertainties, from instruments themselves (calibration), data collection protocols, and data processing algorithms. Then numbers have to be assigned to these uncertainties, either through data analyses or sometimes just as a best (conservative) guess when nothing else is possible. Finally, individual uncertainty assessments have to be combined to derive an overall uncertainty budget.

Recommendation 19: establish uncertainty budgets whenever feasible, in order to provide data with uncertainties. As far as possible, take advantage of current developments in this domain in the international community (in particular current efforts to derive comprehensive error budgets for the two existing SVC sites).

6.2.5 Instrumentation development

Commercial instruments are not necessarily adapted to all research endeavours. For instance, measuring the volume scattering function (VSF) of oceanic particles has long been on hold because no commercial instrument was available since prototypes were developed and used in the US in the 1960s. Few other developments have been attempted more recently, and they allowed making progress on understanding the variability of the VSF. A similar example can be given for the measurement of the underwater 3D radiance field. Such complex developments are not often adapted to become commercial products, however, which is why the research community sometimes lacks appropriate instruments to make breakthroughs.

The current panorama of specialised small to medium enterprises (SMEs) becoming integrated into larger commercial groups make relationships between researchers and their instrument providers less agile. Instruments do not necessarily evolve and, on the contrary, their production might be stopped and continuity compromised.

Some companies produce underwater radiometers that are rather widely used in our community, yet these instruments are not part of their main product stream so that the efforts towards characterization, calibration, and improvements of these instruments are minimal.

This situation probably calls for a re-examination of the total reliance of the Australian bio-optics research community on overseas commercial providers.

Recommendation 20: evaluate options for more in-house developments, provided that there is a clear view of what sort of instrument would be the most amenable to being developed.

Recommendation 21: Explore new sensor technology to extend the radiometric measurements to cover the UV and NIR spectral ranges that are now covered by the next generation of ocean colour satellites such as Sentinel-3 (e.g. 400 nm to 1040 nm).

6.2.6 Improving the uptake of data by the IMOS nodes and the overall Australian science community

Radiometry per se is rather a “niche activity”, and the associated data have value primarily for scientists interested in their collection, processing, and immediate use (the “bio-optics research community”). Because high-quality radiometry measurements will inevitably remain scarce, their use to develop broad scale products from satellite ocean colour radiometric observations is an indirect way to significantly increase their impact.

Therefore, to improve the uptake of those data by a larger research community, at the level of the IMOS nodes or more broadly, higher-level products have to be generated, such as diffuse attenuation coefficient, horizontal visibility or vertical transparency, and primary production (which however involves additional modelling).

These products might be targeted to certain areas of National significance. Then, the community can focus validation exercises in these regions of priority.

In view of facilitating their access and use, the bio-optical community needs to figure out how to organise the data so that it goes into AODN with all the necessary metadata. The success of this type of action will be underpinned by providing control and consistency to the data formats, metadata languages etc..

Recommendation 22: Facilitate simpler access to radiometric data through a system like AESOP, which allows simultaneous extraction of multiple collocated parameters such as in-water optics and concentrations.

Recommendation 23: Use radiometric data from a variety of platforms (e.g., fixed and en-route) for an annual quality assessment of satellite ocean colour produced by the IMOS Ocean Colour Sub-facility.

Recommendation 24: As a community, identify the most critical satellite product to develop, and whether or not we have the corresponding in situ validation data sets. This can be used to prioritise and say where it is essential to improve.

6.2.7 International engagement

Australia's activities in the domain of OCR calibration and validation are fundamental to maintain our connection with the international community and with space agencies that provide satellite data sets. Keeping close links with the international OCR community and space agencies is vital.

Recommendation 25: continuing participation of the Australian community active under IMOS to a number of International groups, such as the ESA's Sentinel3 ocean colour validation team, the CEOS working group on cal/val (WGCV) and upcoming OC missions by NASA, NOAA, ISRO, JAXA etc.. Initiate collaboration with the Korean Space Agency for GOCHI-II (a geostationary Ocean Colour sensor that will also view Australia).

Recommendation 26: On-going support to maintain the IMOS Bio-Optical Data Base that collates bio-optical and radiometric data collected by the Australian research community for provision to the national and international research community for calibration and validation of ocean colour sensors. In other words, making our radiometric data available internationally. Such availability is core criterion for Australia being accepted internationally as an ocean colour expert country.

7 Summary of recommendations, associated needs, and likely impact if implemented

The table below regroups the recommendations proposed under various topics in section 6, and gives some indication as to whether staff and operating needs to take these recommendations onboard are available, and whether new instrumentation would then be needed. The expected impact on the research community and the general benefit for users of radiometry data and associated satellite products is also sketched.

Some important notes about this Table:

- The practical consequences of implementing the recommendations made here, in particular in terms of cost and possible funding sources, have been intentionally left aside from this report. Doing this would mean deriving an **implementation plan** from the recommendations made in this report, which would require additional work and could be done in a next step.
- **No priority ranking** of the recommendations has been attempted for the moment. This would actually be the first thing to do if an implementation plan is put together.
- In the Table below, when the answer is “no” to the question “Staff & operating needs covered?”, it does not mean that we expect IMOS only to eventually fulfil the need. Again, related to the above comments, **multiple supports would have to be attracted** in order for the “big picture” sketched in this report to become reality. Options include, e.g., the state and federal governments, and international space agencies.

Possible new instrumentation needs	Are staff & operating needs covered by existing support (IMOS or others)?	Impact on the research community, general benefit for users of radiometry data and associated satellite products
Recommendation 1: Undertake similar experiments to the ones described in this report every other year. Some core activities would be the same for each of these experiments, and additional more-focused activities would be included depending on the community needs and resources. Ideally, we could include below-water radiometry if supported by enough interest and instruments. It might actually also be feasible to carry out core laboratory calibration activities annually.		
None	<p>Yes if only existing staff involved.</p> <p>No if dedicated staff has to be hired.</p> <p>“marginal” costs are not covered (travel, consumables, shipments, calibrations)</p>	<ul style="list-style-type: none">- Keeping the bio-optics community active and collaborative.- Keeping instruments well calibrated- Progressively building capability in this community, in relation to radiometry measurements
Recommendation 2: establish a list of data sets that could be reprocessed, and implement the necessary changes (for instance to include temperature dependencies)		

None	No	- Quality improvement of existing data sets - Implementation of codes to be used for processing future data sets
Recommendation 3: agree on instrument-specific data processing codes that the community could use in order to improve consistency of end products		
None	Yes	- Improved consistency of radiometry data sets
Recommendation 4: Maintain an inventory of radiometric instruments in use in the Australian community, along with their calibration history (traceability and repeatability), and with a plan for future maintenance, refurbishment and modernisation when needed. Consult with the group before replacing / upgrading instruments. Existing IMOS assets need to be looked after to extend their life as long as possible.		
None initially, then new community-agreed radiometers	No	- Optimised use of assets - Community agreement on future instrumentation
Recommendation 5: work with the Australian Satellite Calibration Working Group (ASCWG) to evaluate the status of the existing radiometric calibration facilities and how they can be used by our community (see Malthus et al., 2015)		
Additional laboratory equipment for advanced radiometers characterisation	Yes	- More and better use of existing calibration facilities by the marine optics community
Recommendation 6: pool together documentation on protocols for easy access by the Australian bio-optics community.		
None	Yes	- Facilitate access to information on protocols, with anticipated improvement in practices
Recommendation 7: Organize training exercises/workshops on various aspects of collecting and processing radiometric quantities.		
None	No	- Keeping the bio-optics community active and collaborative. - Progressively building capability in this community, in relation to radiometry measurements
Recommendation 8: Continued support to maintain LJCO as AERONET-OC site and invest in new sensor technology if recommended by AERONET.		
None	Partly (Proposed to continue under the 2017/19 plan for IMOS Ocean Colour but not sufficiently funded)	- Data available for ocean colour algorithm development and validation. - Uptake by national / international community and space agencies.
Recommendation 9: Enhance the multi-spectral AERONET-OC acquisitions with hyperspectral radiometry for on-going instrument inter-comparison and quality control of radiometric measurements.		

New hyperspectral radiometer(s) if not existing already in the community	No	<ul style="list-style-type: none"> - Data available for ocean colour algorithm development and validation. - Uptake by national/international community and space agencies. - Enables data quality monitoring of radiometric measurements through regular inter-comparison.
Recommendation 10: Reinstate a reduced number of core in-water optical measurements and regular water quality sampling to support ocean colour algorithm development and validation as well as BGC modelling. This would include: in-water measurements of temperature, salinity, spectral total absorption and attenuation as well as spectral backscattering in addition to regular water sampling to determine the concentrations of chlorophyll-a and total suspended matter and the absorption of particulate and dissolved organic matter from laboratory analysis.		
None	No (Proposed under the 2017/22 plan for IMOS Ocean Colour Growth)	<ul style="list-style-type: none"> - Data available for ocean colour algorithm development, validation, BGC process studies and modelling. - Uptake by national/international community and space agencies.
Recommendation 11: Consider LJCO as a platform for regular inter-comparison exercises and testing of new instrumentation including practical training exercises.		
None	Yes if only existing staff involved. No if dedicated staff has to be hired. “marginal” costs are not covered (travel, consumables, shipments, calibrations)	Same as for Recommendation 1: Keeping the bio-optics community active and collaborative. <ul style="list-style-type: none"> - Progressively building capability in this community, in relation to radiometry measurements
Recommendation 12: Work towards characterization and correction of the superstructure shading effects at LJCO		
None	No	<ul style="list-style-type: none"> - Contribution to establishing an uncertainty budget for radiometry measurements at LJCO - Increased confidence in radiometric products. Required for uncertainty budget of radiometric measurements.
Recommendation 13: En-route DALEC deployments under IMOS should be maintained to increase the spatial footprint for satellite ocean colour validation. Existing data sets should be made available as reflectance products for further use.		
One DALEC dedicated to en-route measurements	Likely Yes (Proposed to continue under the 2017/19 plan for IMOS Ocean Colour)	<ul style="list-style-type: none"> - Increased number of radiometric measurements for ocean colour validation across blue and coastal waters. - Uptake by national/international community and space agencies.
Recommendation 14: The IMOS DALEC instruments used for en-route measurements should be inter-compared with the SeaPRISM at LJCO on annual basis.		
None	No	<ul style="list-style-type: none"> - Improved consistency among radiometers. - Increased confidence in radiometric products.

Recommendation 15: purchasing and maintaining a minimum of one profiling radiometer system and use it on research voyages following a plan to be updated twice a year. Identifying one technical staff as being responsible of its deployment, maintenance and of the data processing.		
One profiling radiometer	No	- Increase the benefit from MNF research voyages for the bio-optics community. - Optimised use of assets
Recommendation 16: further evaluate the feasibility of a globally-relevant blue water site off Perth, WA, in terms of deployment conditions, availability of adapted vessels for deployment and recovery of the mooring, and possible funding sources.		
All new equipment for the new site	Yes in terms of evaluating this option, No if it would have to be implemented	- If feasible and implemented, this site would significantly augment the capability of the Australian community in providing essential calibration / validation observations to international space agencies
Recommendation 17: Evaluate cost-effective approaches for local calibration of radiometers integrated on autonomous platforms.		
None	No	- Improved consistency among radiometers used on various platforms
Recommendation 18: Evaluate and assess the quality of radiometry and optical measurements from the IMOS gliders		
None	No	- Improved consistency among radiometers used on various platforms
Recommendation 19: establish uncertainty budgets whenever feasible, in order to provide data with uncertainties.		
None	No	- Improved traceability of data sets
Recommendation 20: evaluate options for more in-house developments, provided that there is a clear view of what sort of instrument would be the most amenable to being developed		
	No	- Decrease reliance on overseas manufacturers - Better fit-for-purpose instruments
Recommendation 21: Explore new sensor technology to extend the radiometric measurements to cover the UV and NIR spectral ranges that are now covered by the next generation of ocean colour satellites such as Sentinel-3 (e.g. 400 nm to 1040 nm).		
Yes if new technology becomes available	No	- Increased spectral range for ocean colour validation

Recommendation 22: Facilitate simpler access to radiometric data through a system like AESOP, which allows simultaneous extraction of multiple collocated parameters such as in-water optics and concentrations.		
None	No	- Increased use and uptake of data
Recommendation 23: Use radiometric data from a variety of platforms (e.g., fixed and en-route) for an annual quality assessment of satellite ocean colour produced by the IMOS Ocean Colour Sub-facility.		
None	Yes	- Increased confidence in satellite ocean colour radiometry served by IMOS
Recommendation 24: As a community, identify the most critical satellite product to develop, and whether or not we have the corresponding in situ validation data sets. This can be used to prioritise and say where it is essential to improve.		
None	Yes for reaching consensus. No for implementation and validation.	- Increased use and uptake of data driven by impact
Recommendation 25: continuing participation of the Australian community active under IMOS to a number of International groups, such as the ESA's Sentinel3 ocean colour validation team, the CEOS working group on cal/val (WGCV) and upcoming OC missions by NASA, NOAA, ISRO, JAXA etc.. Initiate collaboration with the Korean Space Agency for GOCI-II (a geostationary Ocean Colour sensor that will also view Australia).		
None	Yes (staff) Not fully (travel support)	- Increased visibility and recognition of the Australian bio-optics community as a key player in this field
Recommendation 26: On-going support to maintain the IMOS Bio-Optical Data Base that collates bio-optical and radiometric data collected by the Australian research community for provision to the national and international research community for calibration and validation of ocean colour sensors. In other words, making our radiometric data available internationally.		
None	Yes in principle (Proposed to continue under the 2017/19 plan for IMOS Ocean Colour)	- Data available for ocean colour algorithm development, validation and BGC modelling as well as provision to space agencies.

8 References

- Antoine, D. and A. Morel (1999). A multiple scattering algorithm for atmospheric correction of remotely-sensed ocean colour (MERIS instrument) : principle and implementation for atmospheres carrying various aerosols including absorbing ones, International Journal of Remote Sensing, 20, 1875-1916.
- Baird M.E., N. Cherukuru, E. Jones, N. Margvelashvili, M. Mongin, K. Oubelkheir, P. J. Ralph, F. Rizwi, B. J. Robson, T. Schroeder, J. Skerratt, A. D.L. Steven, K. A. Wild-Allen, 2014. Remote-sensing reflectance and true colour produced by a coupled hydrodynamic, optical, sediment, biogeochemical model of the Great Barrier Reef, Australia: Comparison with satellite data, Environmental Modelling & Software 78:pp 79-96.
- Blondeau-Patissier, D., V. E. Brando, K. Oubelkheir, A. G. Dekker, L. A. Clementson, and P. Daniel (2009), Bio-optical variability of the absorption and scattering properties of the Queensland inshore and reef waters, Australia, J. Geophys. Res., 114, C05003, doi:10.1029/2008JC005039.
- Brando, V.E., Dekker, A.G., Park, Y.J. and Schroeder, T. (2012) An adaptive semi-analytical inversion of ocean colour radiometry in optically complex waters, Applied Optics Vol. 51, Issue 15: pp 2808-2833.
- Brando V., J. Lovell, E. King, D. Boddle, R. Scott and T. Schroeder, 2016. The Potential of Autonomous Ship-Borne Hyperspectral Radiometers for the Validation of Ocean Color Radiometry Data, Remote Sensing, 8, 150; doi:10.3390/rs8020150.
- Cherukuru, R. N., Brando, V.E., Schroeder, T., Clementson, L.A. and Dekker, A.G. (2014) Influence of river discharge and ocean currents on coastal optical properties, Continental Shelf Research, Volume 84, 1 August 2014, pp 188-203, <http://dx.doi.org/10.1016/j.csr.2014.04.022>.
- Everett, J. D. and M. Doblin, 2015. Characterising primary productivity measurements across a dynamic western boundary current region. Deep-Sea Research Part I-Oceanographic Research Papers 100 105-116 DOI: 10.1016/j.dsr.2015.02.010
- Gordon, H. R., and Clark, D. K., 1981, Clear water radiances for atmospheric correction of Coastal Zone Color Scanner imagery, Applied Optics 20, 4175-4180.
- Hooker, S.B., 2014. Mobilization Protocols for Hybrid Sensors for Environmental AOP Sampling (HySEAS) Observations, NASA/TP-2014-217518, NASA Goddard Space Flight Center, Greenbelt, MD 20771.
- Hooker, S.B. and A. Morel (2003). Platform and environmental effects on above- and in-water determinations of water-leaving radiances. Journal of Atmospheric and Oceanic Technology, 20, 187-205
- Hooker, S.B., and G. Zibordi, 2005. Platform perturbations in above-water radiometry. Applied Optics, 44(4), 553-567.
- Huang Z., and M. Feng (2015), Remotely sensed spatial and temporal variability of the Leeuwin Current using MODIS data, Remote Sensing of Environment 166, 214–232.
<http://dx.doi.org/10.1016/j.rse.2015.05.028>.
- Johnson, R., P. G. Strutton, S.W. Wright, A. McMinn, and K. M. Meiners (2013). Three improved satellite chlorophyll algorithms for the Southern Ocean, Journal Of Geophysical Research: Oceans, 118, 3694–3703, doi:10.1002/jgrc.20270.
- Malthus, T.J., Karpouzli, E., Thankappan, M., Dekker, A.G, Smith, C. (2014) An audit of satellite calibration and validation facilities and activities in Australia. Report prepared for the Department of Industry Space Coordination Office. CSIRO Future Science Platform in Earth Observation Informatics, Canberra Australia. ISBN 978-1-4863-0490-5.
- Mobley, C. (1999). Estimation of the remote-sensing reflectance from above-surface measurements. *Applied Optics*, 7442-7455.
- Mobley, C. D., F. Chai, P. Xiu, and L. K. Sundman (2015), Impact of improved light calculations on predicted phytoplankton growth and heating in an idealized upwelling downwelling channel geometry, J. Geophys. Res. Oceans, 120, 875-892, doi:10.1002/2014JC010588.
- Mueller, J.L., 1993: The First SeaWiFS Intercalibration Round-Robin Experiment, SIRREX, July 1992. NASA Tech. Memo. 104566, Vol. 14, S.B. Hooker and E.R. Firestone, Eds., NASA Goddard Space Flight Center, Greenbelt, Maryland, 60 pp.
- Mueller J.L., 2003. Ocean Optics Protocols For Satellite Ocean Color Sensor Validation, Revision 4, Volume II: Instrument Specifications, Characterization and Calibration. NASA/TM-2003-21621/Rev-Vol II.
- Mitchell, R. M. and S. K. Campbell (2004), The Australian Aerosol Ground Station Network: Status report and development of a Radiometric Calibration Facility, Optica Pura y Aplicada, 37, 3, 3259-3262.
- Qin, Y., Brando, V. E., Dekker, A. G. and Blondeau-Patissier, D. (2007), Validity of SeaDAS water constituents retrieval algorithms in Australian tropical coastal waters, Geophysical Research Letter, 34, L21603, doi:10.1029/2007GL030599

- Schroeder T., Brando V.E., Cherukuru N., Clementson L., Blondeau-Patier D., Dekker A.G., and Fischer J., "Remote Sensing of apparent and inherent optical properties of Tasmanian coastal waters: Application to MODIS data", In: Proceedings of the XIX Ocean Optics Conference, Barga, Italy, 2008.
- Schroeder, T., Devlin, M. J., Brando, V. E., Dekker, A.G., Brodie, J.E., Clementson, L. & McKinna, L. (2012) Inter-annual variability of wet season freshwater plume extent into the Great Barrier Reef lagoon based on satellite coastal ocean colour observations; Marine Pollution Bulletin MPB5182 [DOI information: 10.1016/j.marpolbul.2012.02.022].
- Steven, A.D.L., Brando, V.E., Clementson, L., Dekker, A.G., Hardman-Mountford, N., Hodge, J., Jones, E., King, E. and Schroeder, T. (2014) "Coastal Ocean Colour of Australian Waters: Progress & Outlook", Ch 18 (pp 123-130) in "Oceans and Society-Blue Planet": Eds. Djavidnia, S., Cheung, V. Ott, M. and Seeyave, S., Cambridge Scholars Publishing. www.oceansandsociety.org
- Wojtasiewicz, B., N. Hardman-Mountford, D. Antoine, F. Dufois, D. Slawinski and T. W. Trull, Use of bio-optical profiling float data in validation of ocean colour satellite products in a remote ocean region, in preparation for submission in July 2017.
- Zibordi, G., D. D'Alimonte, D. van der Linde, J-F.Berthon, S.B. Hooker, J.L. Mueller, G. Lazin, and S. McLean, 2002: The Eighth SeaWiFS Intercalibration Round-Robin Experiment (SIRREX-8), September–December 2001. NASA Tech. Memo. 2003--206892, Vol. 21, S.B. Hooker and E.R. Firestone, Eds., NASA Goddard Space Flight Center, Greenbelt, Maryland, 39 pp.
- Zibordi, G., and F. Mélin, 2017. An evaluation of marine regions relevant for ocean color system vicarious calibration, Remote Sensing of Environment 190 (2017) 122–136,
<http://dx.doi.org/10.1016/j.rse.2016.11.020>

9 Acronyms

AOP	Apparent Optical Property
BGC	Biogeochemistry
BOUSSOLE	BOUée pour l'acquiSition d'une Série Optique à Long termE.
BWG	Bio-optical Working Group
CDOM	Coloured Dissolved Organic Matter
CHL	Chlorophyll
CSIRO	Commonwealth Scientific & Industrial Research Organisation
DALEC	Dynamic Above water radiance and irradiance collector
EC	European Commission
ESA	European Space Agency
EUMETSAT	European Organisation for the Exploitation of Meteorological Satellites
GBR	Great Barrier Reef
IMO	Insitu Marine Optics, a Perth-based SME
IMOS	Integrated Marine Observing System
IOP	Inherent Optical Property
LJCO	Lucinda Jetty Coastal Observatory
MNF	Marine National Facility, i.e., the Australian "Investigator" research vessel
MOBY	Marine Optical Buoy
MODIS	Moderate Resolution Imaging Spectrometer
MSI	Multi Spectral Instrument
NAP	Non-algal particles
NASA	National Aeronautics and Space Administration of the USA
NIR	Near infrared
NIST	National Institute of Standards and Technology of the USA
NOAA	National Oceanic and Atmospheric Administration of the USA
NRS	National Reference Station (IMOS)
OCR	Ocean Colour Radiometry
OLCI	Ocean and Land Colour Imager
PACE	Plankton, Aerosol, Cloud, ocean Ecosystem mission
PP	Primary production
RS	Remote Sensing
RSSRG	Remote Sensing and Satellite Research Group (Curtin Uni.)
RTT	Radiometry Task Team
SARDI	South Australia Research and Development Institute
SeaWiFS	Sea-viewing Wide Field-of-view Sensor
SGLI	Second-Generation Global Imager
SRS	Satellite Remote Sensing Facility (IMOS)
SVC	System Vicarious Calibration
UTS	University of Technology, Sydney
UV	Ultraviolet
VIIRS	Visible Infrared Imaging Radiometer Suite

10 Appendix 1. Error sources in above-water radiometry

We identify below a number of error sources in the determination of R_{rs} from above-water radiometry measurements, as well as sources of differences between instruments. Those with a superscript * have been addressed during the work of the RTT.

Sources of Error from the Instrument and their deployment

Calibration methodology / accuracy*
Cosine Response (E_s)*
Temperature responsivity changes in Offset (DC) and Slope (Fe / Fl)*
Wavelength Calibration*
Linearity (Flux and integration time)*
Instrument tilt (E_s and L_t)
Skylight Reflection (L_t)
Stray Light
Self-Shading (L_t)

Sources of Difference between sensors (other than Error)

Field of View / Footprint*
Integration time*

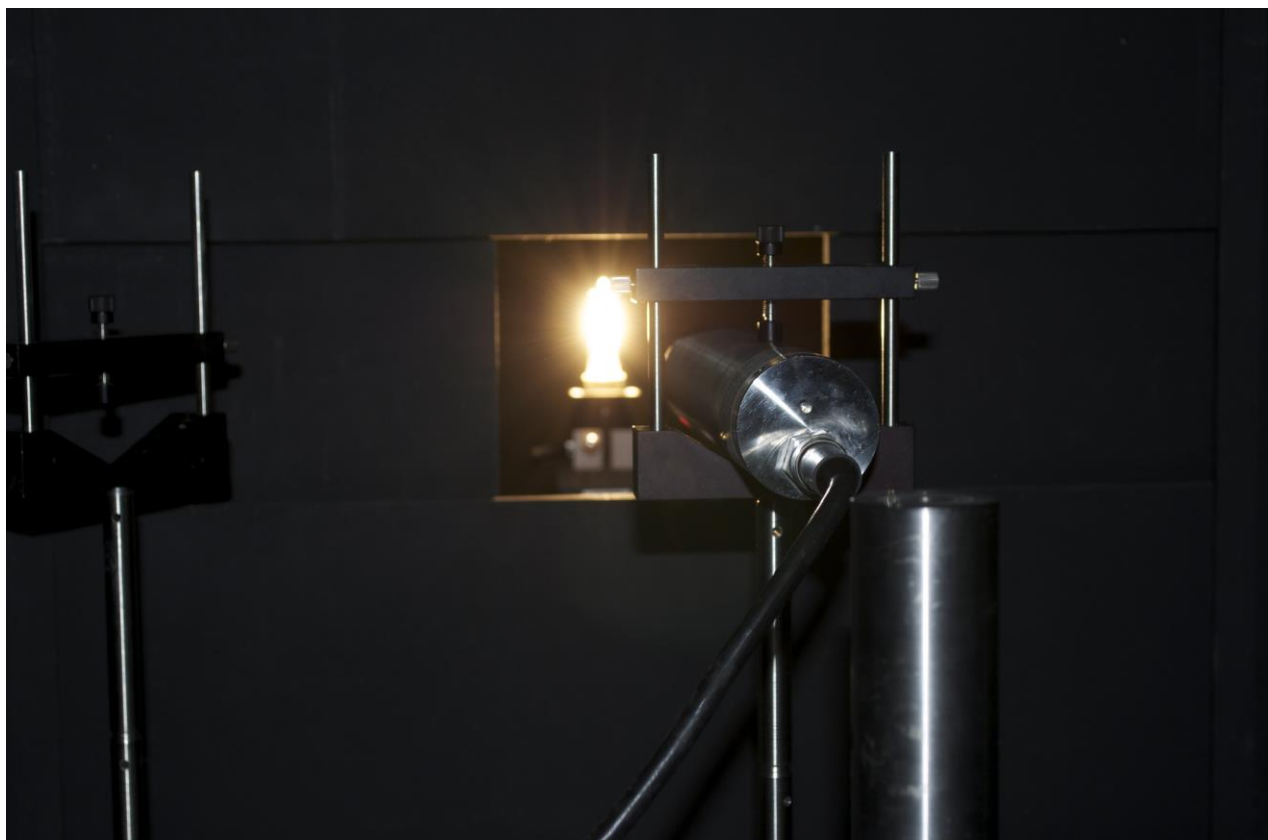
Errors possibly introduced at data processing

Software bugs / quirks *
Software filtering methodology*
Dark correction (related to temperature)*
Application of calibration coefficients (exact approach varies)*
Glint correction (fundamentally tied to FOV / footprint Integration time)
Skylight correction (fundamentally tied to FOV / footprint Integration time)

11 Appendix 2: report of the laboratory characterisation and calibration experiments

Report:

IMOS RTT Absolute Calibration



Prepared by:

 In-situ Marine Optics

Unit 7, 6 Tidal Way
Bibra Lake WA 6163
Australia
ABN: 56126 959 055

Date: 21 October 2016, revised 13/06/2017
IMO#: Curtin-Qu-004b
Client: Prepared for Curtin University Remote Sensing and Satellite Research Group,
under funding from the IMOS "Radiometry Task Team"

Executive Summary

This report outlines the methodology and presents results of absolute radiometric calibration of selected multispectral and hyperspectral radiometers that are commonly used in the Australian ocean colour remote sensing community. Measurements were performed at different temperatures and (where applicable) integration times to assess the applicability of a given lab-based radiometric calibration to those conditions likely to be encountered in the field.

For all spectrometers, sensor temperature was found to have an influence on the spectral calibration coefficient magnitudes - up to 0.56%/°C for blue wavelengths and -0.42%/°C for NIR wavelengths, suggesting that a spectral approach for temperature correction should be investigated for all such devices, and especially when they are to be used outside typical calibration facility “room” temperatures.

Integration time linearity was also investigated, and nonlinearities were observed. In general, the commercial spectrometers were stable within ±4% across different integration times likely to be used in the field. Trends were consistent, so there is a possibility that further compensating the instrument’s response to integration time will improve the accuracy of these devices.

Two different NIST-traceable working standard lamps were measured relative to a third “reference” lamp and differed by no more than 2.0% from their initial NIST calibrations.

Background

A number of different hyperspectral radiometers and one type of multispectral radiometer are used for ocean colour algorithm development, validation and general marine research in Australia. There are a number of manufacturers producing these instruments; optimised for operation above water, in-water or both.

A selection of these radiometers were chosen for the IMOS Absolute Calibration activity, including two DALECs (In-situ Marine Optics and Curtin), two HyperOCRs (Satlantic), six RAMSES (TriOS), a USSIMO (In-situ Marine Optics) and one multispectral sensor, the CIMEL (Cimel Electronique).

The hyperspectral radiometers all incorporate Carl Zeiss UV/VIS miniature monolithic spectrometer modules as the internal light recording device. However, the spectrometer read-out / interface electronics and optical design (diffusers, collimators, filters, etc.) differ between the various instruments. The spectrometer modules incorporate a fibre optic bundle, entrance slit and mirror for light dispersion and a linear Si photodiode array which can record light between approximately 300 nm – 1100 nm into 256 pixels. The Analog to Digital Converter (ADC) electronics and microcontrollers control the amount of exposure to light (integration time) and record the data digitally (counts) to provide a measure of light in terms of a spectrum of counts. It is this raw spectrum that needs to be converted to physical units, in terms of either irradiance ($Wm^{-2}nm^{-1}$) or radiance ($Wm^{-2}sr^{-1}nm^{-1}$).

With silicon-based photodiodes, a thermally-induced background current is present and should be removed from light measurements. This is termed dark current, dark count or dark offset. Different manufactures have slightly different approaches in removing these artefacts. Both the DALEC and USSIMO sensors incorporate UV filters to block out light reaching the first few pixels of the spectrometer array. This provides a measure of the dark current offsets simultaneously to the spectral measurement whilst also reducing the effects of internal stray light. Similarly, the RAMSES sensors block out light in the NIR portion of the silicon array to provide a measure of the dark offsets. The HyperOCR sensors incorporate mechanical shutters that periodically close to provide a spectral measurement of the dark current.

The standard approach in converting the hyperspectral digital counts to a physical radiometric quantity (radiance/irradiance) is to multiply the sensor calibration coefficients to a dark-corrected spectrum of digital counts. The calibration coefficients are typically determined by measuring the sensor response of a high-powered lamp with a known irradiance. This is typically performed for a fixed integration time and temperature in the laboratory by the sensor manufacturer.

Procedure

The calibration approach adopted in this study incorporates the methods outlined in the Ocean Optics Protocols for SeaWiFS Validation, Revision 1 (Mueller and Austin 1995) which recommends the use of a 1000 $WFEL$ standard of spectral irradiance with calibration traceable to NIST and lamp operation with a 0.01% current stable power supply.

Irradiance Calibration Coefficients

The general procedure for computing the calibration coefficients $F_E(\lambda)$ for irradiance sensors requires a calibrated lamp, at a known distance r , to illuminate the front face of the detector, accurately aligned normal to the lamp. Most hyperspectral irradiance sensor responses, $V_r(\lambda)$, are recorded in digital counts. Thus the irradiance calibration factors (in air) are determined as,

$$F_E(\lambda) = \frac{E_{50}(\lambda)}{V_r(\lambda) - V_{amb}(\lambda)} \left[\frac{50}{r} \right]^2, \quad (1)$$

where $E_{50}(\lambda)$ is the known lamp irradiance values for a distance of 50 cm, r is given in cm and $V_{amb}(\lambda)$ are the recorded digital counts of the ambient light when an occulting device is placed in between lamp and detector thus measuring the proportion of scattered light that needs to be subtracted. For most hyperspectral radiometers, the calibration coefficients are determined for a fixed integration time. The calibration coefficients can then be applied to subsequent radiometric measurements to yield spectral irradiance $E(\lambda)$ as,

$$E(\lambda) = F_E(\lambda) V(\lambda) \frac{I_0}{I}, \quad (2)$$

where $V(\lambda)$ is a dark corrected measurement, I is the integration time in milliseconds (ms) during the measurement and I_0 is the integration time during calibration.

Radiance Calibration Coefficients

The general procedure for computing the calibration coefficients $F_L(\lambda)$ for radiance sensors requires a calibrated lamp, at a known distance r , to illuminate a calibrated reflectance plaque, normal to lamp, and the detector viewing the plaque at an angle of $\theta = 45^\circ$, measured from the plaque normal.

The radiance reflected by the plaque and viewed by the sensor in this geometry is determined as,

$$L_p(\lambda) = \frac{1}{\pi} \rho(\lambda, 0^\circ, 45^\circ) E_{50}(\lambda) \left[\frac{50}{r} \right]^2, \quad (3)$$

Where $\rho(\lambda, 0^\circ, 45^\circ)$ are the calibrated reflectance values for 0° illumination and 45° viewing geometry. Using the measured sensor responses, the radiance calibration coefficients (in air) may then be determined as,

$$F_L(\lambda) = \frac{L_p(\lambda)}{V_r(\lambda) - V_{amb}(\lambda)}, \quad (4)$$

The calibration coefficients can then be applied to subsequent radiometric measurements to yield spectral radiance $L(\lambda)$ as,

$$L(\lambda) = F_L(\lambda) V(\lambda) \frac{I_0}{I}, \quad (5)$$

Facility

The IMOS Absolute Calibration measurements were conducted at In-situ Marine Optics' dedicated optics calibration room. The optics calibration room is a 4.5 x 3.5m dark room, painted with black diffuse paint. The room is partitioned at one end in order to separate the irradiance lamp from the detector. An adjustable aperture within the partition wall allows light to enter into the detector-side partition. The optics room houses two 600mm x 900mm (M6) optical benches and various baffles, optical mounts, lamp jigs and sensor holders that can be fixed securely to each bench.

Equipment list

Power Supply	OL83A (Optronics). SN:13221347
Lamp Standards	OL FEL-C (Optronics). SN's: F1227, F793 and F722
Lamp Holder	OL61 (Optronics).
Alignment Jig	OL62 (Optronics).
Reflectance Plaque	SRT-99 12 Inch (Labsphere). SN: 99AA02-031306083
Shunt Resistor	3020-01107-0 (Murata). 0.01 Ω, 0-10 VDC
Digital Multimeter	Fluke-179. SN: 15550370
Optical Mounts	M6 Post mounts and V-Clamps (Thorlabs)
Optical benches	2 x 900 mm x 600 mm. M6 Threaded
Alignment Laser	10 mW 532 nm

Irradiance Calibration Setup

The procedure for aligning the irradiance sensors to be calibrated with respect to the lamp standard were as follows:

- 1) An alignment laser was mounted on the optical bench in room A, approximately 90 cm behind the lamp mount holder.
- 2) The lamp mount holder with alignment jig was mounted approximately 25 cm away from the room partition aperture.
- 3) The irradiance sensor was mounted using v-block holders approximately 50 cm in front of the lamp on the optical bench in room B.

- 4) The alignment laser was powered on, and optical alignment was achieved by adjusting the height and rotation of the alignment jig until the laser beam hit the centre of the alignment jig cross hairs and the laser beam reflected back on itself.
- 5) The alignment of the detector with respect to the lamp was achieved by iteratively rotating, tilting, raising, and lowering the optical bench and v-block mounts until the laser beam targeted the centre of the detector's cosine diffuser and the laser beam reflected back on its own path after placing an optical window flat against the cosine diffuser.
- 6) The distance between the front face of the lamp alignment jig and the front face of the cosine diffuser was measured with a 600 mm metal rule with 1 mm markings and recorded in the calibration log sheets.
- 7) Once aligned, the alignment jig was removed and the lamp standard was placed in the lamp mount ensuring the mounting screws were properly tightened.
- 8) The alignment laser was removed.
- 9) The lamp was turned on and slowly ramped up to full current with the power supply.
- 10) The aperture was adjusted so there were no shadows or diffraction edges on the detector faceplate and any stray light was minimised.
- 11) The lamp was warmed up for at least 20 minutes before any data were recorded.

Radiance Calibration Setup

The procedure for aligning the radiance sensors to be calibrated with respect to a reflectance plaque and lamp standard were as follows:

- 1) The alignment laser, lamp mount holder and alignment jig in room A was set up as for the irradiance calibration setup.
- 2) The reflectance plaque was mounted on the optical bench in room B at a distance greater than 700 mm from the lamp. Depending on what sensor was being calibrated, this distance ranged from 720 mm to 977 mm.
- 3) The plaque alignment was adjusted until the alignment laser struck the centre of the reflectance plaque area and the laser beam reflected back on itself after placement of an optical window pressed flat against the plaque surface.
- 4) The distance between the front face of the lamp alignment jig and the front face of the reflectance plaque was measured with a metal tape measure with 1 mm markings and recorded in the calibration log sheets.
- 5) The radiance sensor was mounted using v-block holders at an angle of 45° off normal to the plaque.
- 6) The sensor was turned on and a live view of the data output was showed in a monitor. The height and rotation of the sensor was adjusted until the maximum signal from the sensor was achieved, indicating that the sensor optics was aligned to the centre of the laser beam being reflected off the plaque.
- 7) Once aligned, the alignment jig was removed and the lamp standard was placed in the lamp mount ensuring the mounting screws were properly tightened.
- 8) The alignment laser was removed.
- 9) The lamp was turned on allowed to ramp up the current with the power supply.
- 10) The aperture was adjusted so there were no shadows or diffraction edges on the reflectance plaque and any stray light was minimised.
- 11) The lamp was warmed up for at least 20 minutes before any data were recorded

Data Collection

Three types of experiments were conducted to investigate the uncertainty with radiometric calibrations. They were to:

- 1) Determine the absolute calibration coefficient using the manufacturer's method for a fixed integration time at room temperature.
- 2) Determine the absolute calibration coefficients over a range of different integration times.
- 3) Determine the absolute calibration coefficients over a range of sensor temperatures.

The calibration experiments were conducted at the In-situ Marine Optics' optics calibration lab between 27th July 2016 and 6th October 2016. Each sensor calibration was performed individually. For each sensor

alignment set up, the sensor was turned on and its supporting software was used to establish communication and data logging.

Experiment 1 (Room Temperature, Fixed Integration time).

Calibration measurements were performed at room temperature ($\sim 24^{\circ}\text{C}$) for a fixed integration time. After a warm up time of 5 minutes, at least 20 or more spectral measurements of the direct lamp or plaque target were collected. Following this, an intervening occulter (on-axis baffle) was placed in front of the lamp to measure the indirect light that reaches the detector. Again at least 20 or more occulted recordings were collected.

Experiment 2 (Range of Sensor Temperatures, Fixed Integration time).

The sequence of direct lamp (or plaque) and ambient light measurements were repeated over 2 extreme sensor temperatures, Cold and Hot. The “cold” measurements were performed first thing in the morning whereby the sensors were cooled overnight due to the cooler night time temperatures, typically $14\text{--}18^{\circ}\text{C}$. For the “hot” measurements, the sensors were placed in a low temperature oven at 40°C for at least 1 hour to reach equilibrium. The DALEC, HyperOCR and USSIMO instruments reported the internal sensor temperatures along with each spectral measurement. Unfortunately, the RAMSES sensors did not provide the internal temperatures so only the temperatures of the RAMSES outer metal housing was measured with a thermocouple at the start and end of the experiment. Note: “cold” calibrations were not performed for the RAMSES sensors since the outer metal housing rapidly increased in temperature during the lamp warm up time.

Experiment 3 (Room Temperature, Range of Integration times).

The sequence of direct lamp (or plaque) and ambient measurements were repeated over a range of each sensors allowable integration time settings until the point of near saturation in direct lamp (or plaque) readings.

Table 1: A summary of the calibration measurements performed and associated ancillary information required for data processing.

Date	Sensor	Type	Integration Time (ms)	Sensor Temp ($^{\circ}\text{C}$)	Lamp Distance (mm)	Lamp Hours
26/07/2016	CIMEL (SN: 658) (CSIRO)	L	n/a	18 38 14	720.0	63.7
27/07/2016	DALEC (SN:0001) (CSIRO)	Ed	500 1 – 1024 (incremental) 500	10 29 41	518.0	71.3
27/07/2016	DALEC (SN:0001) (CSIRO)	Lu	1000 1 – 2048 (incremental) 1000	20 30 40	518.0	72.5
27/07/2016	DALEC (SN:0001) (CSIRO)	Lsky	1000 1 – 2048 (incremental) 1000	17 26 41	518.0	74.0
9/08/2016	HyperOCR (SN:346) (CSIRO)	Ed	512 8 – 1024 (incremental) 512	16 26 37	511	77.2
9/08/2016	RAMSES (SN:5039) (CSIRO)	Ed	4 – 512 (incremental) 256	21 34	511	78.6
10/08/2016	RAMSES (SN:8035) (CSIRO)	Ed	4 – 512 (incremental) 256	21 34	511	79.5
10/08/2016	RAMSES (SN:506D) (UTS)	Ed	4 – 512 (incremental) 256	23 31	511	81.5
10/08/2016	RAMSES (SN:8375) (UTS)	Ed	4 – 512 (incremental) 256	21 34	511	82.0
11/08/2016	HyperOCR (SN:287) (CSIRO)	Lu	512 8 – 1024 (incremental)	21 25	932	84.0

			512	38		
11/08/2016	RAMSES (SN:8494) (CSIRO)	Lu	4 – 512 (incremental) 256	15 32	932	85.1
11/08/2016	RAMSES (SN:506F) (UTS)	Lu	4 – 512 (incremental) 256	15 32	932	87.2
5/10/2016	DALEC (Curtin)	Ed	2500 8 – 6500 (incremental) 2500	23 30 42	519	103.4
5/10/2016	DALEC (Curtin)	Lu	3000 8 – 6500 (incremental) 3000	26 30 45	977	104.8
5/10/2016	DALEC (Curtin)	Lsky	3000 8 – 6500 (incremental) 3000	20 30 46	977	106.6

Software

Six types of software were used to control instrumentation and data acquisition during this calibration experiments. DALECview (v4.0), MSDA_XE (8.8.19), SatView (2.9.2), SatCon (1.5.1), USSIMOView (2.2) and DALEC_on_Transect.

A quirk was found in the MSDA_XE software that was used to operate the RAMSES sensors. Intermittent data loss was experienced whereby pixel # 30 of the spectrometer array reported values near the dark current magnitude and also appeared to shift the spectrum for data after pixel # 30. Figure 1 shows an example of the corrupt and non-corrupt raw spectra, captured with the RAMSES Ed (SN:) sensor.

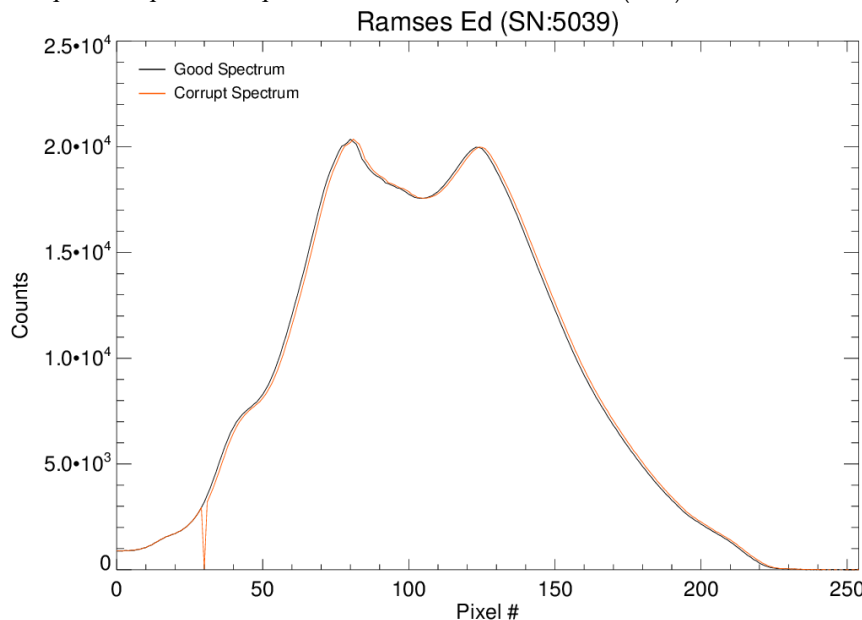


Figure 1. Example of corrupt and non-corrupt raw lamp spectrum captured with the MSDA_XE software.

These errors occurred for both the calibrated and raw data files as output by the control software. This quirk occurred on 3 separate computers and on 2 different controller units and all 6 spectrometers.

Power Supply Stability

At various stages of the calibration exercise, the power supply current was monitored by measuring the voltage drop across a calibrated precision shunt resistor ($0.01\Omega \pm 0.25\%$), connected in series with the Lamp standard. Using a 4 decimal place voltmeter, the voltage across the resistor was measured and consistently gave a reading of 80.0 mA. Using $V=IR$, the current was calculated to be stable at $8.00\text{ A} \pm 0.25\%$.

Lamp comparisons

Three FEL lamps were inter-compared to provide confidence in the working lamp standard (F1227) used throughout the calibration experiments. The lamp hours of the working Lamp standard at the beginning of

the IMOS RTT calibrations was 59 hours. Over the course of the calibration experiment a total of 48 lamp hours were accumulated during the comprehensive calibration tests. The lamp hours of the two Curtin lamps were 66 and 110 hours for F722 and F793, respectively. Using the HyperOCR (SN:346) irradiance sensor as the transfer radiometer, each lamp was measured. The experimental setup followed the standard alignment approach as in section **Irradiance Calibration Setup**. The room air conditioning was set to 24°C. A lamp and sensor warm up of 20 minutes was used for each lamp measurement. Using newly derived calibration coefficients for the transfer radiometer from the F1227 lamp measurements, the reproduction of each lamp was calculated. Figure 2 shows the irradiance of each lamp as measured by the transfer radiometer. The comparison between manufacturer supplied NIST irradiance values and calculated transfer radiometer shows a very close agreement within a relative errors between ±1.32% at 400 nm and ±0.3% at 800 nm (see Table 2).

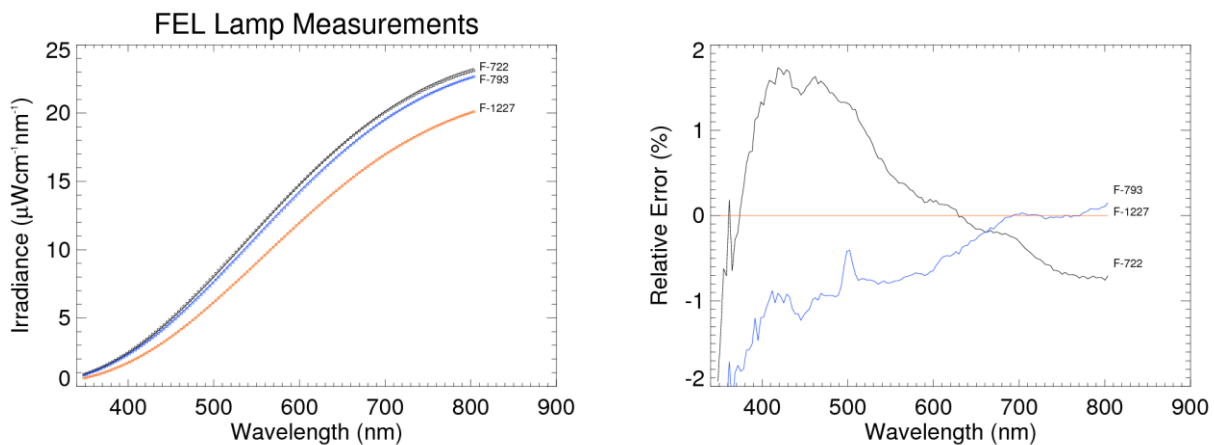


Figure 2. Comparison of 3 lamp standards. Solid lines are the manufacturer supplied irradiance scale and the symbols are the transfer radiometer derived irradiance scale (left). The spectral error of transferred lamp irradiance relative to the F1227 lamp irradiance. (right).

Table 2. Summary of Lamp relative errors at 400nm and 700nm along with the uncertainty in NIST irradiance scale and distance.

Lamp SN	Orig. Cal Date	Lamp Hours	Error @ 400nm (%)	Error @ 700nm (%)	NIST Lamp + Dist Uncertainty @ 400nm (%)	NIST Lamp + Dist Uncertainty @ 700nm (%)
F-722	02/2003	66	1.32	-0.30	1.49	1.26
F-793	01/2005	110	-1.20	0.01	1.49	1.26
F-1227	04/2013	102	n/a	n/a	n/a	n/a

Spectralon Plaque Characterisation

The manufacturer supplied reflectance values for the Labsphere plaque are given for an 8° illumination and hemispherical viewing geometry. Since the geometry for radiance sensor calibration was taken at 0° illumination and 45° view, the plaque reflectance for this geometry is required. The plaque reflectance for 0° illumination and 45° viewing geometry was determined using the ratio between spectral measurements taken 8° view and 45° view. The lamp and Spectralon plaque was setup as for the **Radiance Calibration Setup** procedure with a lamp to plaque distance of 720 mm. A Zeiss spectrometer module, with an ARC-72 (Ocean Optics, Inc) collimator attachment was positioned to view the centre of the spectralon plaque at a distance of 45 cm in front of the plaque at 8° from normal. At this distance the narrow field of view of the collimator resulted in a viewing footprint of approximately 25 mm in diameter at the centre of the plaque. After a lamp warm up time of 20 minutes, 100 spectral readings of direct plaque and occulted plaque were collected with the Zeiss MMS1 spectrometer module. The collimator was repositioned to view the centre of the plaque at 45° from normal. Again, 100 spectral readings of direct plaque and occulted plaque were collected. Using the ratio

between occult corrected 8 and 45° measurements, the reflectance at 45° was transferred from the supplied Spectralon calibration values.

Figure 3 shows the manufacturer supplied and measured reflectance values for the Spectralon plaque. As a reference, the Labsphere spectral reflectance at (0°, 45°) is shown (blue line), calculated using published tabulated data taken from the Labsphere Technical Guide document.

(<https://www.labsphere.com/site/assets/files/2553/a-guide-to-reflectance-materials-and-coatings.pdf>). The plaque was characterised post the CIMEL and DALEC (SN:0001) calibrations on the 01/08/2016 (orange line in Fig 3). At this time, it was noticed that the Spectralon surface was lightly soiled. Subsequently, the plaque was cleaned thoroughly using isopropyl alcohol and delicate tissue wipes and the (0°, 45°) measurements were repeated (lime line in Fig 3). The measured reflectance's of the cleaned Spectralon showed lower reflectance values. This could be due to changes in the surface properties post cleaning. The reflectance values from the uncleaned measurements were used in the calculation of the CIMEL and DALEC (SN:0001) radiance calibration coefficients. For all other radiance sensors, the reflectance values of the cleaned measurements were used since those measurements were conducted after cleaning of the plaque.

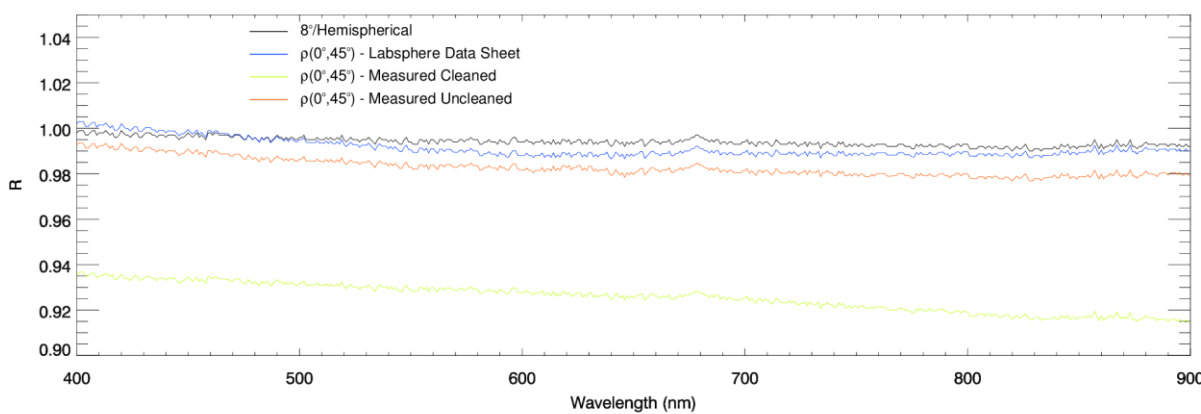


Figure 3. Supplied spectralon reflectance values for 8°/Hemispherical geometry and the measured reflectance's at (0°, 45°) geometry.

Results and Discussion

The calibration coefficients for the irradiance and radiance sensors were calculated using Eq 1 and Eq 3, respectively. The average direct lamp response, $V_r(\lambda)$, and associated occluded response, $V_{amb}(\lambda)$, were calculated for the various sensor temperatures tested using the fixed integration time, as was used during factory calibration (See Table 1).

For the DALEC and RAMSES sensors, $V_r(\lambda)$ and $V_{amb}(\lambda)$ were corrected for dark current offsets whereby the digital counts of the dark pixels within each spectral record was subtracted. For the DALEC sensors, the mean counts of pixels 1 to 3 of each raw spectrum was used. For the RAMSES sensors, the mean counts of pixels 238 to 254 for each raw spectrum was used. Additionally, the RAMSES data were quality controlled by removing the corrupt spectra as recorded by the MSDA_XE software. For the HyperOCR sensors, there was a consistent difference between the dark readings (closed shutter) during direct lamp and occulted readings in the order of 400 counts. This suggests that there may be some light leakage or improper closing of the internal shutter that is used to provide dark reading. Therefore, $V_r(\lambda)$ and $V_{amb}(\lambda)$ were not dark corrected for the HyperOCR analysis. However, since the series of direct lamp and occult measurements were conducted in quick succession (1 to 2 minutes) of each other, any thermally induced dark offsets should be accounted for in the occulted measurement.

The left panels in figures 4 to 8 show the derived spectral calibration coefficients for the sensors calibrated during this study. The solid black lines represent the calibration coefficients derived at "room" temperature as per the standard approach used by the various instrument manufacturers. Although the laboratory air-conditioning was set at 24°C during the measurements, the actual temperatures of the sensors ranged between

21°C and 30°C due to internal heating of the instruments electronics. (See Table 1 for a list of sensor temperatures recorded for each calibrated sensor). The blue and orange lines show the derived calibration coefficients for “cold” and “hot” sensor temperatures. For reference, each instruments’ factory calibration coefficients are also provided, denoted as black dashed lines. Generally, the calibration coefficients for each sensor resemble a similar spectral shape when compared with each other. The calibration coefficients are relatively low in the visible wavelength range and steadily increase in magnitude toward the NIR wavelengths where the sensitivity of the spectrometer module itself diminishes.

The centre panels in figures 4 to 8 shows the percent difference of calibration coefficients relative to “room” temperature derived calibration coefficients (IMOS Cal). All irradiance and radiance sensors showed differences in calibration coefficients derived for both “cold” and “hot” sensor temperatures. Generally, positive differences are observed for “cold” calibrations and negative differences for “hot” sensor temperatures, especially for wavelengths approaching the NIR. This indicates that the sensor’s photosensitivity is lower at colder temperatures and higher at hotter temperatures.

For the DALEC Ed (SN:0001) and HyperOCR Ed (SN:346) sensors, the differences in both “cold” and “hot” calibration coefficients tend to be more pronounced at increasing wavelengths. The same is evident with “hot” calibrations for the RAMSES Ed sensors. Both sensors show relatively large differences in ‘cold’ and ‘hot’ calibrations, ranging from approximately $\pm 3\%$ for blue wavelengths up to $\pm 10\%$ toward NIR wavelengths. The RAMSES Ed sensors showed differences of approximately 2% in the blue region and -8% in the NIR region for “hot” calibrations. However, the temperature ranges during the RAMSES Ed measurements were markedly lower ($\Delta T \approx 13^\circ\text{C}$) than that for the DALEC Ed (SN:0001) and HyperOCR Ed (SN:346) measurements ($\Delta T \approx 30^\circ\text{C}$ and 20°C , respectively). The DALEC Ed (SN:Curtin) sensor shows a reverse trend, whereby, the differences of the “hot” calibration coefficients are positive for visible wavelengths, ranging from +10% at 400 nm to -4% at 900 nm. A similar situation occurs for the radiance sensors where positive differences occur at blue wavelengths and decrease toward negative differences approaching the NIR wavelengths. The differences for “cold” and “hot” derived calibration coefficients are generally within $\pm 5\%$ for the radiance sensors, except for the RAMSES Lu sensors with differences down to -10%.

The comparison between each instruments manufacturer’s calibration coefficients and the IMOS Cal derived calibration coefficients, in terms of percent difference, are shown in the centre panels (dashed line). The IMOS Cal shows good agreement for the HyperOCR Ed (SN:346) and RAMSES Ed (SN: 8035) sensors with relative differences within $\pm 2.5\%$ of the supplied factory calibrations. The comparison for the RAMSES Ed (SN: 5039) sensors shows relative differences between -5% and -8% within the 400 nm – 600 nm wavelength range. These differences could be explained by the influence of the dirty teflon diffuser that was noted during the calibration. Prior to calibration, the diffuser was cleaned with isopropyl alcohol and delicate wipes; however, some black streaks still remained within the diffusers uneven surface. The RAMSES Ed (SN:506D and SN:8375) both showed a poor comparison between IMOS and factory supplied calibration with relative differences between -20% and -10% for visible wavelengths. This suggests significant sensor responsivity degradation since the time of this IMOS calibration (Aug 2016) and the factory calibrations (Jul 2011). The comparison between the IMOS and factory calibration for the DALEC Ed (SN:0001) shows relative differences between -0.5% and -2.5% for visible wavelengths and -7% at 900 nm. This is the same trend as seen for the “hot” calibration. Since the DALEC instrument houses 3 spectrometer modules, a microcomputer, motor and ancillary sensors in the one unit, the internal temperature of the instrument generally runs “hot” in normal operation. Because of this, the standard factory calibration was performed at $\sim 40^\circ\text{C}$ which is close to the “hot” calibration performed in this study. The factory calibration coefficients for the DALEC Ed (SN:Curtin) sensor was not supplied at the time of writing this report therefore no comparisons were made. The comparison between the IMOS and factory calibration for the radiance sensors are generally within 5%, except for the RAMSES Lu (SN:506F) sensor which shows differences of -10% at 400 nm.

Table 3. Summary of the calculated slope (Δ) of calibration coefficients at 400 nm and 700 nm as a function temperature for each sensor.

Sensor	SN	Type	$\Delta(400\text{nm})$ (%°C ⁻¹)	$\Delta(700\text{nm})$ (%°C ⁻¹)	Tmin (°C)	Tmax (°C)	N
DALEC	0001	Ed	-0.1335	-0.306	10	41	3
HyperOCR	0346	Ed	-0.1342	-0.4184	16	37	3
RAMSES	5039	Ed	-0.0761	-0.2284	21	34	2
RAMSES	8035	Ed	-0.0671	-0.2724	21	34	2
RAMSES	506D	Ed	0.30956	-0.0895	23	31	2
RAMSES	8375	Ed	0.14942	-0.1112	21	34	2
DALEC	Curtin	Ed	0.56462	0.02605	23	44	3
DALEC	0001	Lu	-0.0029	-0.123	20	40	3
DALEC	0001	Lsky	0.04303	-0.1365	17	41	3
HyperOCR	0287	Lu	0.12297	-0.0923	22	38	3
RAMSES	8494	Lu	0.08971	-0.1587	15	32	2
RAMSES	506F	Lu	0.03585	-0.2387	15	32	2
DALEC	Curtin	Lu	0.31678	-0.0399	26	45	3
DALEC	Curtin	Lsky	0.2117	0.09882	20	46	3

The irradiance calibration coefficients, F_E , and radiance calibration coefficients, F_L , at 400 and 700 nm (normalised to 1 at 24 °C) as a function of sensor temperature, for each sensor, are shown in figures 4 to 8 (right panels). Generally, normalised $F_E(700)$ and $F_L(700)$ decreases with increasing sensor temperature, with the exception of the DALEC Ed and Lsky (SN:Curtin) channels which shows the reverse trend. The slope (Δ) of normalised F_E and F_L at 400 nm and 700 nm versus sensor temperature are displayed within each plot and summarised in Table 3. At 400 nm, the slopes range from -0.13%°C⁻¹ to +0.56%°C⁻¹. This is equivalent to calibration coefficient differences of -2.7% to +11.3% at 400 nm over a temperature range of 20°C. At 700 nm, the slopes range from -0.42%°C⁻¹ to 0.10%°C⁻¹, equivalent to differences in calibration coefficients of -8.4% to +2.0% over a temperature range of 20°C.

Figure 6 shows the derived radiance calibration coefficients of the multispectral CIMEL sensor for “cold”, “room” (IMOS Cal) and “hot” sensor temperatures along with a recent NASA (Feb 2016) calibration as reference. The calibration coefficients measured at the “cold” sensor temperature shows large percent differences relative to the standard room calibration derived coefficients by up to 25% relative difference for blue wavelengths (centre plot). The calibration coefficients for the “hot” sensor temperature show relative differences in the order of 1% to 3.5% for visible wavelengths and -5% at 1020 nm. The comparison of the recent NASA performed calibration with this calibration exercise shows excellent agreement with relative differences within ±1% for visible wavelengths and ±1.5% for NIR wavelengths. The 1020 nm channel shows a linear relationship between normalised F_L and sensor temperature with a calculated slope of -0.31%°C⁻¹ (right plot).

Irradiance Calibration Coefficients

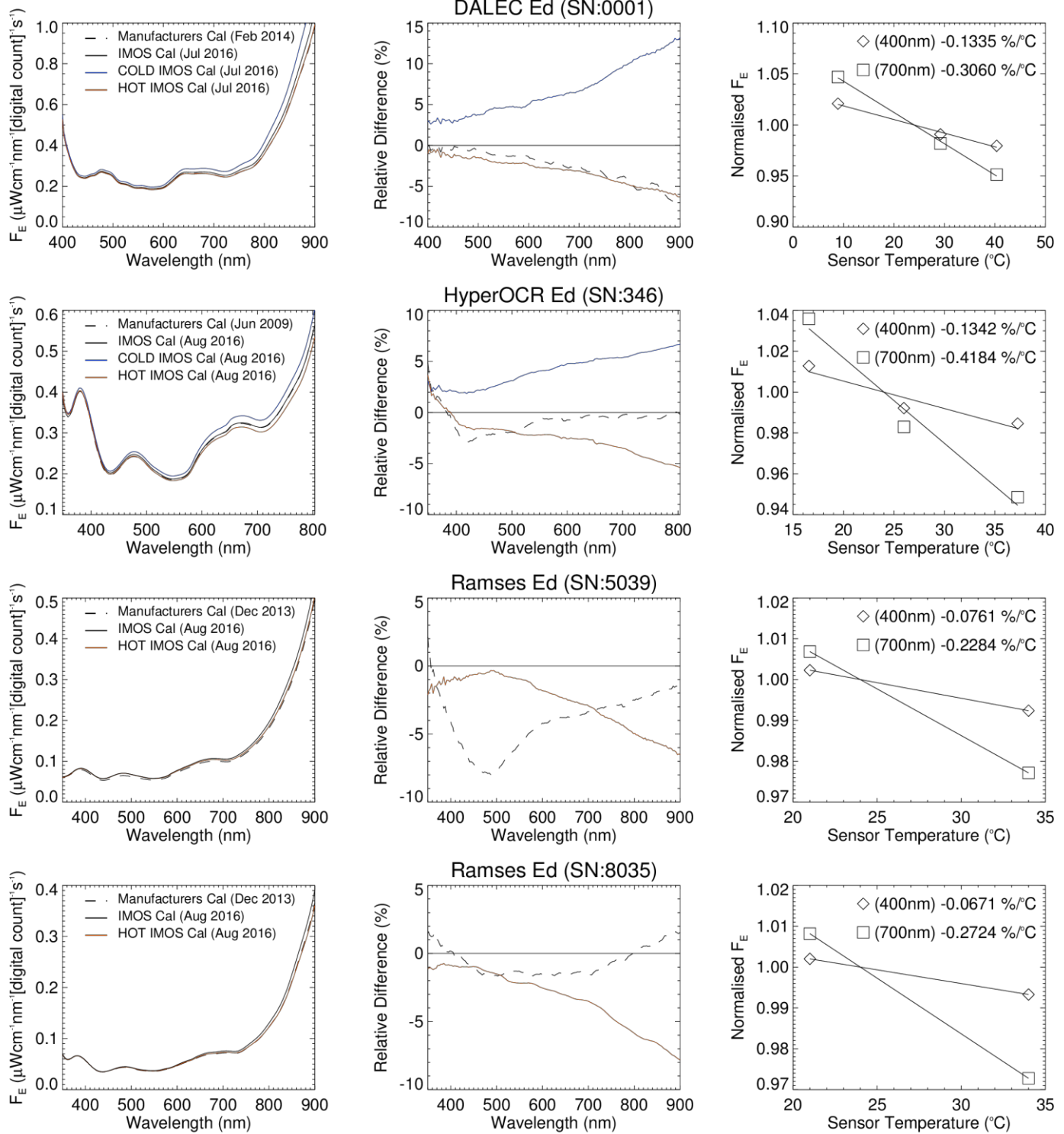


Figure 4: Irradiance calibration coefficients determined for cold, room (IMOS Cal), and hot sensor temperatures, along with the manufacturer's factory calibration coefficients (left panels). Percent difference of cold, hot and factory calibration coefficients relative to IMOS Cal calibration coefficients (centre panels) and irradiance calibration coefficients at 400 nm and 700 nm as a function of sensor temperature (right panels).

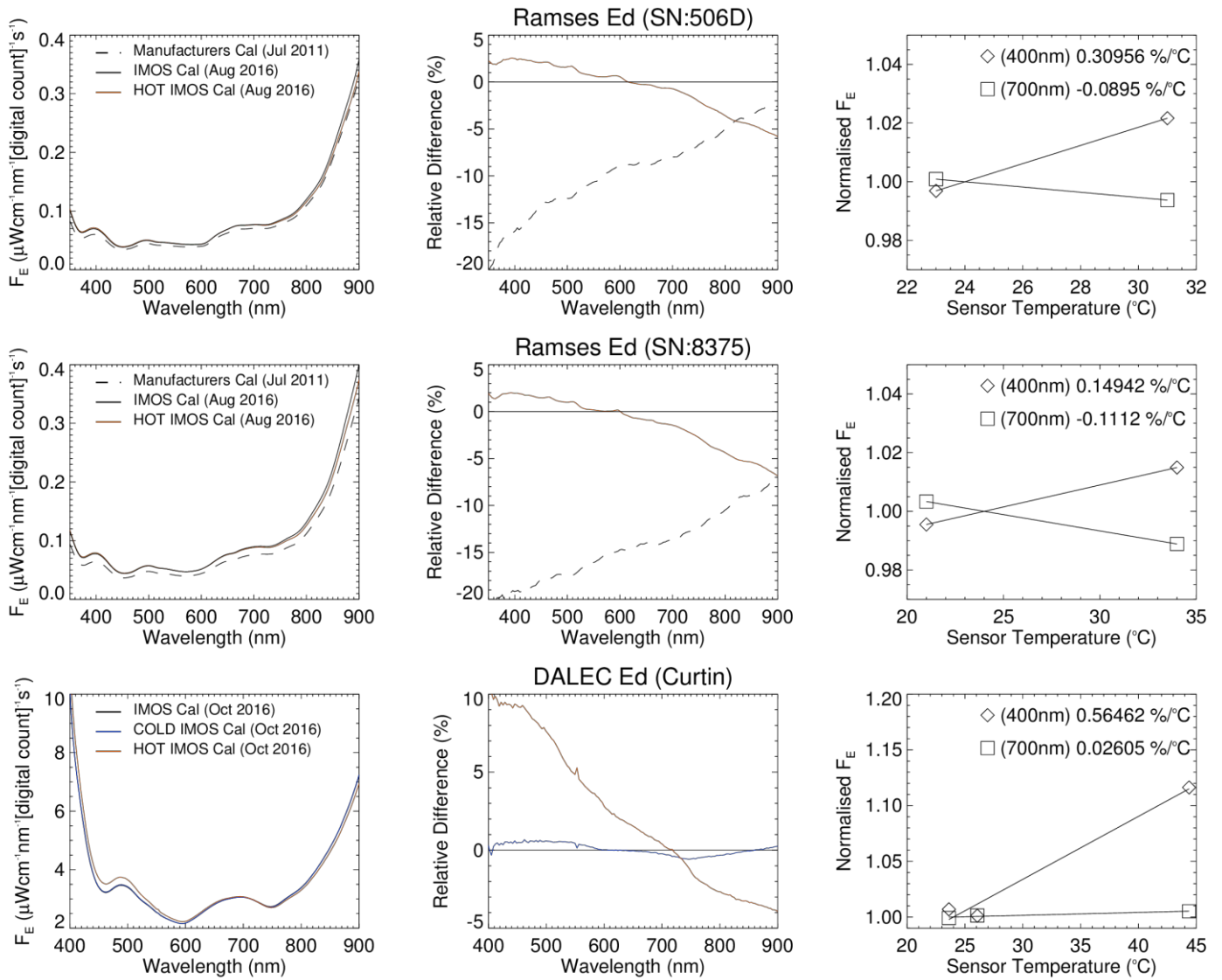


Figure 5. Irradiance calibration coefficients determined for cold, room (IMOS Cal), and hot sensor temperatures, along with the manufacturers factory calibration coefficients (left panels). Percent difference of cold, hot and factory calibration coefficients relative to IMOS Cal calibration coefficients (centre panels) and irradiance calibration coefficients at 400 nm and 700 nm as a function of sensor temperature (right panels).

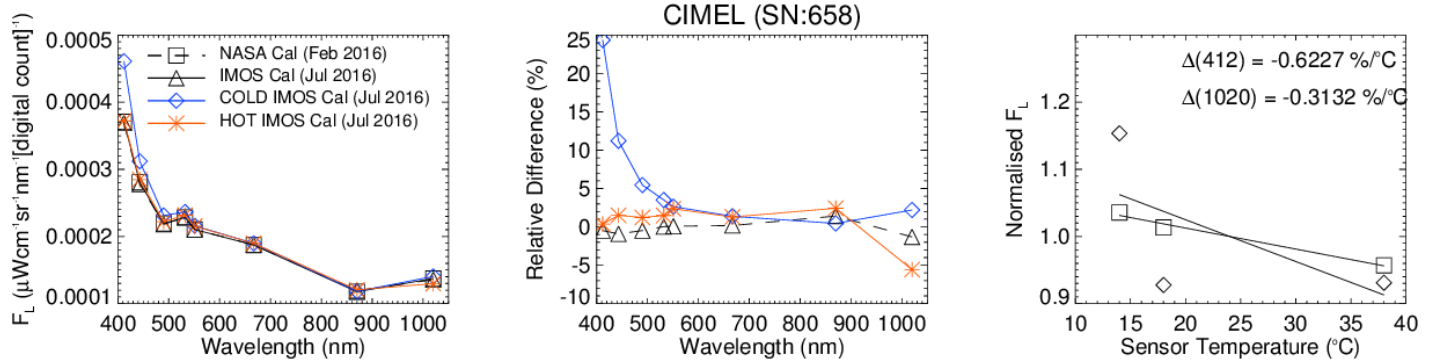


Figure 6. Radiance calibration coefficients determined for cold, room (IMOS Cal), and hot sensor temperatures, along with the manufacturers factory calibration coefficients (left panels). Percent difference of cold, hot and factory calibration coefficients relative to IMOS Cal calibration coefficients (centre panels) and radiance calibration coefficients at 412 nm and 1020 nm as a function of sensor temperature (right panel).

Radiance Calibration Coefficients

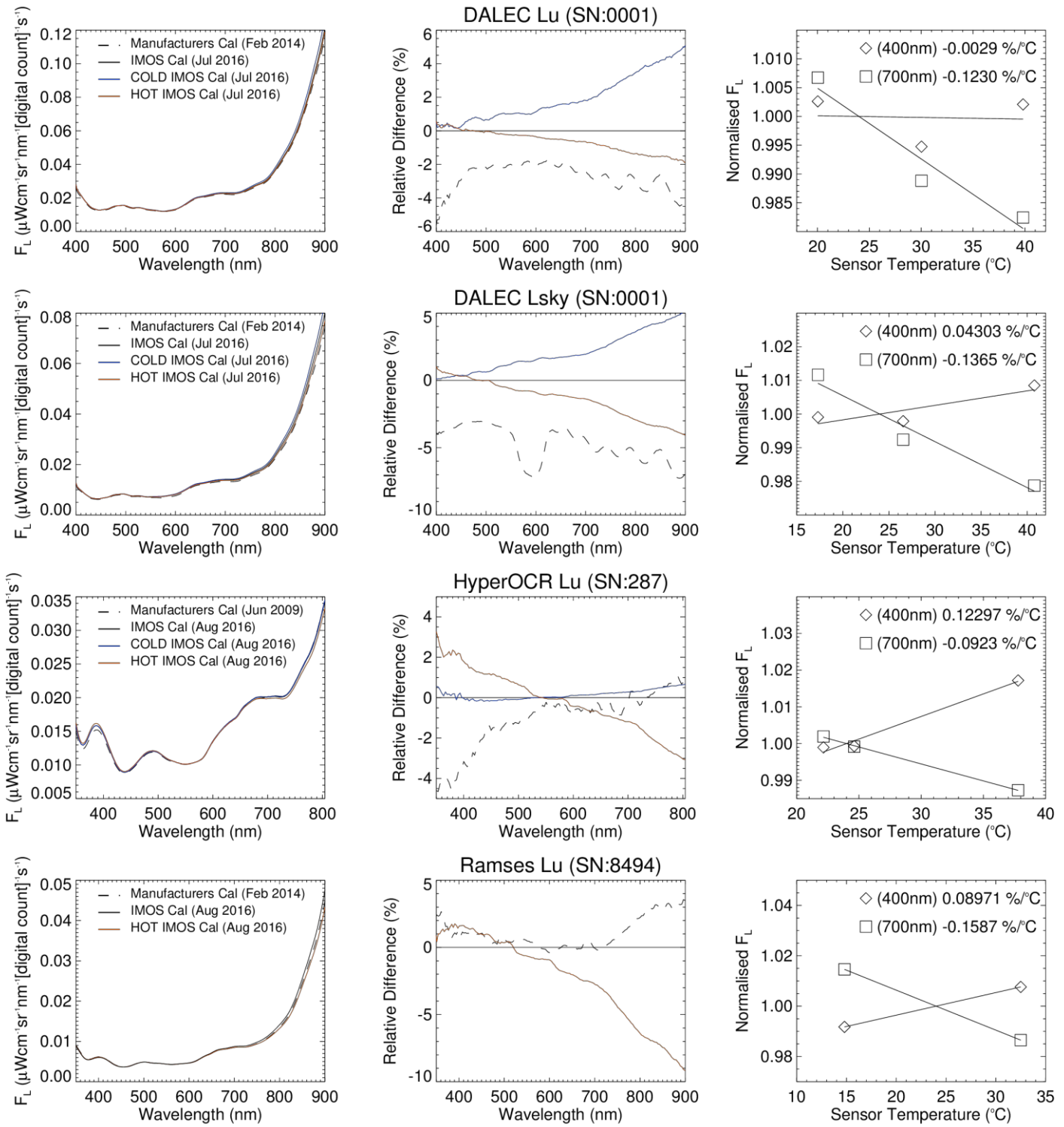


Figure 7. Radiance calibration coefficients determined for cold, room (IMOS Cal), and hot sensor temperatures, along with the manufacturers factory calibration coefficients (left panels). Percent difference of cold, hot and factory calibration coefficients relative to IMOS Cal calibration coefficients (centre panels) and radiance calibration coefficients at 400 nm and 700 nm as a function of sensor temperature (right panels).

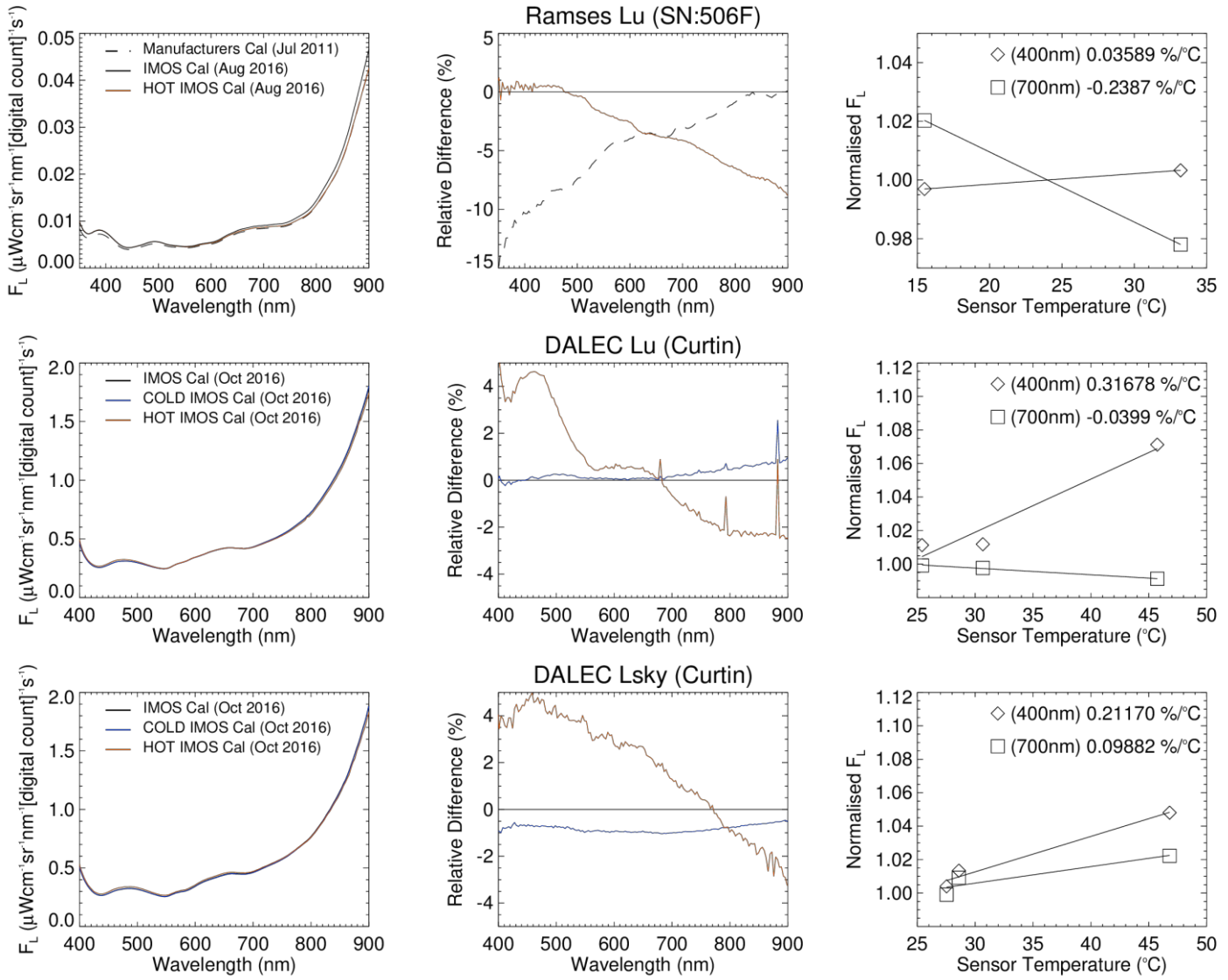


Figure 8. Radiance calibration coefficients determined for cold, room (IMOS Cal), and hot sensor temperatures, along with the manufacturers factory calibration coefficients (left panels). Percent difference of cold, hot and factory calibration coefficients relative to IMOS Cal calibration coefficients (centre panels) and radiance calibration coefficients at 400 nm and 700 nm as a function of sensor temperature (right panels).

Integration Time Linearity

The application of Eq 2 and Eq 5 in determining irradiance and radiance from field measurements assumes perfect linearity with respect to integration time. For example, the detector response of a constant light flux measured with a particular integration time should double when the integration time doubles. In other words, the count rate (counts per second) of a sensor should remain constant regardless of how many counts are recorded. The integration time linearity of the above sensors were assessed from direct lamp (or plaque) readings captured at a variety of integration times in order to collect counts across a large portion of the dynamic range of the detectors. The average and standard deviation of sensor responses were calculated for each integration time setting. Figure 5 (left plots) shows the dark current corrected average sensor responses collected for a range of integration times. The count rate (CR) was calculated as,

$$CR = \frac{V_r(\lambda) - V_{dark}(\lambda)}{t}, \quad (6)$$

where, t is the integration time in seconds.

Figures 9 to 13 (right plots) show example count rates at 600 nm for each of the sensors as a function of detector counts. The count rates at 600 nm were normalised to 1 at an arbitrary integration time to show the relative changes. The value of 600 nm was chosen in figures 9 to 13 because this is near the maximum spectral count range achievable without saturation. All sensors tested showed non-linearity with respect to integration time in the order of 2% to 4% for most sensors.

For improved accuracy in radiometric processing, the non-linearity of each sensor should be corrected for. The DALEC sensors show large departures from ideal at very low integration times in the order of 100%. However, the DALEC manufacturers radiometric processing software (DALECproc) incorporates integration time linearity correction as standard (See DALEC calibration file header for description) which adequately accounts for this.

The current radiometric processing techniques adopted for the HyperOCR and RAMSES sensors do not incorporate integration time linearity, so variability in the normalised count rate can essentially be interpreted as error due to integration time non-linearity for the HyperOCR and RAMSES sensors.

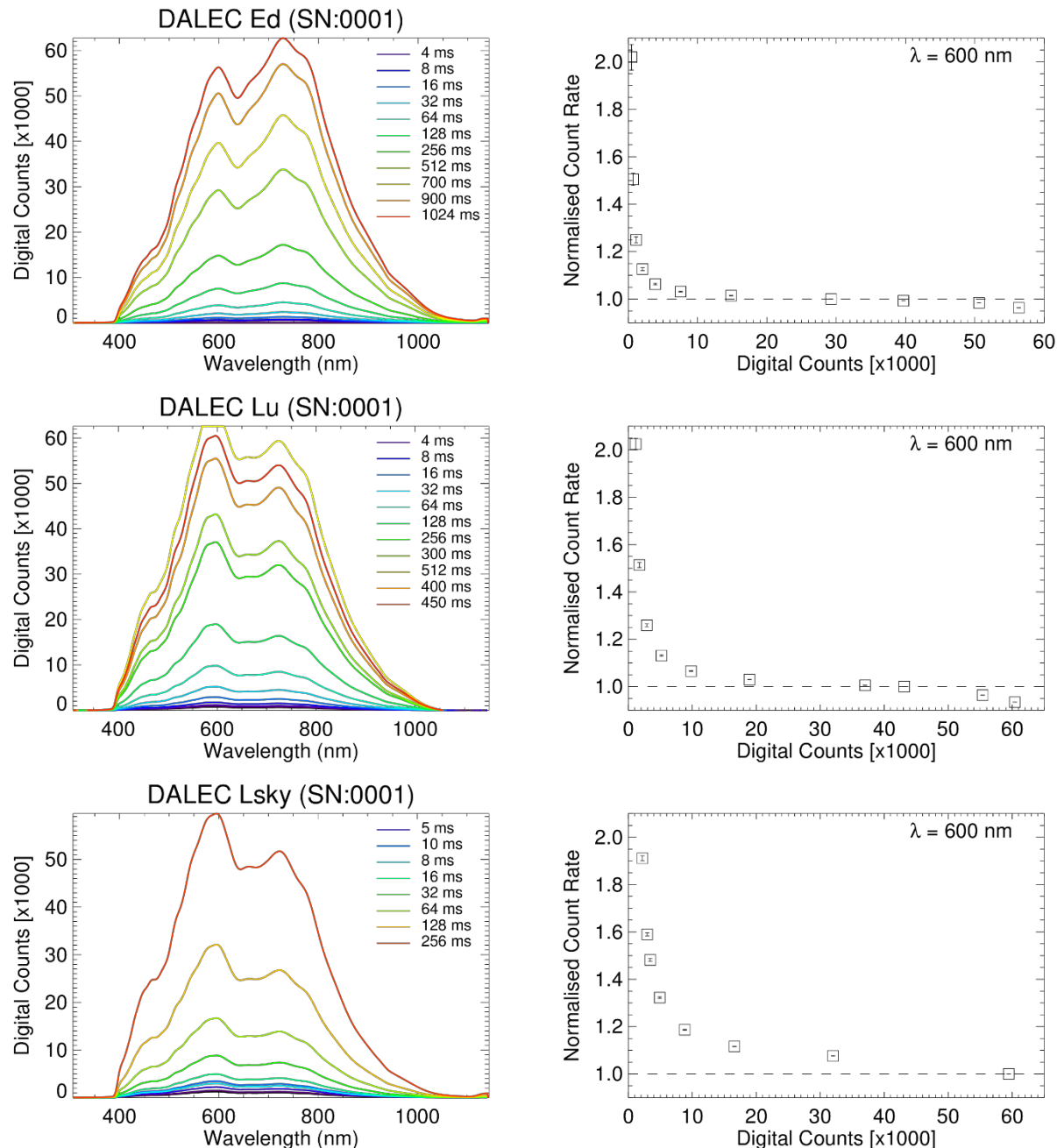


Figure 9. Dark corrected average lamp response measured at a variety of integration times (left). Normalised count rate at $\lambda = 600 \text{ nm}$ as a function of detector counts (right).

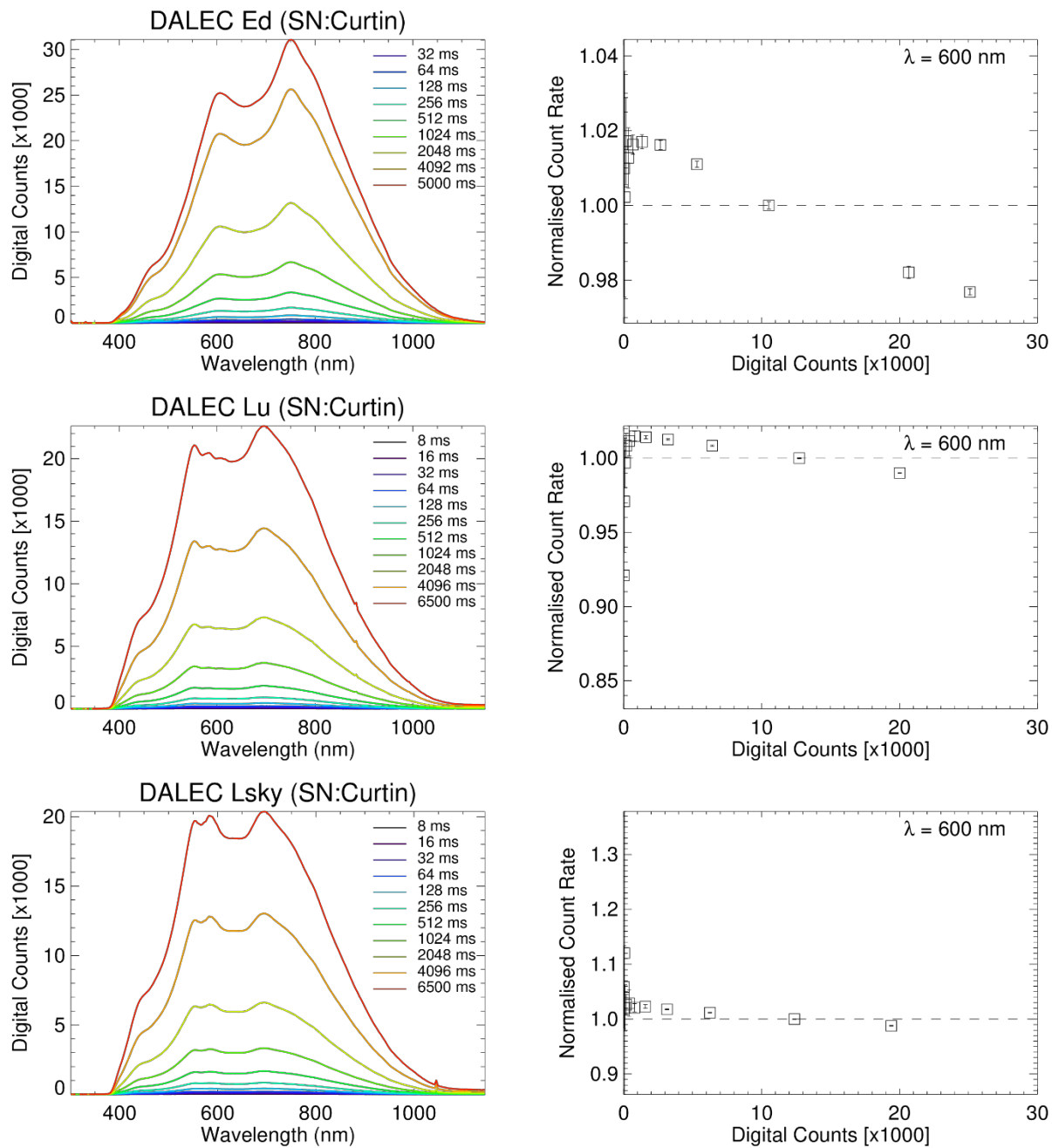


Figure 9. Dark corrected average lamp response measured at a variety of integration times (left). Normalised count rate at $\lambda = 600 \text{ nm}$ as a function of detector counts (right).

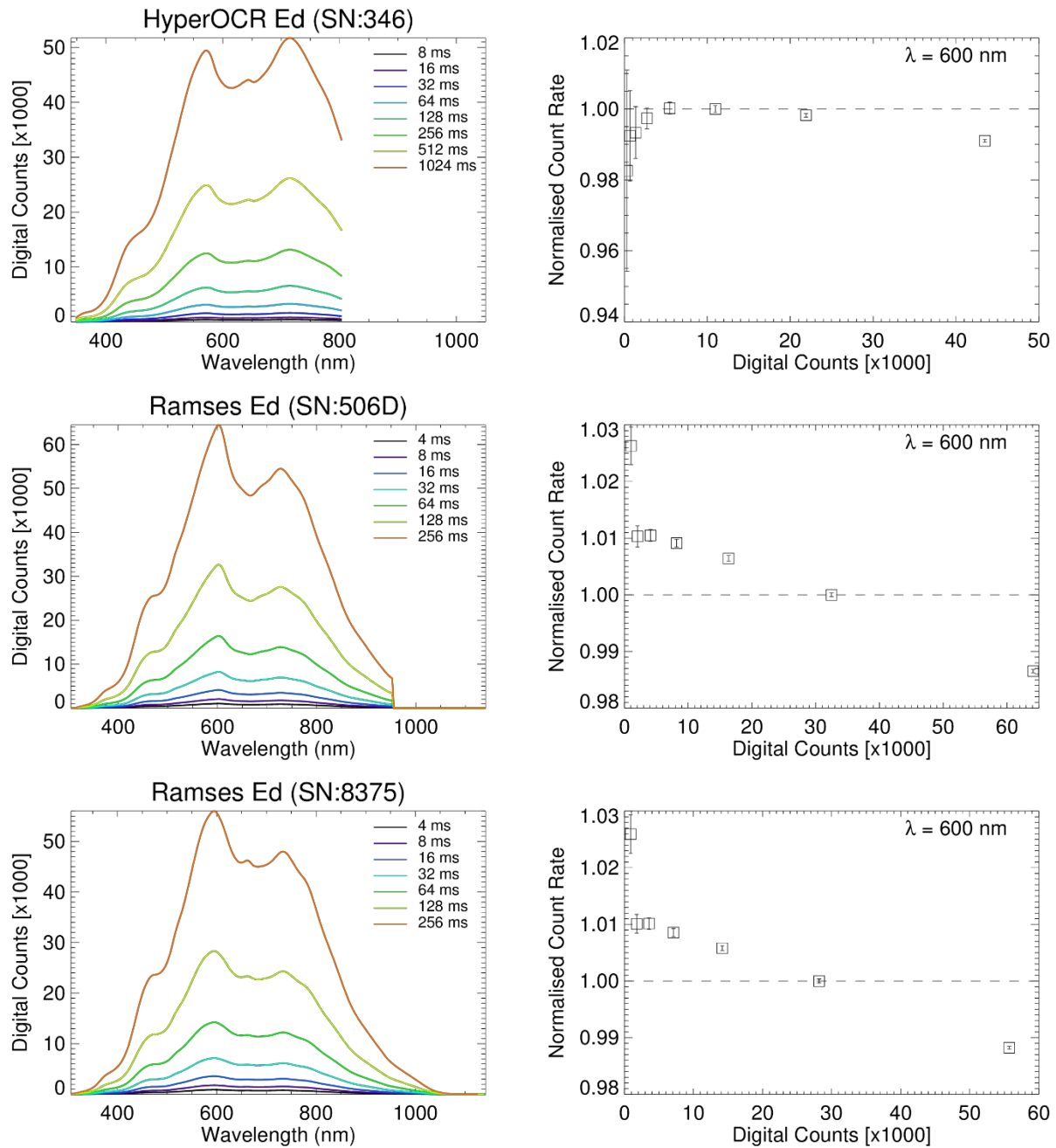


Figure 10. Dark corrected average lamp response measured at a variety of integration times (left). Normalised count rate at $\lambda = 600 \text{ nm}$ as a function of detector counts (right).

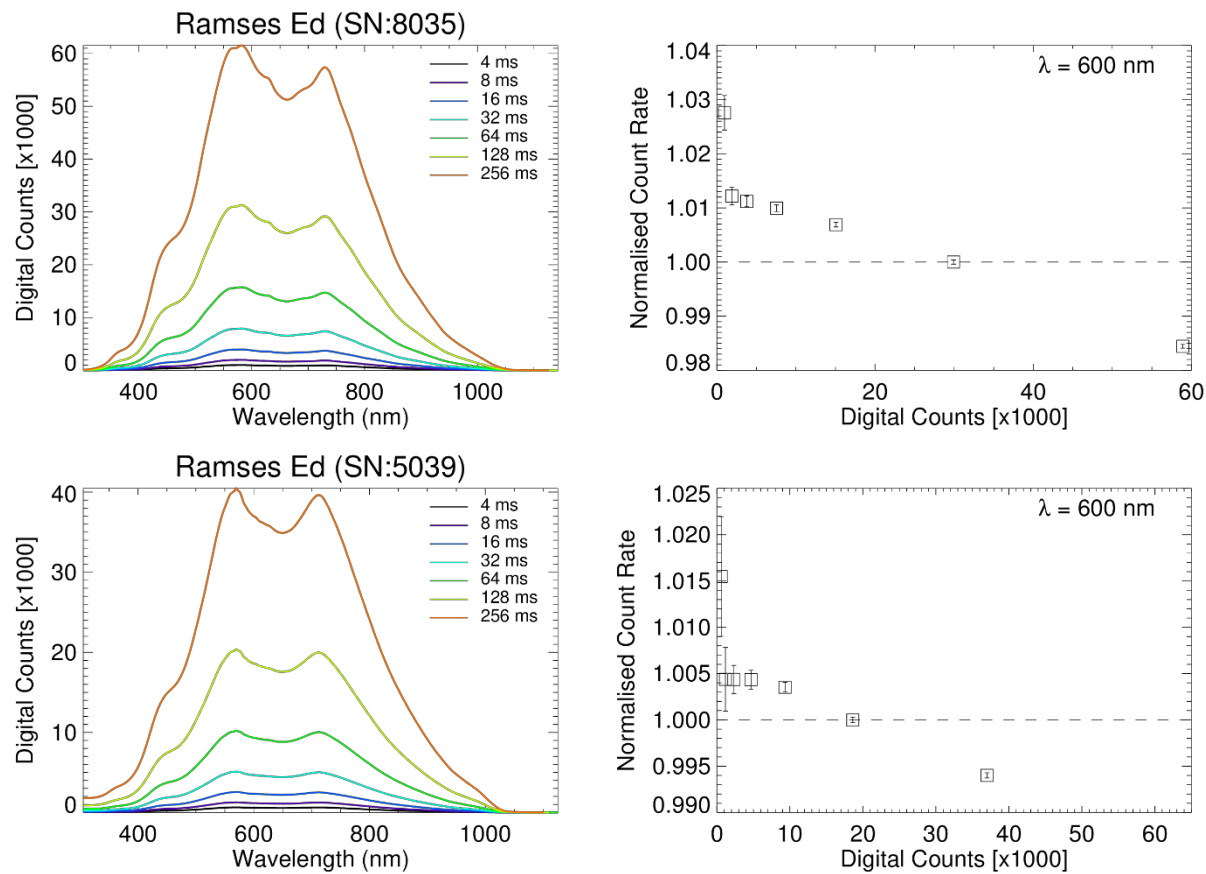


Figure 12. Dark corrected average lamp response measured at a variety of integration times (left). Normalised count rate at 600 nm as a function of detector counts (right).

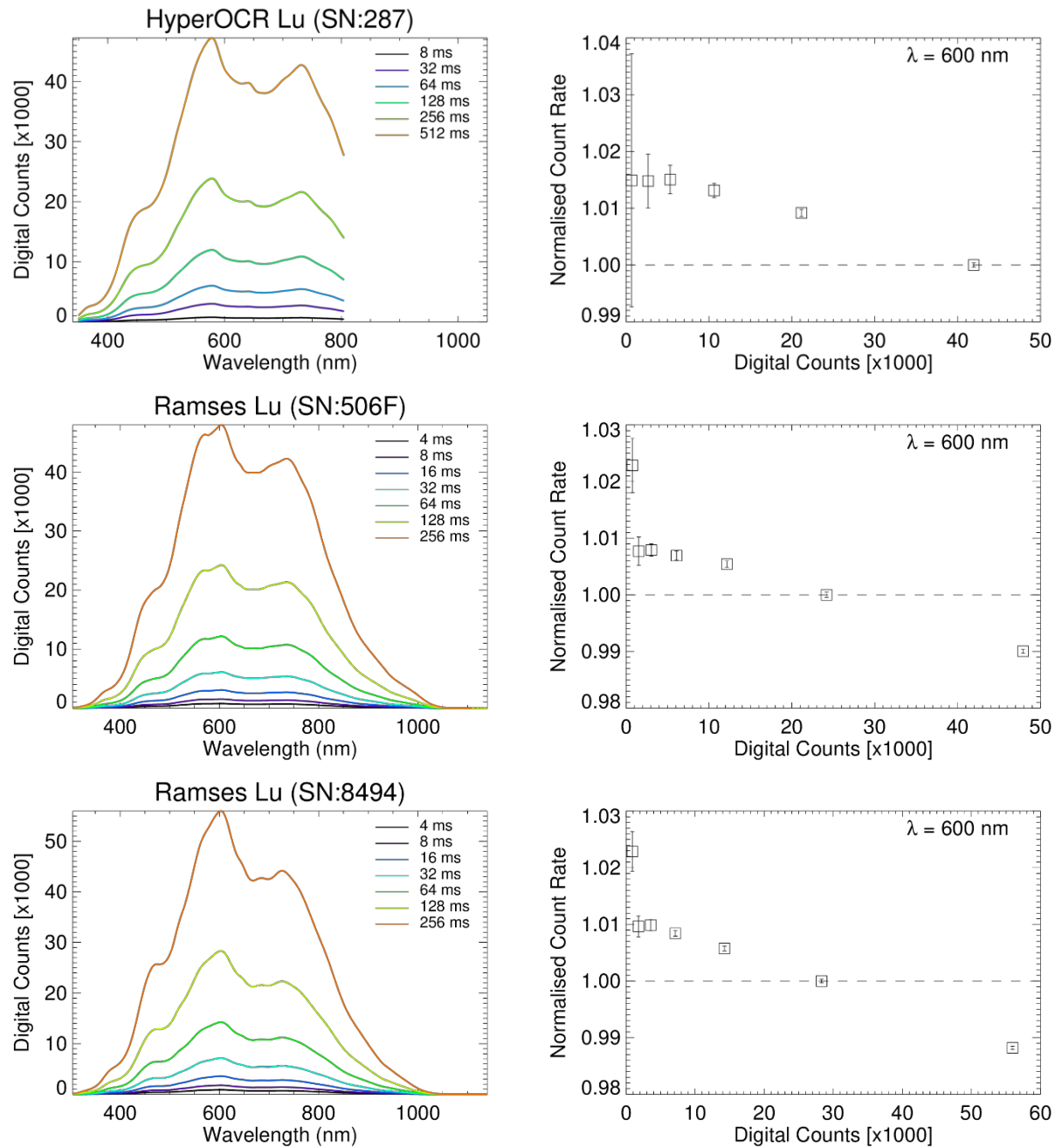


Figure 11: Dark corrected average lamp response measured at a variety of integration times (left). Normalised count rate at $\lambda = 600 \text{ nm}$ as a function of detector counts (right).

Conclusion

Absolute radiometric calibrations were performed on a number of hyperspectral irradiance and radiance sensors and one multispectral radiance sensor for the IMOS RTT project. Prior to the calibration measurements, In-situ Marine Optics' working lamp standard (F1227) was tested against Curtin's two lamp standards (F722 and F793) using a HyperOCR as the transfer radiometer. The calculated lamp irradiances agreed with each other to within $\pm 1.35\%$ at 400 nm and $\pm 0.09\%$ at 800 nm. The power supply current was monitored with a calibrated precision shunt resistor and reported a stable current supply of $8.00 \text{ A} \pm 0.25\%$ throughout the calibration measurements.

The absolute radiometric calibrations were performed at cold ($\sim 14\text{-}18^\circ\text{C}$), room ($21\text{-}26^\circ\text{C}$) and hot ($32\text{-}41^\circ\text{C}$) sensor temperatures. The most significant finding in this study was that sensor temperature was found to have a measurable influence on the spectral calibration coefficient magnitudes, typically around 2.5% for blue wavelengths up to 15% for NIR wavelengths, suggesting that an approach for temperature correction post-processing should be investigated to improve the radiometric accuracy of radiometers deployed in field conditions. The RAMSES sensors did not measure internal temperature.

The IMOS radiometric calibrations generally agreed well with each sensors factory calibrations, however, was difficult to assess properly due to the confounding effects of sensor temperature differences between factory calibrations and measurements made during this study. Large differences, in the order of 20% at blue wavelengths, between factory supplied and IMOS calibration coefficients occurred for the three (UTS) RAMSES sensors (SN's 506D, 506F and 8375), which could not be explained by temperature effects. This suggests significant sensor degradation since their respective factory calibrations.

Detector response as a function of integration time (integration time linearity) was assessed for the hyperspectral instruments. All irradiance and radiance sensors exhibited non-linear behaviour. The DALEC sensors showed the largest non-linear deviation at low integration times, however as noted earlier, this non-linearity is corrected for within the In-situ Marine Optics DALECPROC software package. It is suggested that a similar approach in linearity correction be adopted for the Curtin DALEC, RAMSES and HyperOCR sensors to improve their radiometric accuracy by $< 3\%$.

12 Appendix 3: report of the field experiment at the LJCO

Introduction

This report outlines a series of concurrent field radiometric measurements made at the Lucinda Jetty Coastal Observatory (LJCO) with a variety of mainly commercially-available sensors used by the Australian scientific community. Within 2 months prior to the field campaign, each sensor was calibrated by the same laboratory using methods based on the NASA Ocean Optics Protocols of Ocean Colour Validation.

Field data collection and post-processing methodologies were kept as close as possible to what would be considered ‘standard’ for a particular instrument and task team participant, including using manufacturer-provided post processing software.

An above-water measurement regime was selected to facilitate more practical simultaneous data acquisition of the same parameter from different instruments, whilst minimising uncertainties due to spatial and temporal variability.

This work then studies the potential differences between instruments during optimal field conditions experienced at the LJCO.

Equipment

A representative selection of radiometric instruments used by Australia marine researchers was included in the RTT fieldwork. The same radiometers were also calibrated and characterised in the laboratory component of this initiative.

Table 4: Radiometers used in both the Laboratory and Field Studies. E denotes “Irradiance” and L denotes “Radiance” measurements. The DALEC instruments contain two Radiance sensors and one irradiance sensor.
*) Non-commercial.

Manufacturer	Instrument	Operator	Serial No.	Type
In-situ Marine Optics	DALEC	IMOS/CSIRO	1	2L, 1E
Curtin (Klonowski)*	DALEC	Curtin	1	2L, 1E
In-situ Marine Optics	USSIMO	In-situ Marine Optics	2	E
Satlantic	HyperOCR	CSIRO	346	E
TriOS	RAMSES	CSIRO	5039	E
TriOS	RAMSES	CSIRO	8035	E
TriOS	RAMSES	CSIRO	8375	E
CIMEL Electronique	SeaPRISM	IMOS/CSIRO	658	L
Satlantic	HyperOCR	CSIRO	287	L
TriOS	RAMSES	UTS	8494	L
TriOS	RAMSES	UTS	506F/836D	L

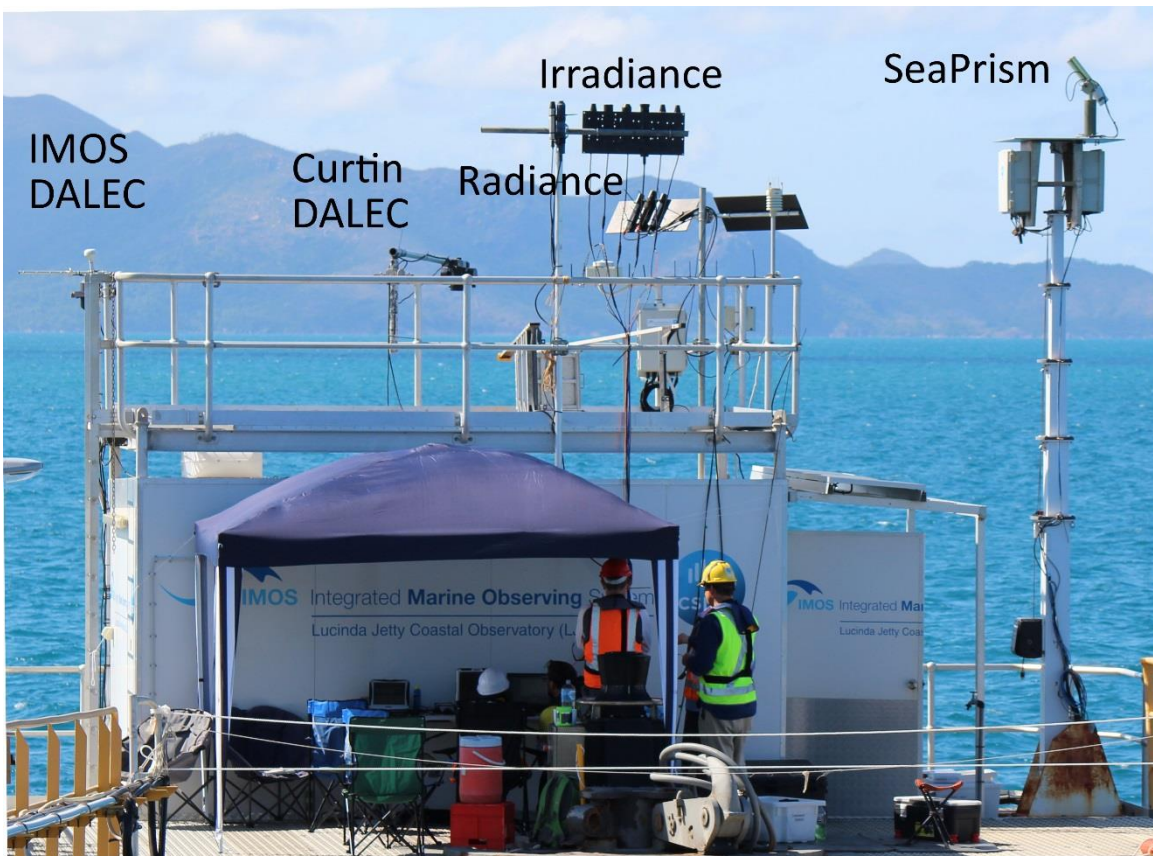


Figure 12: The Lucinda Jetty Coastal Observatory platform equipped with Radiometry Task Team Instrumentation. (Note IMOS DALEC is partially obscured by hand-railing).

With the exception of the SeaPRISM, all radiometers are hyperspectral devices that incorporate a fibre optic input monolithic spectrometer (all likely to be based on the Zeiss MMS-1 module). These devices contain a holographic blazed diffraction grating that spreads the incident light according to its wavelength onto a fixed linear diode array. Integrating circuitry collects the photocurrent incident on each pixel in the photodiode array over a user-selectable time period referred to as the *integration time*.

Although it is likely that the same spectrometer module is used across all devices, the devices differ in their ‘read-out’ electronics, which takes the integrated photocurrent and then amplifies and digitises the resulting photocurrent to be represented as “counts”. The digital control interface that governs the actual integration time chosen for a given measurement also differs amongst manufacturers. In addition, there are differences to the optical design and output communications interfaces. All use a RS232 serial data protocol, however some encode data in binary or human-readable, or both.

The SeaPRISM contains two silicon photodiodes; one set for low brightness targets (Sea and Sky measurements) and the other for high brightness targets (the Sun). A rotating optical filter wheel is placed between the target and the photodiodes. It is unclear whether the detector electronics are photocurrent-integrating at a factory-fixed integration time, or transimpedance (instantaneous photocurrent to voltage conversion) based.

Methods

Irradiance

All single-unit Irradiance (E) radiometers were mounted in a row, with their diffusers at equal height to avoid shading. The inclination of each radiometer was adjusted individually to less than approximately 2 degrees by using spirit level observations on 2 axes.



Figure 13: Irradiance Radiometers: from right to left, RAMSES 5039, RAMSES 8035, HyperOCR 346, USSIMO 0002, MS8 Prototype, RAMSES 506D, IMOS HyperOCR (not included in the RTT lab and field inter-comparison) and RAMSES 8375. The smallest instrument (5th from the left) is a prototype multispectral sensor not included in this work.

The two DALEC instruments (Tab 1.) were attached to boom poles that were lower in elevation than the single-unit irradiance sensor line (see Figure 14 and Figure 15), and approximately 6 meters towards the Nor-Nor-West from the sensor line (See TOP view diagram). The internal pitch and roll on the IMOS DALEC was typically +/- 1.0 degree for the duration of the experiment.



Figure 14: The boom-mounted DALEC spectroradiometers (IMOS DALEC on left, Curtin DALEC on right).

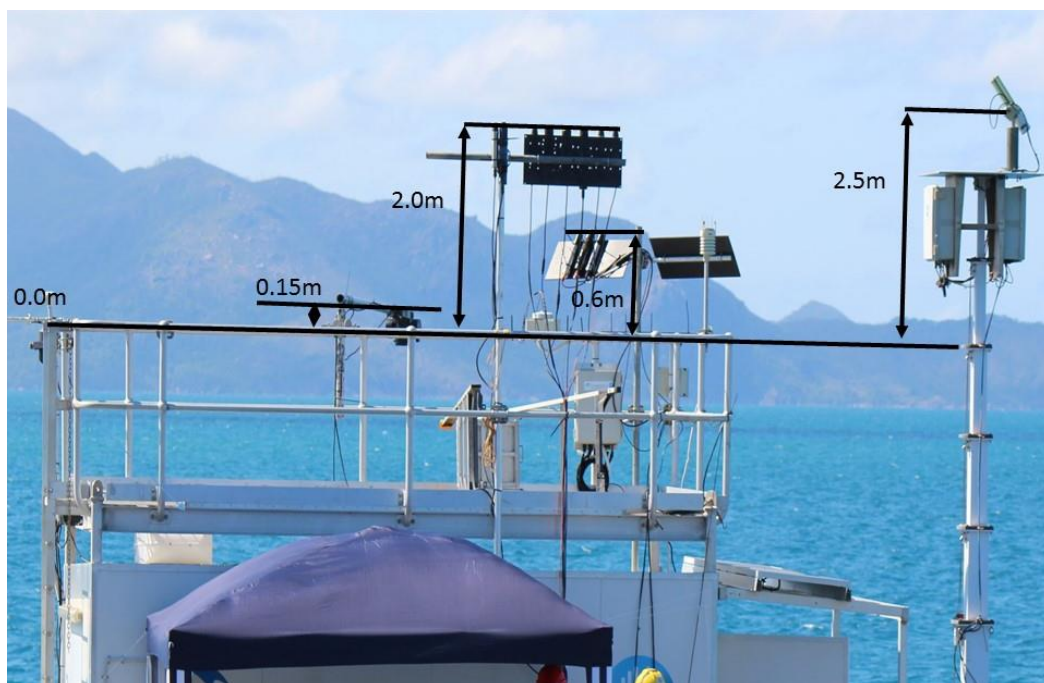


Figure 15: Approximate relative heights between cosine collectors (where applicable) and the handrail. Note - IMOS DALEC Irradiance cosine collector is level with the handrail.

The Curtin DALEC was operated with software called DALEConTRANSECT.exe, which collected Ed, Lt and Lsky sequentially with automatic light integration times. The time differences between data collection from the different radiometers is typically less than 1 second. In addition to the radiometric quantities, compass heading, internal temperature and pitch and roll were recorded during light integration.

The IMOS DALEC was operated with DALECView 4.0. The USSIMO data was collected with USSIMOview 2.0, the HyperOCR data was captured by SatView 2.9.5_7 and the RAMSES data was captured by MSDA_XE 8.8.13.

Radiance

All single-unit Radiance (L) radiometers were mounted in a row on a flat black plastic panel. The azimuth and view angle of this panel could be altered such that users could rapidly alternate between sea and sky radiance

measurements, and also attach occluders in order to collect manual dark offset spectra. All radiometers on this panel had consistent azimuth and view angles, within about 2 degrees (See Figure 16).

The SeaPRISM radiance sensor was mounted on its own mast, higher up on the LJCO platform (See Figure 15), and its configuration was not altered from the standard AERONET-OC mode.

The DALEC instruments both feature 2 radiance spectrometers, $L_t(40^\circ)$ and $L_{sky}(40^\circ)$. Both DALEC sensors were mounted on boom poles, however the DALEC operated under IMOS features a motor and can rotate on its axis to provide optimal sun-relative azimuth angles without needed to move the boom pole, whereas the Curtin DALEC's boom pole needed to be re-aligned as the sun transited the sky.

The radiance sensors collect light over different Fields Of View (FOV). The Full-Width-Half-Maximum (FWHM) angles in air are shown in Table 5.

Table 5: Radiance Sensor Fields of View.

Sensor	Full Angle FOV (°)
HyperOCR	23
SeaPRISM	1.2
Ramses	7
IMOS	
DALEC	10
Curtin DALEC	20



Figure 16: Radiometers attached to black panel in Sky Radiance Mode (Curtin DALEC in background on the left, where the L_t sensor head can be seen pointing to the ocean, 40° from Nadir. The other side of the DALEC features the L_{sky} sensor which is pointing to the sky, 40° from Zenith. Hemispherical web-camera (not used for radiometric measurements) can be seen in the foreground, mounted to railing.



Figure 17: Radiometers in Sea Radiance Mode.

Atmospheric Model Reference Irradiance Approach

Adjacent to the Irradiance and Radiance spectroradiometers, the photodiode and filter wheel-based multispectral SeaPRISM was deployed to automatically measure the radiance of the solar disk, sky and sea surface at regular intervals throughout the duration of the experiment. The SeaPRISM was shown to be one of the most temperature-stable and possibly most temporally-stable radiometer during the IMO laboratory calibration and characterisation exercise (excluding the 'cold' radiance measurement which likely suffered from condensation, and the 1020 nm channel), so information derived from the SeaPRISM was used as a reference from which to measure other radiometers performance.

Based on the solar disk radiance measurements, the SeaPRISM data is processed by NASA AERONET in delayed-mode to determine a series of atmospheric products such as Aerosol Optical Thickness, and precipitable water vapour. This data was downloaded from the AERONET site and used as input into the RADTRAN solar irradiance model (Gregg & Carder, 1990), along with relative humidity, pressure, wind speed, and time data collected at LJCO adjacent to the radiance sensor panel.

The RADTRAN model was run using the Thuillier exo-atmospheric solar irradiance spectrum as input (Thuillier, et al., 2003). For comparisons with the other spectrometers, the modelled spectrum was temporally interpolated to provide irradiance occurring at the mid-point of the 5 minute measurement period and was spectrally convolved to a Gaussian spectral response function with a FWHM of 10 nm to suit the Zeiss MMS-1 spectrometer modules which are likely used in these commercial products. An example of the spectrally interpolated, modelled irradiance spectrum is shown later in Figure 23, along with spectra from a selection of other radiometers near noon.

Reference Radiance Approach

For Sky and Sea radiance reference, the AERONET-Ocean Color Data Download Level 1.0. Real Time Data was used. The band centres for CIMEL are 412, 441, 491, 530, 551 668 and 870nm.

Instrument Radiometric Calibration Files

The laboratory calibration exercise demonstrated temperature dependence on the instrument responsivity by observing instrument responses at “Room” and “Hot” temperatures. Room temperature represents the normal ambient temperature conditions commonly experienced in calibration laboratories (22–25 degrees), whereas “Hot” calibration temperatures were closer to 35 to 40 degrees – assumed to be closer to the conditions expected in the Australian Tropics.

Based on these laboratory measurements, instrument-specific calibration files were generated for both “room” and “hot” laboratory calibration temperatures. For Satlantic and TriOS sensors, this required characterising both the “dark” spectrum and normalised responsivity coefficients. Calibration files were produced to match the format of the respective factory calibration file examples, such that the manufacturer’s native processing software could be used to process the data from each sensor. As a result, for every measurement, there was a “room” and “hot” dataset.

Measurement Sequence:

Table 6: Measurement Sequences performed on Day 1:

Date	Local Time	ID	Type	Solar Zenith Angle (deg)	Solar Azimuth (deg)	Wind Speed (m/s)	Matching SeaPRISM Time
9th Nov 2016	11:29	S02	Sea	6.0	85.7	6.0	-
9th Nov 2016	12:11	S03	Sea	3.6	278.1	6.0	12:05
9th Nov 2016	12:17	S03	Sky	5.1	275.4	6.1	-
9th Nov 2016	12:32	S04	Sea	8.5	272.3	6.3	12:32
9th Nov 2016	12:36	S04	Sky	9.9	271.6	6.3	-
9th Nov 2016	13:31	S05	Sea	22.6	267.8	5.9	13:32
9th Nov 2016	13:36	S05	Sky	23.9	267.5	6.1	-
9th Nov 2016	14:17	S07	Sky	33.3	265.6	6.9	-
9th Nov 2016	14:21	S07	Sea	34.3	265.4	6.9	-
9th Nov 2016	14:25	S07	Sky 2	35.4	265.2	6.9	14:32
9th Nov 2016	14:43	S08	Sky	39.5	264.4	7.1	-
9th Nov 2016	14:48	S08	Sea	40.7	264.1	7.2	-
9th Nov 2016	14:53	S08	Sky 2	41.7	263.9	7.2	-
9th Nov 2016	15:13	S09	Sky	46.6	263.0	6.8	15:10
9th Nov 2016	15:20	S09	Sea	48.4	262.6	6.5	-
9th Nov 2016	15:30	S09	Sky 2	50.7	262.1	6.2	-
9th Nov 2016	15:40	S10	Sky	53.3	261.6	6.2	-
9th Nov 2016	15:45	S10	Sea	54.4	261.4	6.2	-
9th Nov 2016	15:50	S10	Sky 2	55.3	261.2	6.2	-
9th Nov 2016	16:02	S11	Sky	58.5	260.5	6.2	16:00
9th Nov 2016	16:08	S11	Sea	59.6	260.3	6.2	-
9th Nov 2016	16:12	S11	Sky 2	60.6	260.0	6.2	-
9th Nov 2016	16:26	S12	Sky	64.2	259.2	6.2	-
9th Nov 2016	16:32	S12	Sea	65.4	258.9	6.3	16:30
9th Nov 2016	16:37	S12	Sky 2	66.5	258.7	6.4	-
9th Nov 2016	16:56	S13	Sky	70.8	257.7	6.8	-
9th Nov 2016	17:00	S13	Sea	71.8	257.4	6.9	-
9th Nov 2016	17:04	S13	Sky 2	72.8	257.1	6.9	-

Table 7: Measurements Sequences performed on Day 2:

Date	Local Time	ID	Type	Solar Zenith Angle (deg)	Solar Azimuth (deg)	Wind Speed (m/s)	Matching SeaPRISM Time
10th Nov 2016	9:39	S14	Az 2	32.8	94.3	4.7	-
10th Nov 2016	9:46	S14	Az 3	31.4	94.0	5.0	-
10th Nov 2016	9:49	S14	Az 4	30.4	93.8	5.2	-
10th Nov 2016	9:53	S14	Az 5	29.5	93.7	5.4	-
10th Nov 2016	9:58	S14	Az 6	28.3	93.4	5.7	-
10th Nov 2016	10:02	S14	Az 7	27.3	93.8	5.8	-
10th Nov 2016	10:07	S14	Az 8	26.2	93.6	5.9	-
10th Nov 2016	10:19	S15	Sky	23.2	93.1	6.3	-
10th Nov 2016	10:26	S15	Sea	21.5	92.7	6.5	-
10th Nov 2016	10:29	S15	Sky 2	20.5	92.5	6.7	-
10th Nov 2016	10:45	S16	Sky	17.1	91.8	7.7	-
10th Nov 2016	10:50	S16	Sea	16.0	91.6	8.0	-
10th Nov 2016	10:54	S16	Sky 2	15.1	91.4	8.3	-
10th Nov 2016	11:06	S17	Sky	12.1	90.7	8.7	-
10th Nov 2016	11:11	S17	Sea	11.2	90.4	8.7	-
10th Nov 2016	11:15	S17	Sky 2	10.0	90.1	8.7	-
10th Nov 2016	11:26	S18	Sky	6.7	88.8	8.8	-
10th Nov 2016	11:33	S18	Sea	5.6	88.2	8.6	-
10th Nov 2016	11:38	S18	Sky 2	4.3	87.2	8.5	-
10th Nov 2016	11:58	S19	Sky	0.3	322.8	7.9	-
10th Nov 2016	12:02	S19	Sea	1.6	279.2	7.9	-
10th Nov 2016	12:07	S19	Sky 2	2.5	275.5	7.9	12:05
10th Nov 2016	12:54	S20	Sky	13.6	269.0	8.5	12:32
10th Nov 2016	12:58	S20	Sea	14.5	268.7	8.6	-
10th Nov 2016	13:02	S20	Sky 2	15.5	268.5	8.8	13:04
10th Nov 2016	13:14	S21	Sky	18.4	267.9	9.4	-
10th Nov 2016	13:18	S21	Sea	19.4	267.7	9.6	-
10th Nov 2016	13:23	S21	Sky 2	20.6	267.5	9.8	-
10th Nov 2016	13:29	S21	Sea 2	21.8	267.2	10.1	13:32
10th Nov 2016	13:42	S22	Sky	24.9	266.6	10.3	-
10th Nov 2016	13:46	S22	Sea	25.9	266.4	10.4	-
10th Nov 2016	13:50	S22	Sky 2	26.9	266.3	10.5	14:04

Results

Instrument Wavelength Calibration

For each spectrometer, individual field spectral measurements were initially compared in order to identify any wavelength calibration issues amongst the spectrometers. By inspection of the Fraunhofer absorption lines and broader absorption bands evident in Figure 18, Figure 19 and Figure 20, it is clear that both DALEC instruments deviated from the other spectrometers. For the IMOS DALEC, this deviation has been identified as an error from the spectrometer module manufacturer's front-end electronics; whereby data from the first pixel (UV) is not reported and the last pixel value reported is not exposed to light. This then creates a

mismatch between the Zeiss factory wavelength calibration polynomial coefficients and the spectrometer data output. This issue occurred across all 3 spectrometers inside IMOS DALEC³.

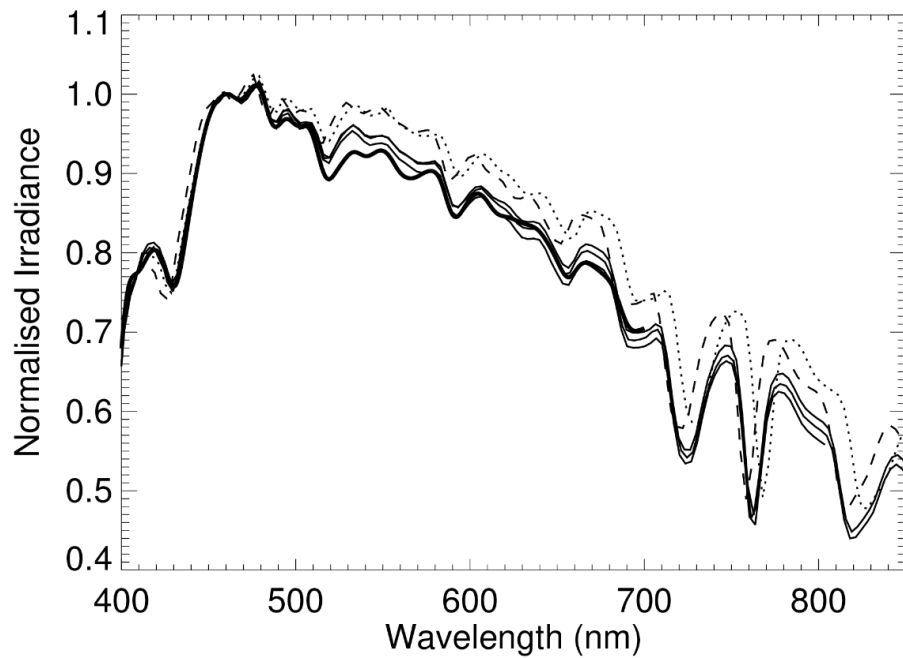


Figure 18: Normalised Irradiance spectra (reference wavelength = 460nm). Note NIR wavelength calibration issues with the Curtin DALEC (dotted line), and a 1 pixel ($\sim 3.3\text{nm}$) translation error in the IMOS DALEC 1 (dashed line). Gaussian-interpolated RADTRAN model output shown from 400 to 700nm in bold line. The thin solid lines are the spectra from the USSIMO and one RAMSES spectrometer.

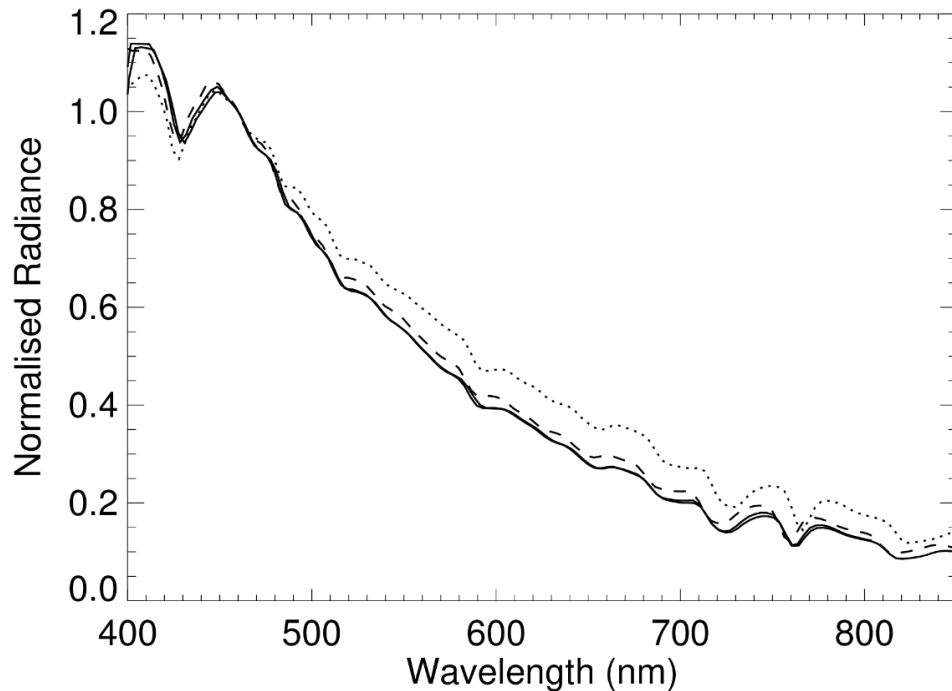


Figure 19: Normalised Sky Radiance spectra (reference wavelength = 460nm). Note NIR wavelength calibration issues with the Curtin DALEC (dotted line), and a 1 pixel ($\sim 3.3\text{nm}$) translation error in the IMOS DALEC (dashed line).

³ Note, the USSIMO the same spectrometer front end electronics from the same OEM manufacturer, however this module did not have the error.

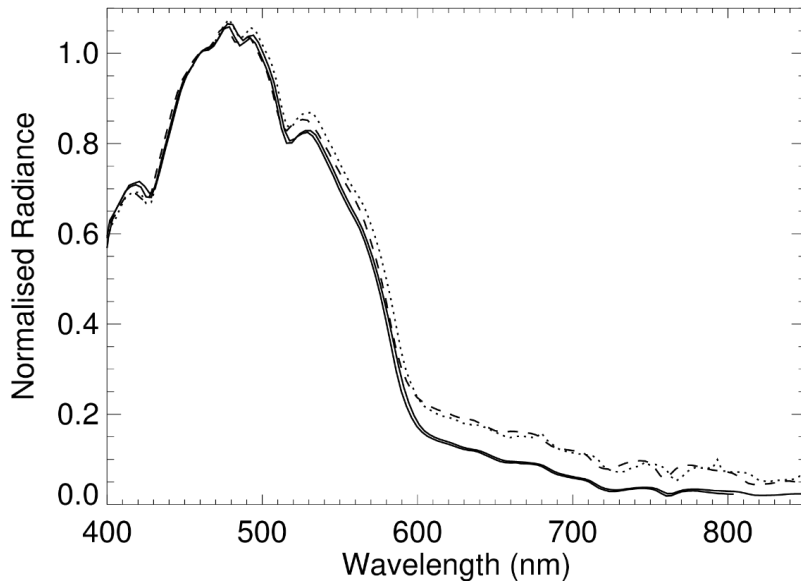


Figure 20: Normalised Raw Sea Radiance spectra (reference wavelength = 460nm). Note NIR wavelength calibration issues with the Curtin DALEC (dotted line), and a 1 pixel ($\sim 3.3\text{nm}$) translation error in the IMOS DALEC (dashed line).

Unfortunately, the incorrect wavelength calibration of the IMOS DALEC was used during the IMOS RTT calibration exercise, and this introduces a spectrally-dependent error, up to 6% at 400nm. Figure 21 shows the fractional error of the uncorrected calibration coefficients for all IMOS DALEC spectrometers (Fractional error was determined by the uncorrected spectrum, divided by the corrected spectrum). This spectral curvature is directly defined by the fractional difference in the calibration lamp response of an erroneously shifted wavelength calibration. After correction for both wavelength calibration and responsivity, the spectral features of IMOS DALEC agree well with the USSIMO, Hyper-OCR and RAMSES spectrometers (See Figure 22).

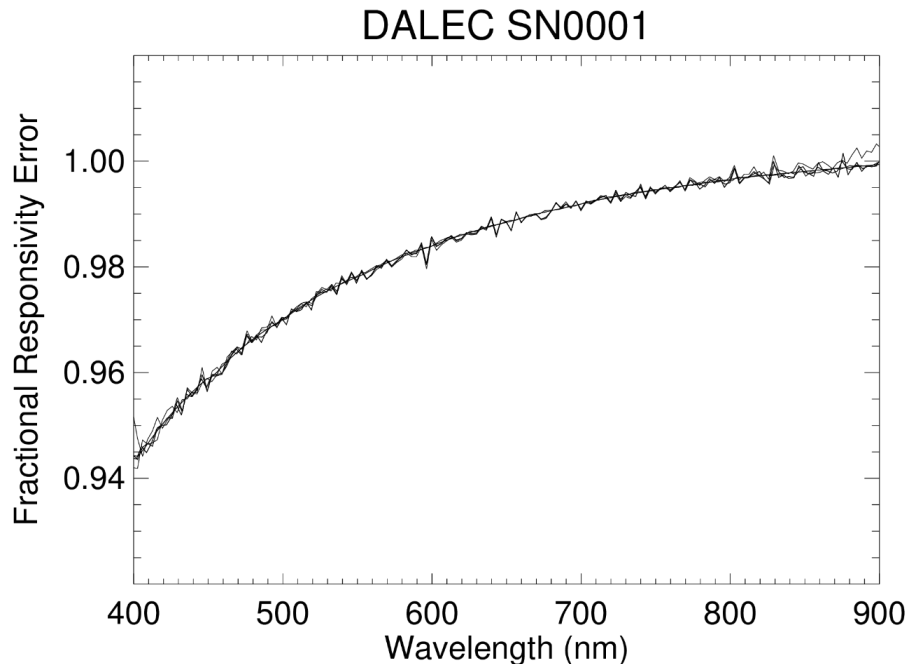


Figure 21: The Fractional spectral error in the initial IMOS DALEC data introduced by a $\sim 3.3\text{nm}$ wavelength calibration translation error during radiometric calibration. Data from E_d , L_{sky} and L_t are overplotted.

For the Curtin DALEC, the wavelength calibration variation is more difficult to correct. The source of the error on this instrument is most likely due to aging of the spectrometer modules. The spectrometers in the Curtin DALEC are approximately 18 years old (circa 1999) and the original wavelength calibration was still being applied to the instrument. Wavelength calibrations for all 3 spectrometers (E_d , L_t and L_{sky}) were tested to see if the spectrometer modules were mislabelled, however this did not reconcile any of the mismatched Fraunhofer and molecular absorption lines evident in the spectra (See Figure 22). As a result of these spectrometers requiring more characterisation measurements to reconcile (i.e. using an emission line source), and given that the wavelength calibration appears satisfactory in the visible region, the wavelength calibration and resultant radiometric calibration was left uncorrected.

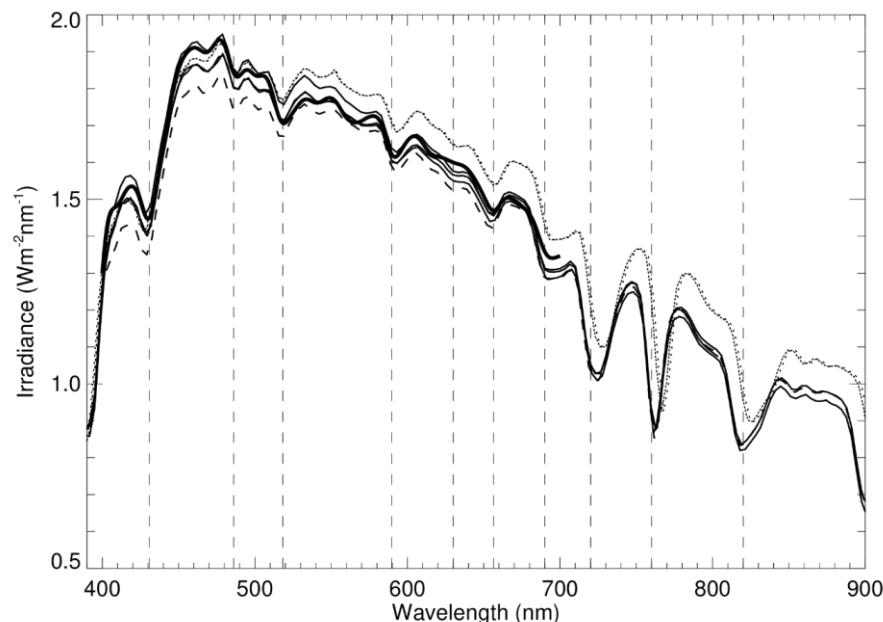


Figure 22: Spectral features in Downward Irradiance. The Curtin DALEC irradiance with 3 different wavelength calibrations is plotted in dotted lines. The solid, thin lines are from the USSIMO, Hyper-OCR and RAMSES. The thin, dashed spectrum is from IMOS DALEC after wavelength and radiometric correction, where differences can be seen between 400 and 500nm. The solid thick line is the RADTRAN output. The vertical dashed lines are the approximate Fraunhofer or molecular absorption band centres.

Irradiance Responsivity

During the Lucinda field campaign, the lowest solar zenith angle (θ_z) measurement was performed at 0.3 degrees. At this solar angle, irradiance differences can primarily be attributable to sensor calibration accuracy and to a much lesser extent, pointing accuracy (sensor tilt).

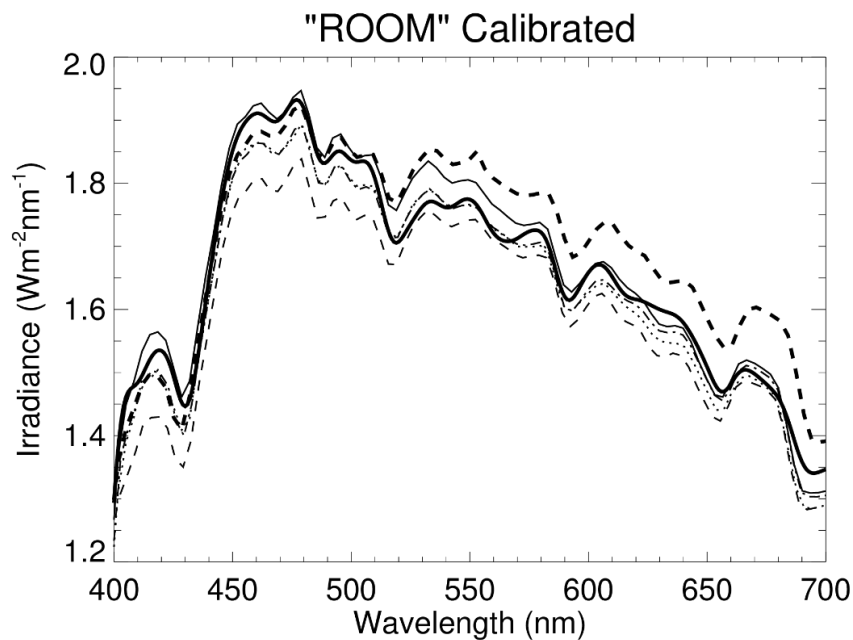


Figure 23: Example Irradiance Spectra measured at $\theta_z = 0.3$ degrees showing spectrally interpolated RADTRAN reference spectrum with thick solid line. The thin dashed line is the IMOS DALEC, dotted line is the USSIMO, dot-dashed line is a RAMSES and the solid thin line is the HyperOCR. The thick dashed line is the Curtin DALEC. "Room" temperature calibrations applied.

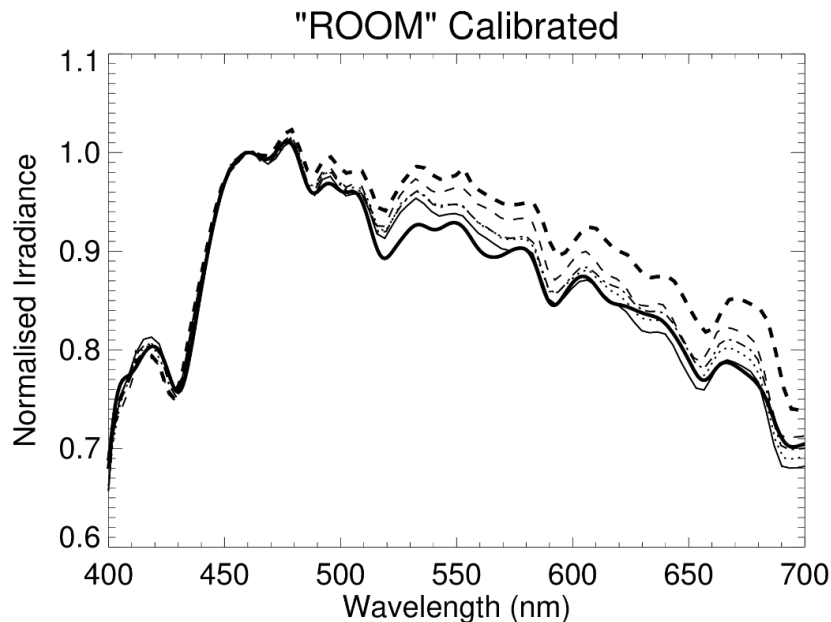


Figure 24: As in Figure 23, however all data normalised to 460nm.

By normalising all example noon irradiance spectra to 460 nm, Figure 24 shows spectral differences in the downward irradiance data that cannot be attributed to spectrally flat calibration errors or cosine response. The choice of 460 nm was made because it this region appears relatively free of Fraunhofer or broad spectral absorption features which could introduce variation due to differences in the spectral bandwidths of the respective spectrometers.

Figure 25 shows the "Fractional Error" (ratio) of the example spectra from each spectrometer measured at noon compared to the RADTRAN reference. It is important to realise that the jagged nature of these spectral errors are not sourced from radiometric calibration or performance, but the more the differences in spectral band responses between the instruments and the Gaussian-convolved RADTRAN Spectrum.

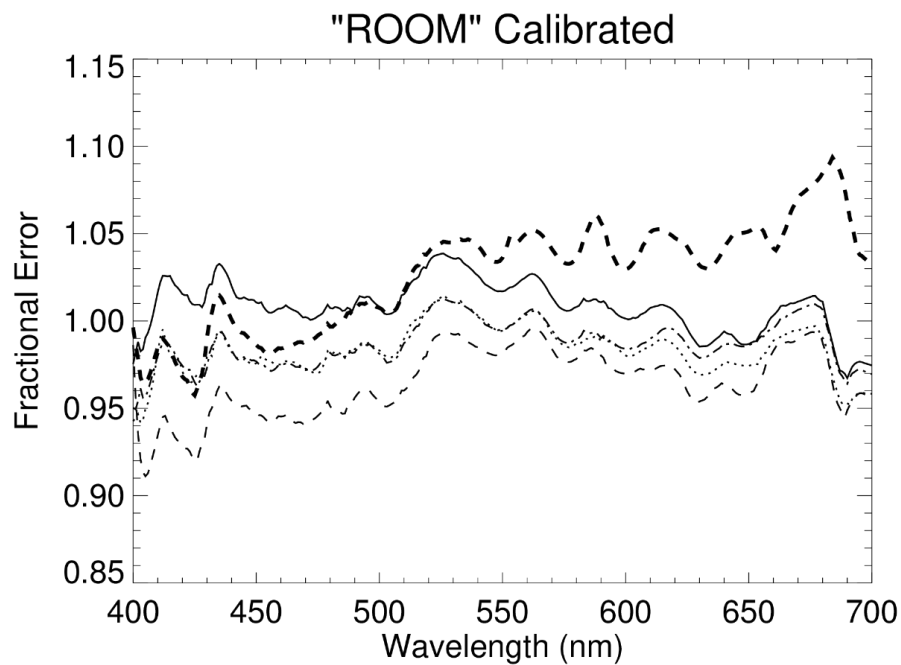


Figure 25: Fractional errors in example spectra shown previously in Figure 12, calculated by normalising sensor spectra by the RADTRAN spectrum. The thin dashed line is the IMOS DALEC, dotted line is the USSIMO, dot-dashed line is a RAMSES, the solid thin line is the HyperOCR and the thick dashed line is the Curtin DALEC.

In order to estimate the level of uncertainty attributable to spectral mis-match (in separation from systematic calibration or instrument responsivity), the normalised fractional errors were calculated by dividing the fractional error by the spectrally-averaged (400–700nm) fractional error. These are shown in Figure 26. These plots reveal the magnitude of spectral deviation expected when comparing different spectrometers with different band centres and spectral responses with the 10 nm FWHM Gaussian-convolved RADTRAN spectrum.

This spectral data was then further reduced by calculating a spectral RMSE (See Table 8) and the maximum zero-mean spectral error (See Table 9) that provides estimate of the likely confidence interval of using the RADTRAN spectrum as a reference⁴.

⁴ Ignoring any overall inaccuracies of RADTRAN which may be up to a few percent in addition.

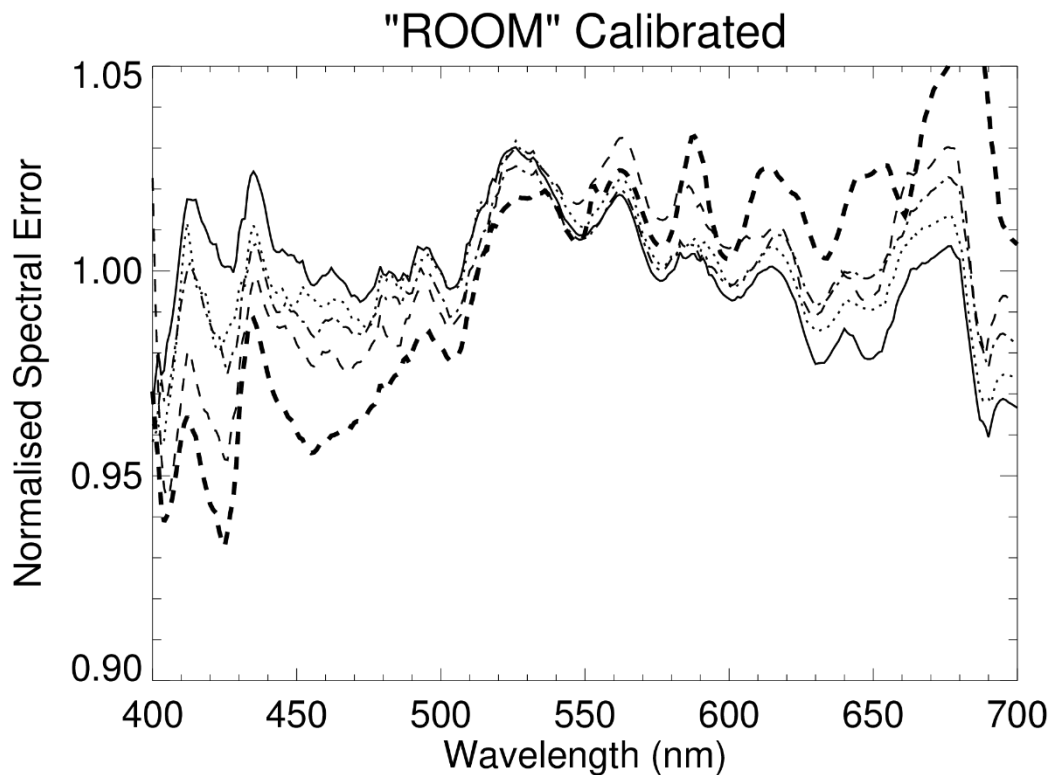


Figure 26: Zero-mean Spectral Error of Example Spectra showing spectral artefacts. The thin dashed line is the IMOS DALEC, dotted line is the USSIMO, dot-dashed line is a RAMSES, the solid thin line is the HyperOCR and the thick dashed line is Curtin DALEC. The Note – using the RAMSES or USSIMO irradiance as the reference results in smoother lines, suggesting very comparable spectral bandwidths between Zeiss-based spectrometers. Room temperature calibrations applied.

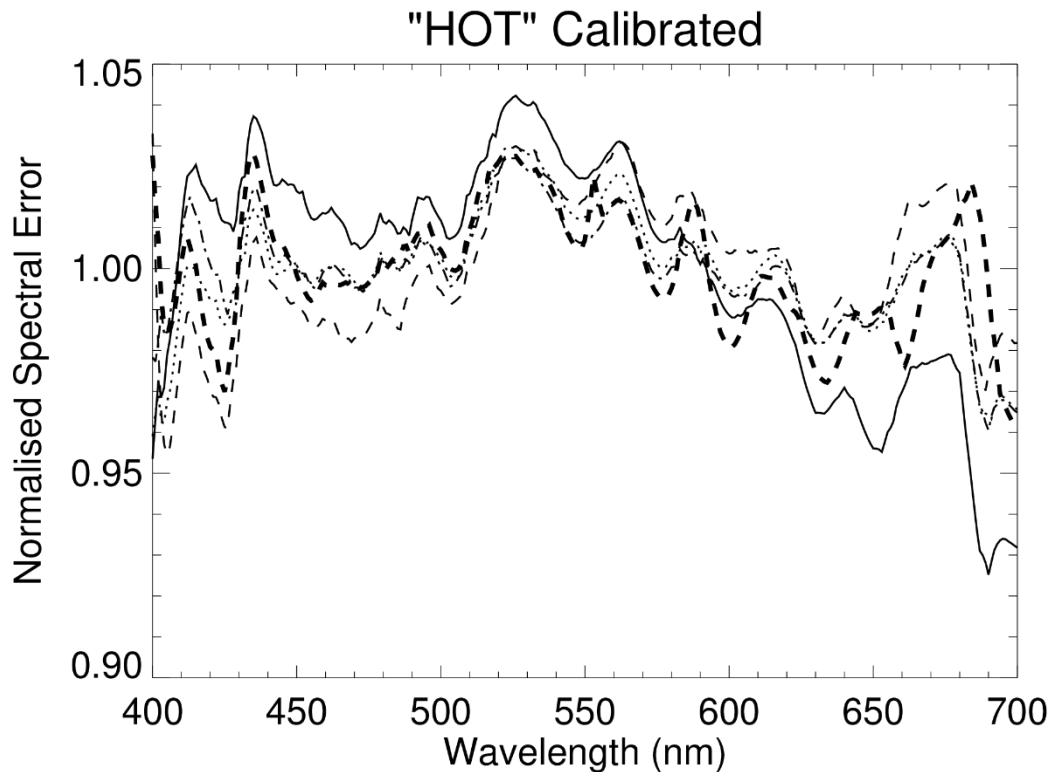


Figure 27: As in Figure 26, but with "Hot" calibrations applied.

Table 8: Root Mean Square normalised spectral errors of the near noon Irradiance measured by 5 spectrometers, using the RADTRAN irradiance as a reference.

RMSE	USSIMO	RAMSES	IMOS DALEC	CURTIN DALEC	HOCR
ROOM	1.1%	1.0%	1.7%	2.5%	1.1%
HOT	1.1%	0.9%	1.5%	1.2%	2.3%

Table 9: Maximum spectral errors of the near noon Irradiance measured by 5 spectrometers, using the RADTRAN irradiance as a reference.

MAX	USSIMO	RAMSES	IMOS DALEC	CURTIN DALEC	HOCR
ROOM	4.3%	3.8%	5.5%	6.7%	4.1%
HOT	4.1%	4.0%	4.5%	3.9%	7.5%

Thus, a comparison for any given wavelength using RADTRAN (or any other hyperspectral radiometer) could yield errors up to 5%. In this estimate, the Curtin DALEC and HOCLR Maximum errors are ignored due to pronounced temperature related spectral errors. In the following plots, this +/- 5% envelope is added to indicate the estimated confidence interval of the RADTRAN-based irradiance comparisons.

Figure 28 and Figure 29 show the 5 minute averaged irradiance values measured at 411 nm for 4 different radiometers, along with the RADTRAN-based irradiance used as the reference. Generally, all radiometers exhibited the expected cosine-like reduction in intensity as a function of solar zenith angle. Subtle deviations in between consecutive 5-minute averages were apparent. These were attributed to subtle angular alignment changes as a result of using manual covers / occults during dark current quality control checks and also possibly physical sagging of the LJCO mounting booms throughout the experiment.

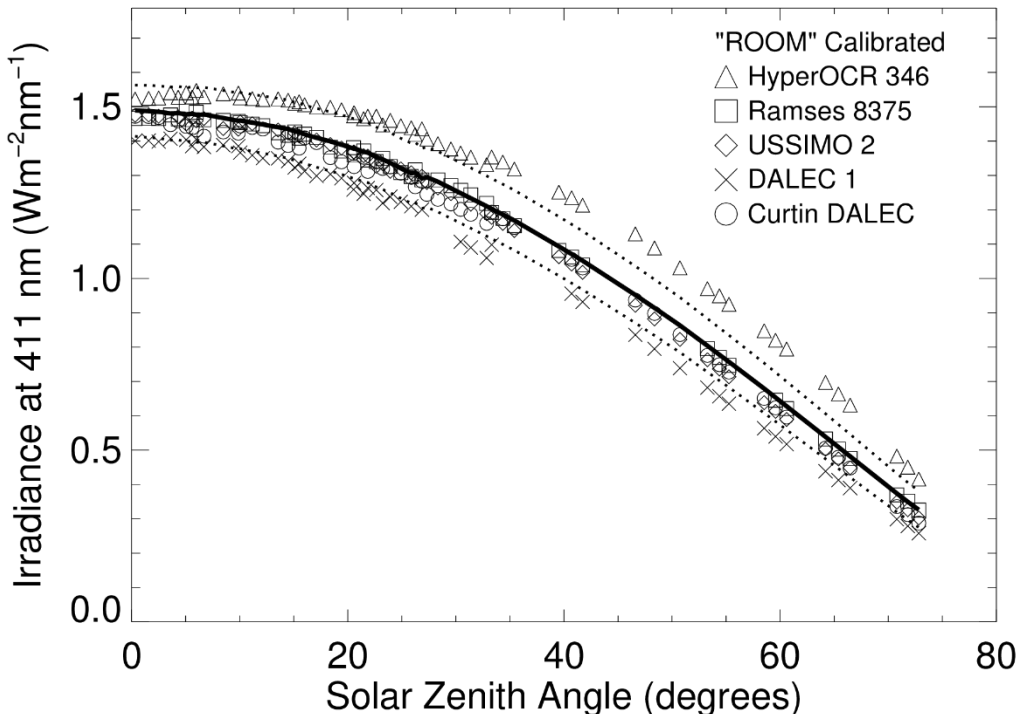


Figure 28: Five minute average irradiance collected on the 9th and 10th of November 2016 at 411 nm vs. Solar Zenith Angle for 4 different radiometers calibrated at “Room” temperature. The RADTRAN-based reference irradiance is shown in the solid line. The dotted lines are the estimated +/- 5% error due to spectral mismatch,

combined with a +/- 2-degree tilt error. Sensor data is marked in the legend. Note, the HyperOCR device was optimised for underwater use, so is expected to overestimate irradiance at large above-water solar zenith angles. All 5-minute standard deviations were smaller than the plot symbols, so were omitted.

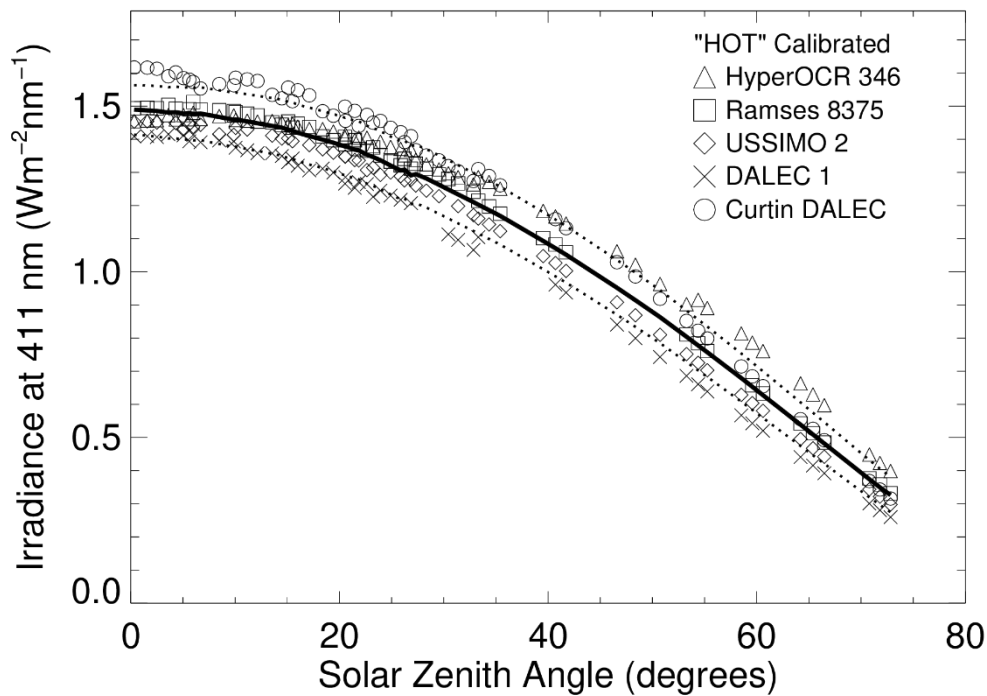


Figure 29: As in Figure 28, but for “Hot” calibrations.

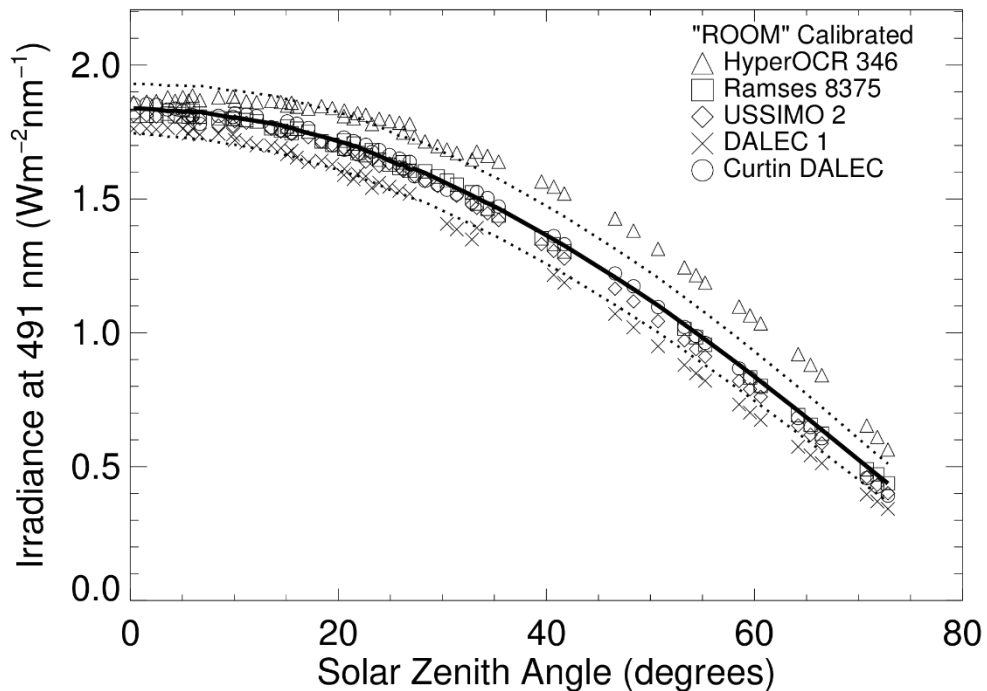


Figure 30: Five minute average irradiance collected on the 9th and 10th of November 2016 at 490nm *vs.* Solar Zenith Angle for 4 different radiometers calibrated at “Room” temperature. The RADTRAN-based reference irradiance is shown in the solid line. The dotted lines are the estimated errors from +/- 5% error due to spectral mismatch, combined with a +/- 2 degrees tilt error. Sensor data is marked in the legend. Note, the HyperOCR device was optimised for underwater use, so is expected to overestimate irradiance at large above-water solar zenith angles. All 5-minute standard deviations were smaller than the plot symbols, so were omitted.

water solar zenith angles. All 5-minute standard deviations were smaller than the plot symbols, so were omitted.

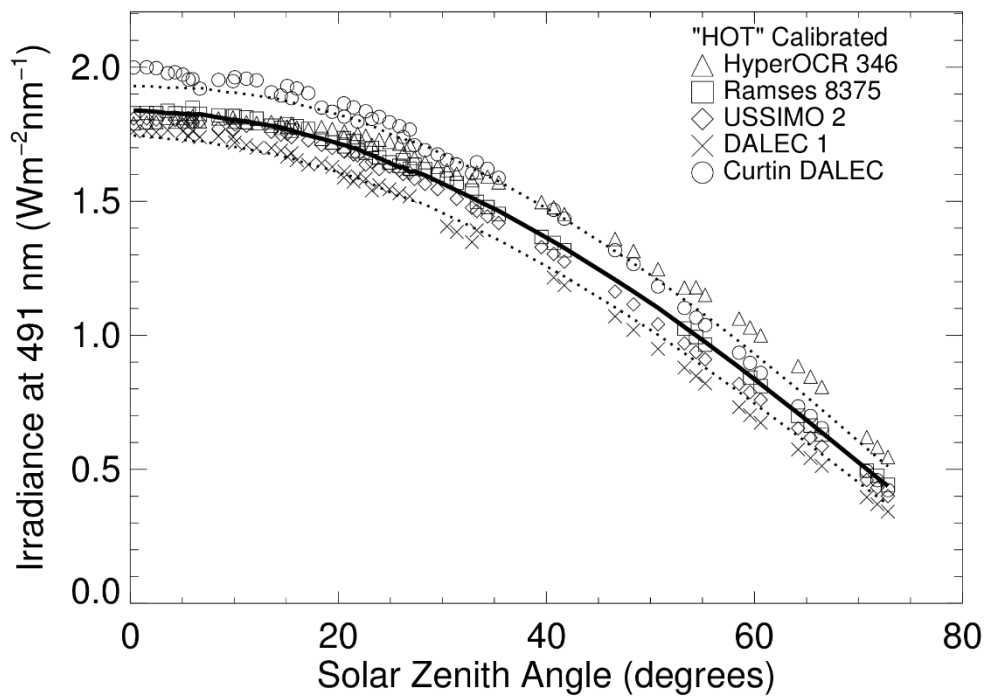


Figure 31: As in Figure 30, but for "Hot" calibrations.

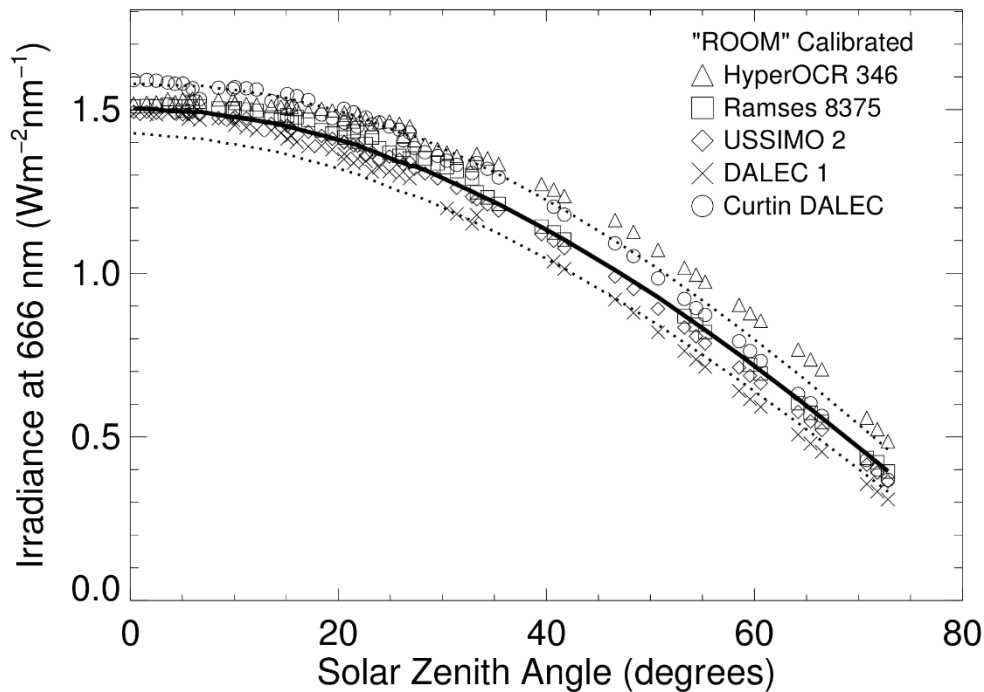


Figure 32: Five minute average irradiance collected on the 9th and 10th of November 2016 at 666nm *vs.* Solar Zenith Angle for 4 different radiometers calibrated at "Room" temperature. The RADTRAN-based reference irradiance is shown in the solid line. The dotted lines are the estimated errors from +/- 5% error due to spectral mismatch, combined with a +/- 2 degrees tilt error. Sensor data is marked in the legend. Note, the HyperOCR device was optimised for underwater use, so is expected to overestimate irradiance at large above-water solar zenith angles. All 5-minute standard deviations were smaller than the plot symbols, so were omitted.

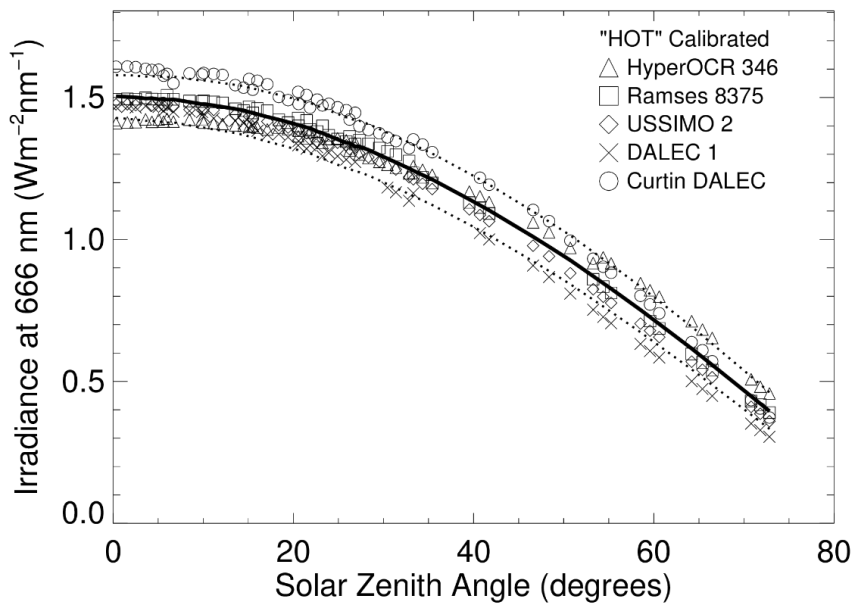


Figure 33: As in Figure 32, but for “Hot” calibration

Figure 34 to Figure 39 show the fractional errors (sensor irradiance divided by RADTRAN irradiance) for 4 different radiometers, at three different wavelengths as a function of solar zenith angle for “Room” and “Hot” calibration coefficients. The errors vary between sensors and wavelengths⁵. There appears to be angular dependence on the fractional errors. The IMOS DALEC fractional errors were slightly larger than expected for the dataset. The tilt of the DALEC was measured and typically varied by no more than 1.5 degrees during the experiment, so errors cannot be explained by a consistent tilt offsets.

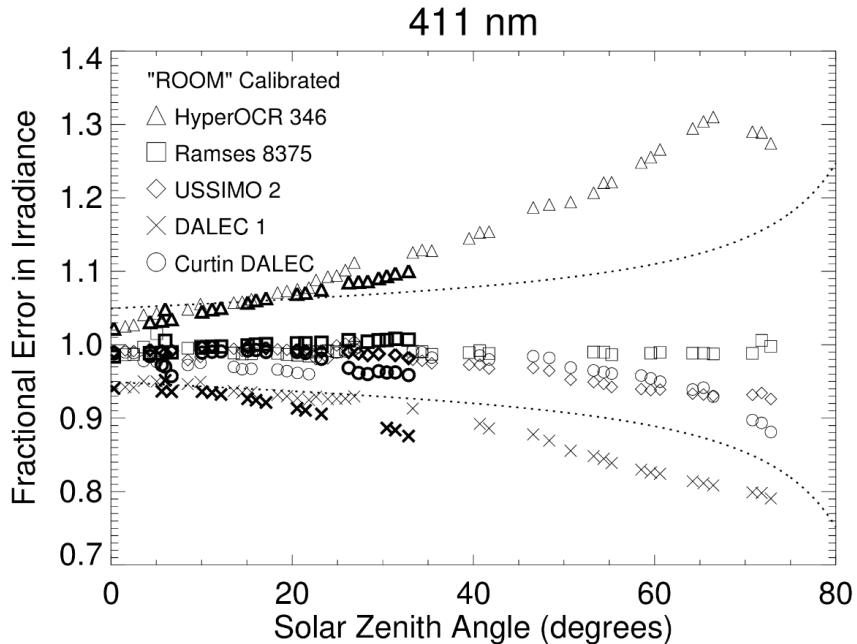


Figure 34: Fractional Error at 411nm (instrument irradiance divided by RADTRAN-based reference irradiance) for the different radiometers as a function of Solar Zenith Angle. Data collected from the ascending

⁵ The internal temperature of the RAMSES spectrometer was not available, however it may be possible to determine a relationship between the average counts collected on non-illuminated portions of the spectrometer array and internal temperature.⁵

sun is shown with bold symbols. The dotted lines show the combined $\pm 5\%$ radiometric uncertainty and a ± 2 degrees tilt angle uncertainty.

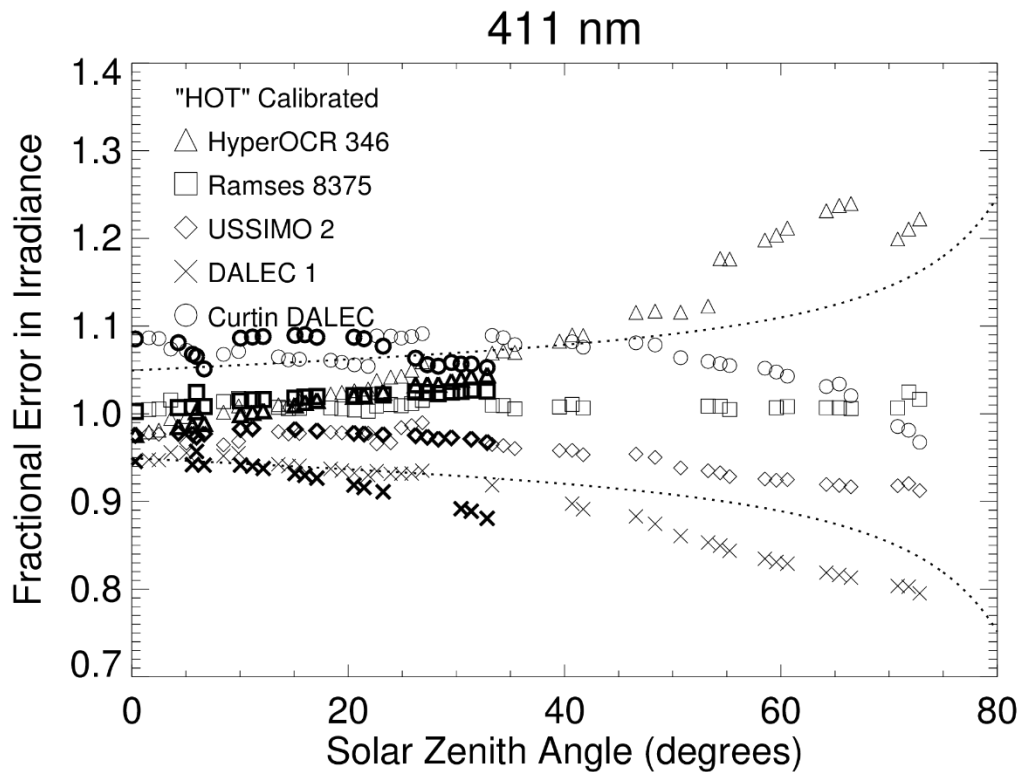


Figure 35: As in Figure 34, but for "Hot" calibration.

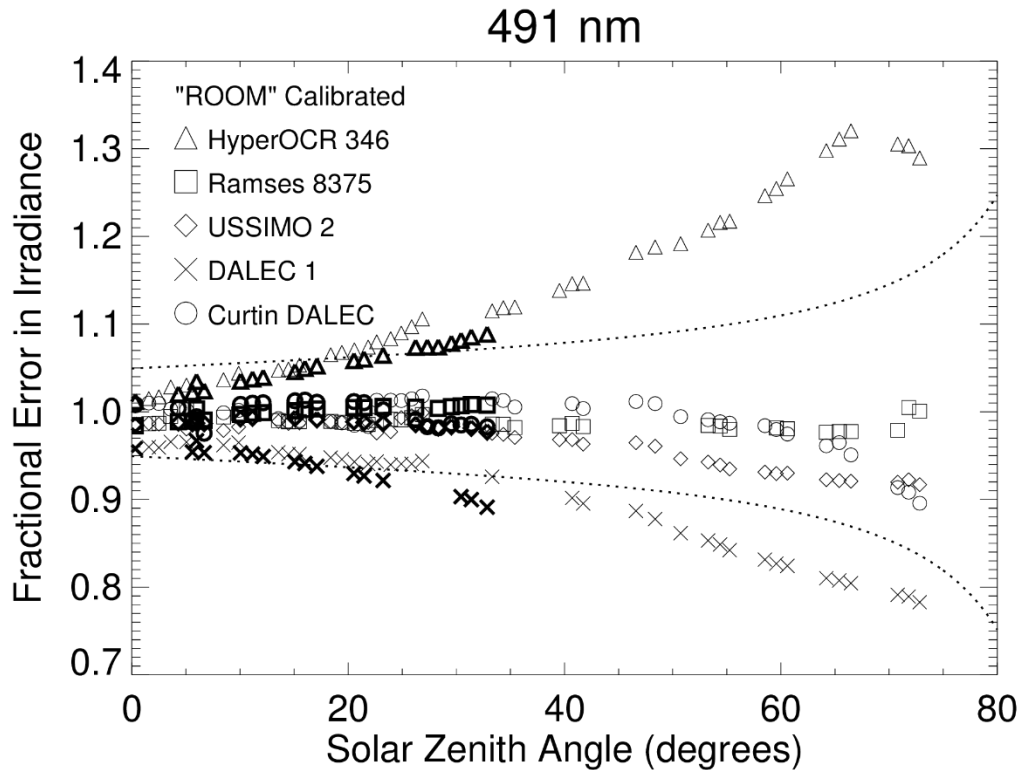


Figure 36: Fractional Error at 491nm (instrument irradiance divided by RADTRAN-based reference irradiance) for the different radiometers as a function of Solar Zenith Angle. Data collected from the ascending sun is shown with bold symbols. The dotted lines show the combined $\pm 5\%$ radiometric uncertainty and a ± 2 degrees tilt angle uncertainty.

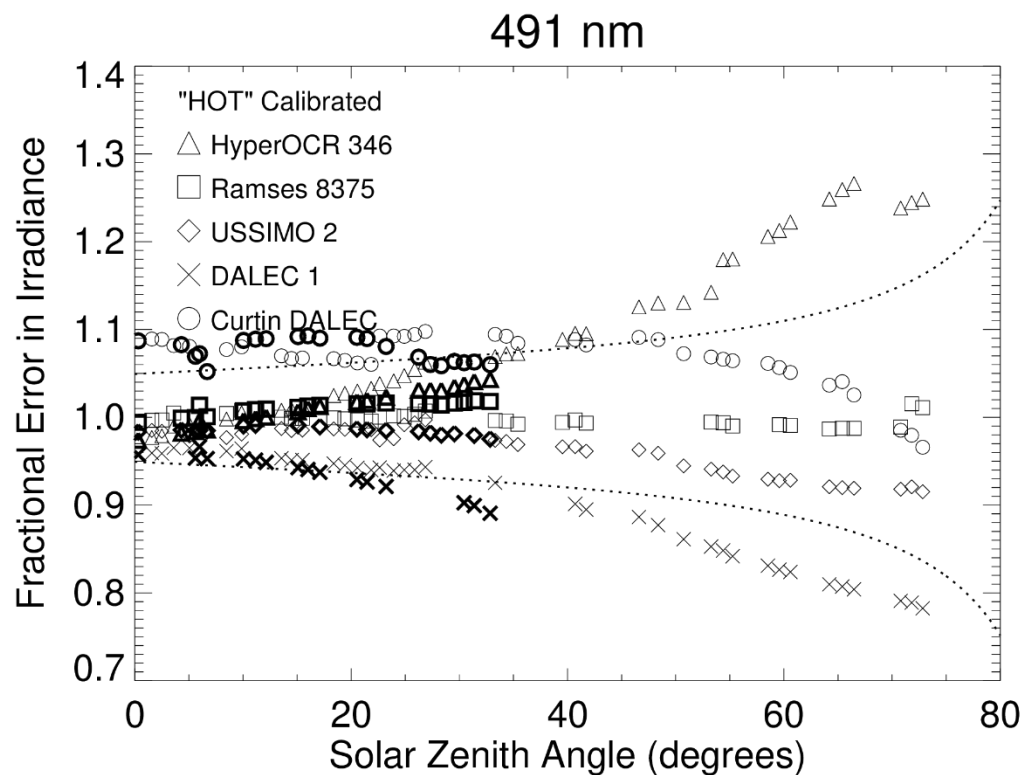


Figure 37: As in Figure 36, but for “Hot” calibration

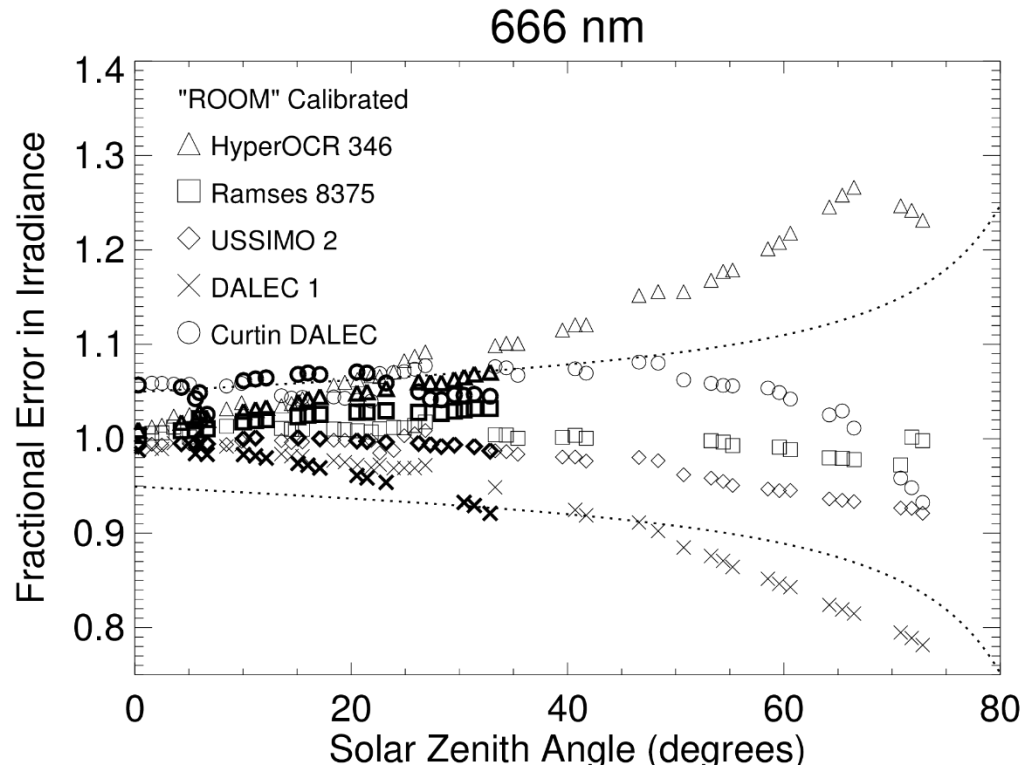


Figure 38: Fractional Error at 666nm (instrument irradiance divided by Cimel-based reference irradiance) for the different radiometers as a function of Solar Zenith Angle. Data collected from the ascending sun is shown with bold symbols. The dotted lines show the combined $\pm 5\%$ radiometric uncertainty and a ± 2 degrees tilt angle uncertainty.

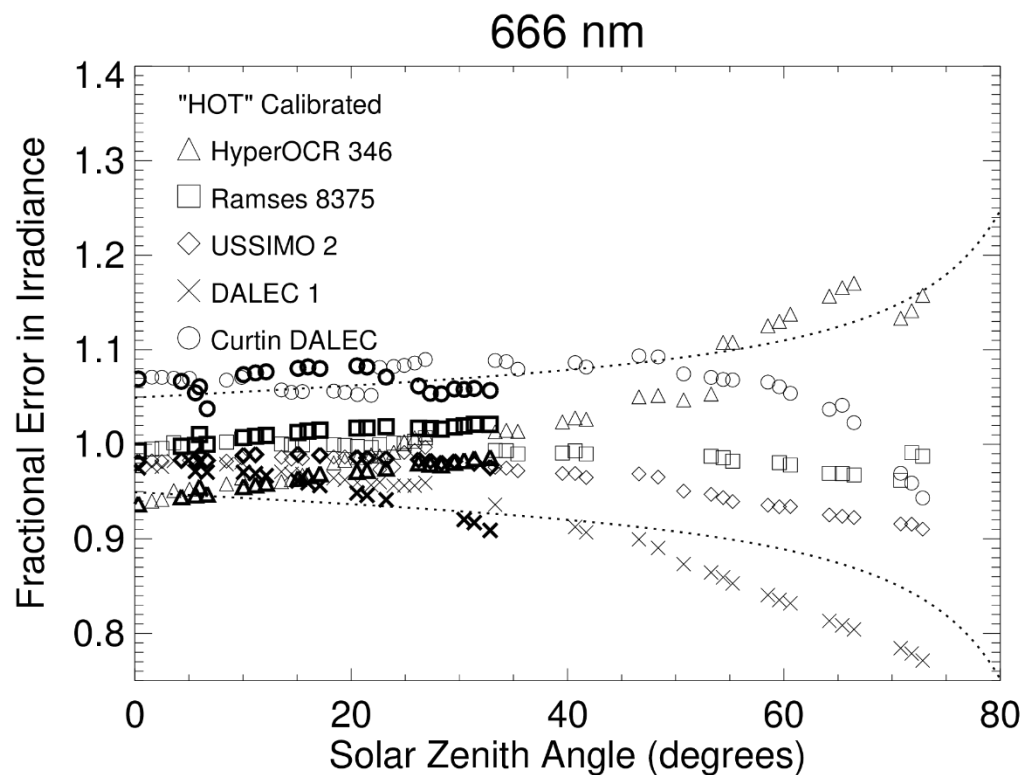


Figure 39: As in Figure 38, but for “Hot” calibration.

To observe the temperature dependency of sensor radiometric responsivity, the near-normal incidence irradiance measurements were processed with both “Room” and “Hot” calibrations, and plotted as a function of temperature difference between calibration temperature and field temperature (See Figure 40).

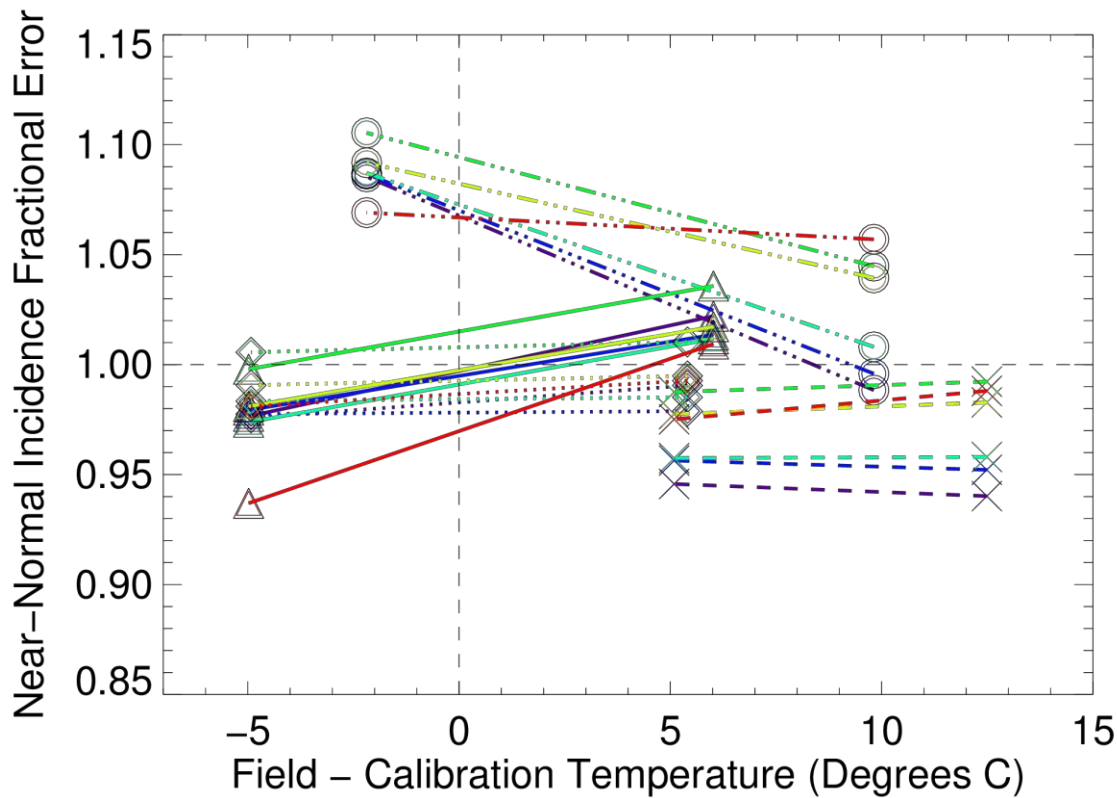


Figure 40: Near-Normal Incidence Fractional Error (Sensor / RADTRAN Reference) versus temperature differences in internal sensor temperatures between calibration and field conditions. The solid lines and triangles are from the HyperOCR and the dotted lines and diamonds are from the USSIMO. The crosses and dashed lines represent the IMOS DALEC, which was 5 degrees hotter than the hottest calibration measurement. The circle and dot-dash lines show the Curtin DALEC. Lines are colour coded by their apparent colour: (412nm is violet, 442nm is blue, 490nm is cyan, 530nm is green, 555nm is lime green, 666nm is red).

This figure demonstrates that for at least the USSIMO and Hyper-OCR, errors can be minimised if radiometric calibrations are performed closer to the temperature encountered during fieldwork (i.e. to achieve a Field - Calibration Temperature difference of zero).

To remove the effects of any systematic errors during calibration from the dataset and reveal the combined effects of sensor angular / cosine response⁶, the irradiance data from each respective sensor was normalised by its respective near-normal – incidence irradiance data. This normalised response was then further normalised by the equivalent near-normal – incidence normalised RADTRAN model output to produce an estimate fractional error in angular response.

⁶ Although note that internal temperature and SZA are coupled.

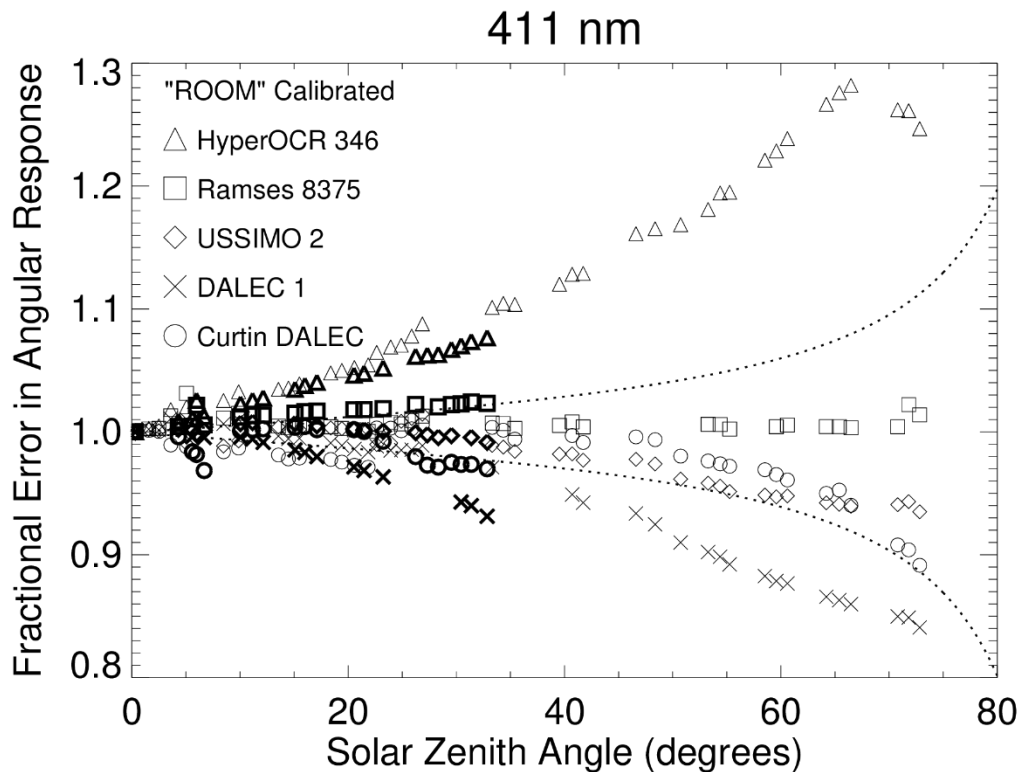


Figure 41: Fractional Error in Irradiance sensor angular response at 411nm. The dotted lines show a +/- 2 degrees tilt angle uncertainty. Data collected from the ascending sun is shown with bold symbols.

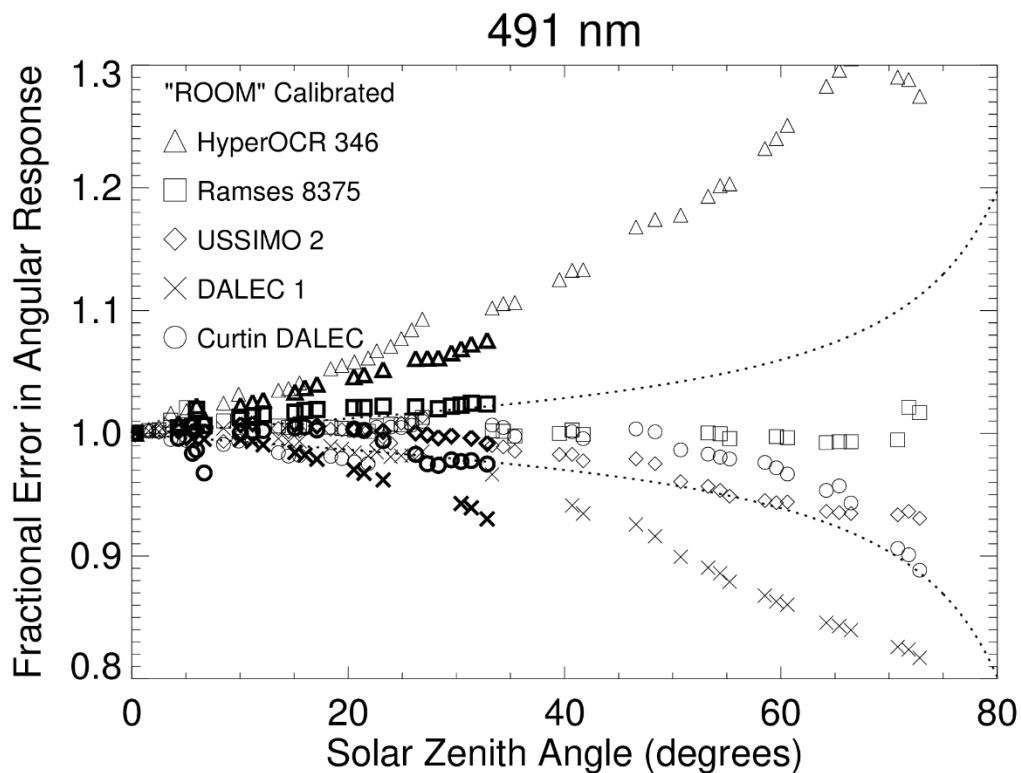


Figure 42: Fractional Error in Irradiance sensor angular response at 491nm. The dotted lines show a +/- 2 degrees tilt angle uncertainty.

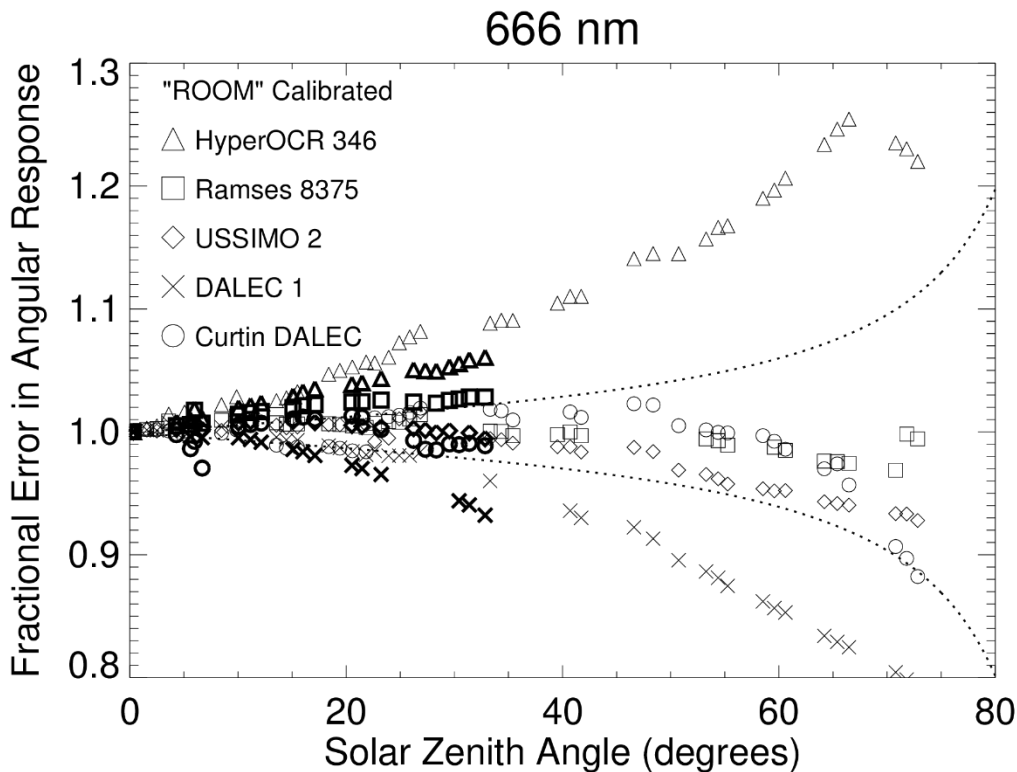


Figure 43: Fractional Error in Irradiance sensor angular response at 666nm. The dotted lines show a +/- 2 degrees tilt angle uncertainty.

Sea Radiance

Above water, sea viewing radiance measurements (L_t) contain contributions from below the water surface (L_w), which contain spectral information about hydrosols and particles suspended in the ocean. Even in ideal situations where there are no land or observer-introduced perturbations, above water radiance measurements are also influenced by skylight (ρL_{sky}), additional perturbations may occur from sun reflections and spectrally neutral foam from the air-water interface (ϵE_d), and also other contributions such as fluorescence and floating algae (k) if present. All of these terms are wavelength dependent.

$$L_t = L_w + \rho L_{sky} + \epsilon E_d + k$$

As a result of the surface-derived contributions, the measured sea viewing radiance is subject to high frequency temporal variability due to the wind-roughened nature of sea surface. For a given radiance sensor view angle, this introduces variability in the signal due to wind speed (wave facet angle changes and whitecaps / foam) and also solar zenith angle. In addition, differences in optical design, software and electronics amongst the different radiometers can affect this variability when viewing a dynamically changing target from a fixed ocean-sensor distance and view angle.

A given radiance sensor's Field Of View (FOV) will serve to spatially average surface-reflected contributions, so sensors with larger FOVs should exhibit less temporal variability if all other variables are held constant. In addition, sensors with higher integration times (i.e. the time over which photocurrent is collected prior to digitization) will also serve to smooth out temporally varying signals. This makes the sensors difficult to compare over short time scales (e.g. less than one minute).

Table 10 shows the details of the Sea radiance measurements performed during the LJCO experiment, including Solar Zenith Angle, Wind Speed and Sun-Relative Sensor Azimuth angle (RELAZ). Note, the SeaPRISM measurement on 9 Nov at 17:09 was only used in the radiance inter-comparison.

Table 10: Sea-viewing Radiance sensor related information

Date (2016)	Local Time	ID	SZA (deg)	SAZ (deg)	Wind (m/s)	IMO DALEC RELAZ (deg)	SAT RELAZ (deg)	Curtin DALEC RELAZ (deg)	RAMSES RELAZ (deg)	Matching SeaPRIS M Time
9th Nov	11:29	S02	6.0	85.7	6.0	96.7	25.7	-	25.7	-
9th Nov	12:11	S03	3.6	278.1	6.0	72.1	21.9	-	21.9	12:05
9th Nov	12:32	S04	8.5	272.3	6.3	80.3	27.7	85.5	27.7	12:32
9th Nov	13:31	S05	22.6	267.8	5.9	85.8	32.2	90.9	32.2	13:32
9th Nov	14:21	S07	34.3	265.4	6.9	-	34.6	88.5	34.6	14:32
9th Nov	14:48	S08	40.7	264.1	7.2	88.9	35.9	87.4	35.9	14:32
9th Nov	15:20	S09	48.4	262.6	6.5	87.4	37.4	85.8	37.4	15:10
9th Nov	15:45	S10	54.4	261.4	6.2	88.6	83.6	84.5	83.6	-
9th Nov	16:08	S11	59.6	260.3	6.2	89.7	84.7	83.5	84.7	16:00
9th Nov	16:32	S12	65.4	258.9	6.3	91.1	86.1	82.2	86.1	16:30
9th Nov	17:00	S13	71.8	257.4	6.9	92.6	87.6	80.7	87.6	(17:09)
10th Nov	9:39	S14	32.9	94.3	4.7	91.3	-	91.8	-	-
10th Nov	9:46	S14	31.6	94.1	5.0	89.1	-	101.1	-	-
10th Nov	9:49	S14	30.4	93.8	5.2	91.8	-	111.8	-	-
10th Nov	10:26	S15	21.5	92.7	6.5	87.3	77.7	111.5	77.7	-
10th Nov	10:50	S16	16.0	91.6	8.0	85.4	76.6	110.6	76.6	-
10th Nov	11:11	S17	11.2	90.4	8.7	82.6	75.4	109.4	75.4	-
10th Nov	11:33	S18	5.6	88.2	8.6	81.8	73.2	107.1	73.2	-
10th Nov	12:02	S19	1.6	279.2	7.9	62.2	65.8	118.2	65.8	12:05
10th Nov	12:58	S20	14.4	268.8	8.6	85.8	76.2	109.4	76.2	12:32
10th Nov	13:18	S21	19.4	267.7	9.6	83.7	77.3	108.3	77.3	13:04
10th Nov	13:29	S21	21.8	267.2	10.1	86.2	77.8	107.8	77.8	13:32
10th Nov	13:46	S22	25.9	266.4	10.4	86.4	78.6	73.1	78.6	14:04

Figure 44 shows an example 5-minute Sea-viewing Radiance time series, featuring the data from 4 different radiometers. Note that most plot symbols are overlapping, indicating good agreement, however there are outliers that may be due to differences in FOV or integration time.

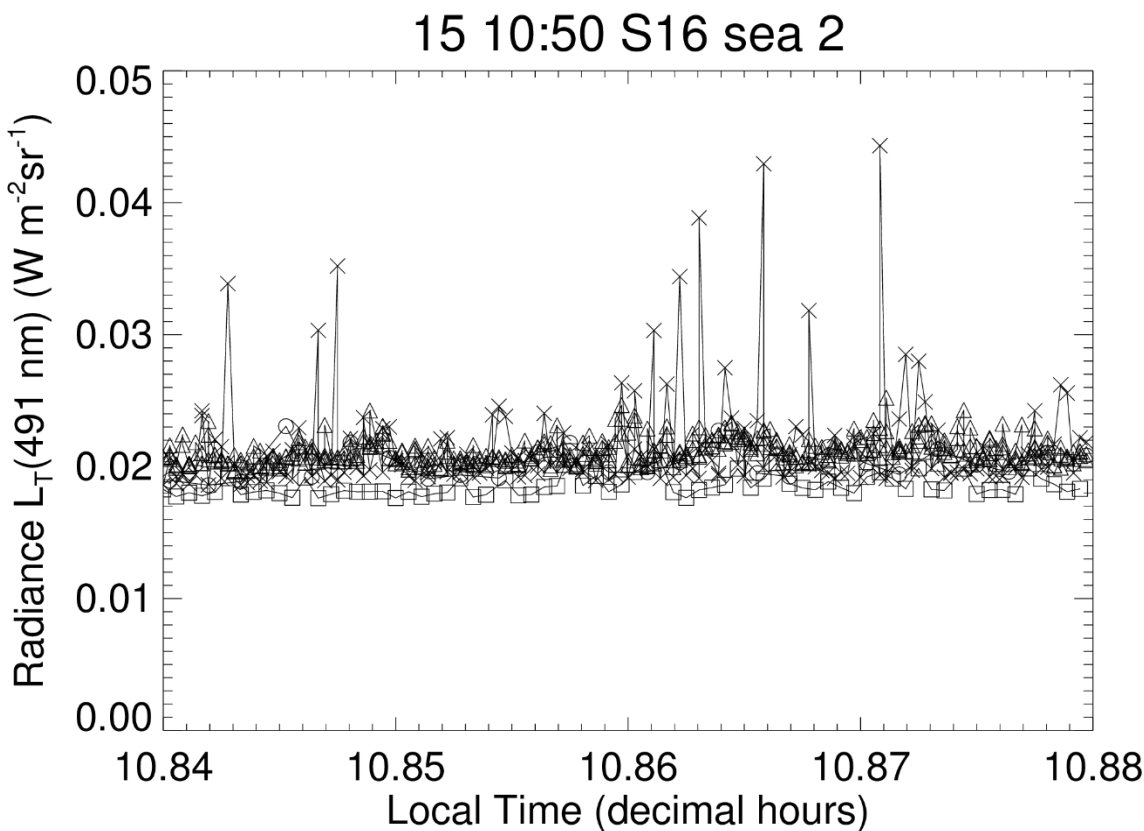


Figure 44: Example 491 nm Sea Radiance time series. Hyper-OCR data shown in triangles, RAMSES shown in squares, Curtin DALEC shown in circles, and IMOS DALEC shown with crosses. Note – the IMOS DALEC was viewing due north at a sun-relative azimuth angle of 91 degrees whereas the Curtin DALEC was at 110 degrees relative to the sun. The RAMSES and Hyper-OCR radiometers were pointed closer to 75 degrees from the sun.

Figure 45 shows example 5 minute averaged sea-viewing radiance (L_T) spectra for the 4 different types spectrometers used during this study. This data was collected with a high solar zenith angle of 16 degrees, a wind speed of 8 ms⁻¹ and sun-relative azimuth angles between approximately 75 and 110 degrees. All spectral shapes look consistent, however the RAMSES instrument exhibits a lower offset.

Figure 46 shows the normalised histograms of the same 5-minute sampling interval (shown previously in Figure 44) for the 4 different sea-viewing radiometers. Note that the IMOS DALEC has a larger spread of values than the Curtin DALEC, but comparable full-width half max deviation compared with the RAMSES and the Hyper-OCR. The IMOS DALEC dataset contains low numbers of high radiance values, and this may be attributable to differences in FOV, integration times or sun-relative view angles. Figure 47 shows the spectral standard deviation of the same dataset. Variation is partly due to changes in irradiance due to solar angle during the 5-minute sampling interval, however this spectral shape suggests sun glint may be a contributor. It is apparent that the IMOS DALEC sees more sun glint, more often than the other spectrometers. By viewing the spectrally normalised standard deviation, it can be seen that each spectrometer receives a slightly different sky-glint contribution, however the two radiometers aligned perfectly (RAMSES and HyperOCR) had more similar spectral standard deviations. Based on this observation, it is recommended that comparisons between sea-viewing radiometers only be performed based on skyglint-corrected data; where some variations due to different view angles will be minimised.

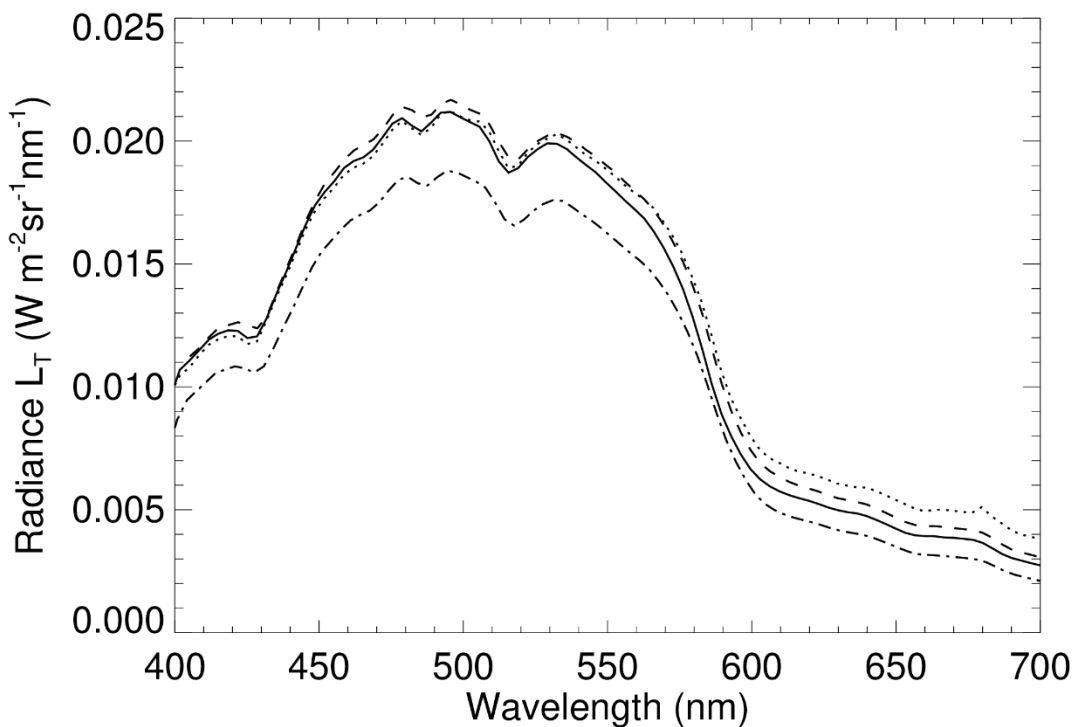


Figure 45: Example time-averaged Radiance (L_T) spectra from the data presented in Figure 44. The dashed line is IMOS DALEC (Corrected), the solid line is Hyper-OCR, the dotted line is Curtin DALEC and the dot-dashed line is the RAMSES. The “Room” temperature calibrations were used.

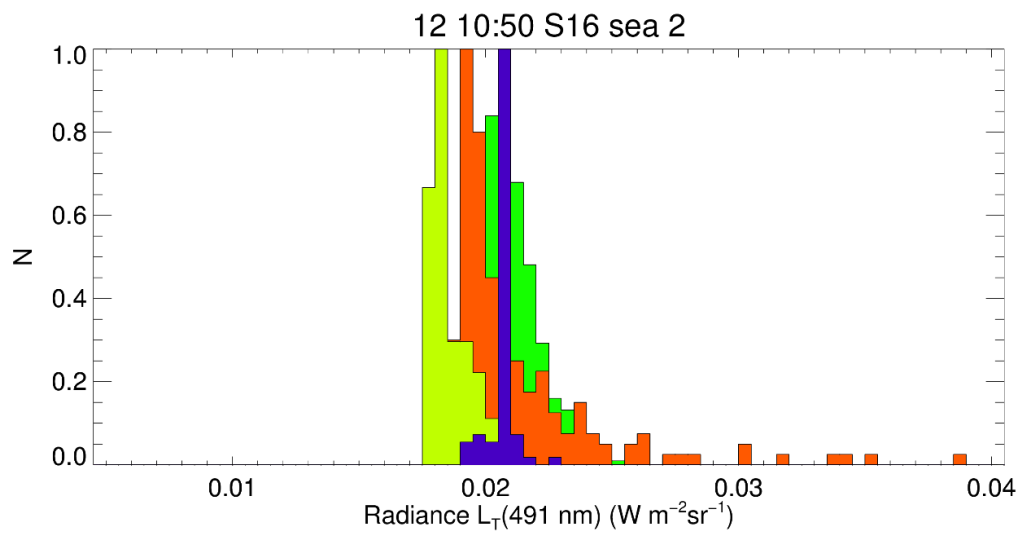


Figure 46: Example 5-minute time-series normalised histogram. RAMSES data shown in yellow, IMOS DALEC shown in orange, Hyper-OCR shown in green, and Curtin DALEC shown in Royal Blue. This data is the same 5-minute interval as shown in Figure 44 and Figure 45. Note – the IMOS DALEC, Curtin DALEC and RAMSES / Hyper-OCR had different sun-relative azimuth angles during this measurement.

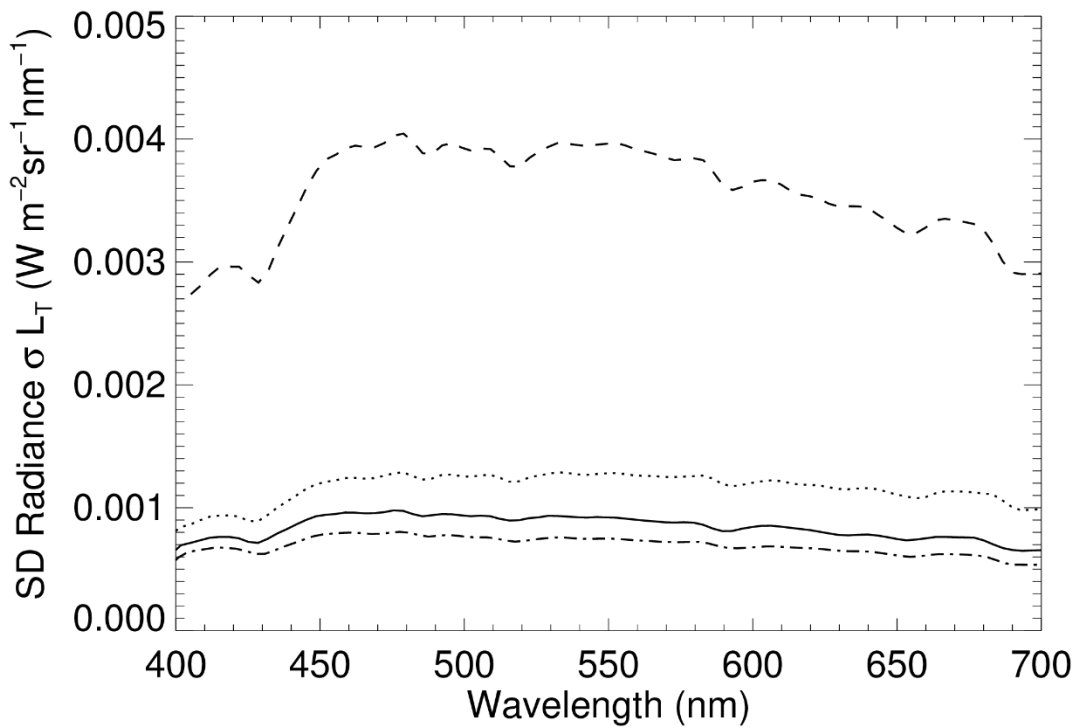


Figure 47: Example Standard Deviation Radiance (L_T) spectra from the data presented in Figure 30. The dashed line is IMOS DALEC (Corrected), the solid line is Hyper-OCR, the dotted line is Curtin DALEC and the dot-dashed line is the RAMSES.

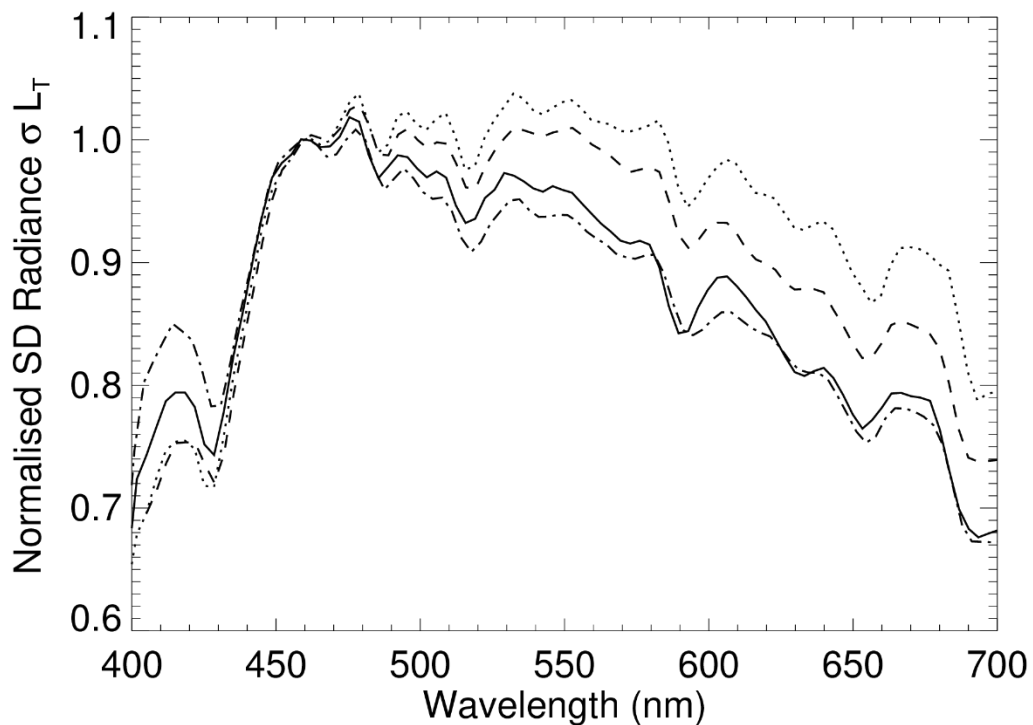


Figure 48: Normalised Standard Deviation (L_T) spectra from the data presented in Figure 30 (Reference wavelength for normalisation is 460nm). The dashed line is IMOS DALEC (Corrected), the solid line is Hyper-OCR, the dotted line is Curtin DALEC and the dot-dashed line is the RAMSES.

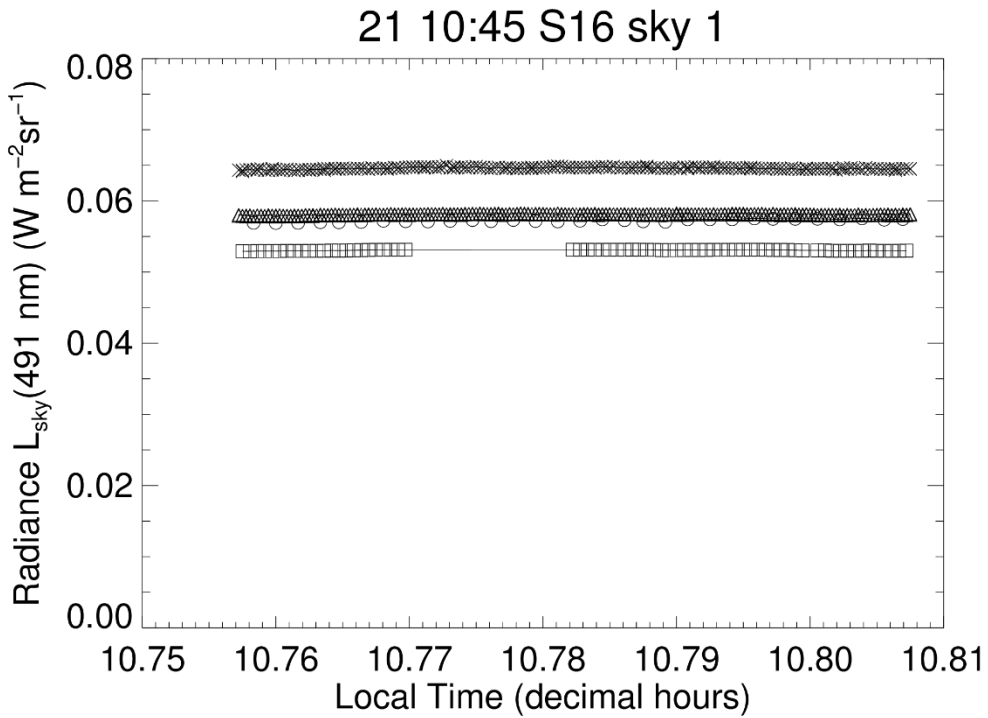


Figure 49: Example 491 nm Sky Radiance time series. Hyper-OCR data shown in triangles, RAMSES shown in squares, Curtin DALEC shown in circles, and IMOS DALEC shown with crosses. Note – the IMO DALEC was viewing due north at a sun-relative azimuth angle of 91 degrees whereas the Curtin DALEC was at 110 degrees relative to the sun. The RAMSES and Hyper-OCR radiometers were pointed closer to 75 degrees from the sun. Note data gap in RAMSES time series.

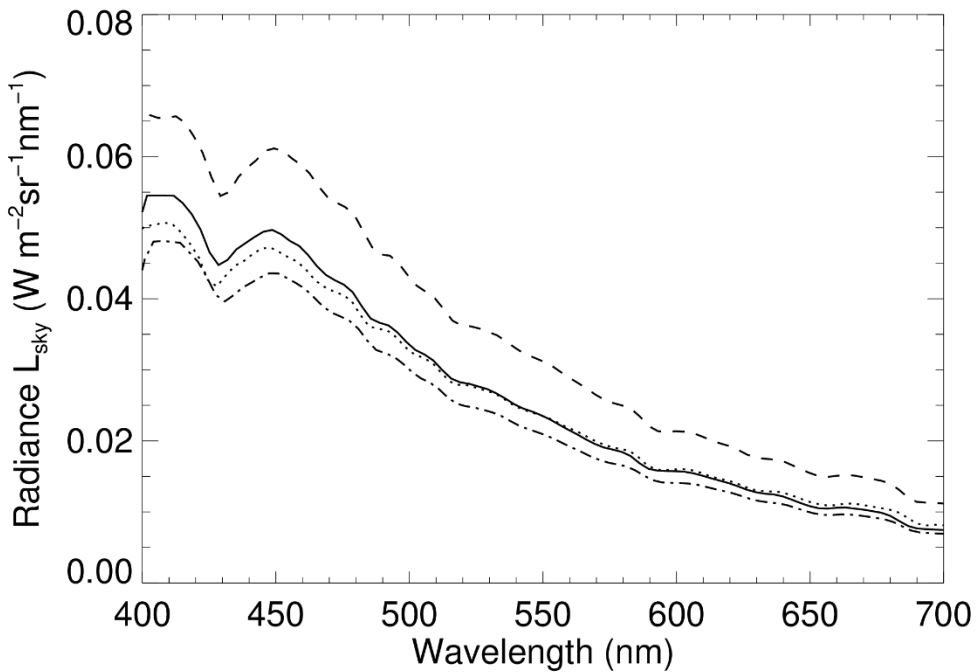


Figure 50: Example time-averaged Sky Radiance (L_{sky}) spectra from the data presented in Figure 30. The dashed line is IMOS DALEC (Corrected), the solid line is Hyper-OCR, the dotted line is Curtin DALEC and the dot-dashed line is the RAMSES. The “Room” temperature calibrations were used.

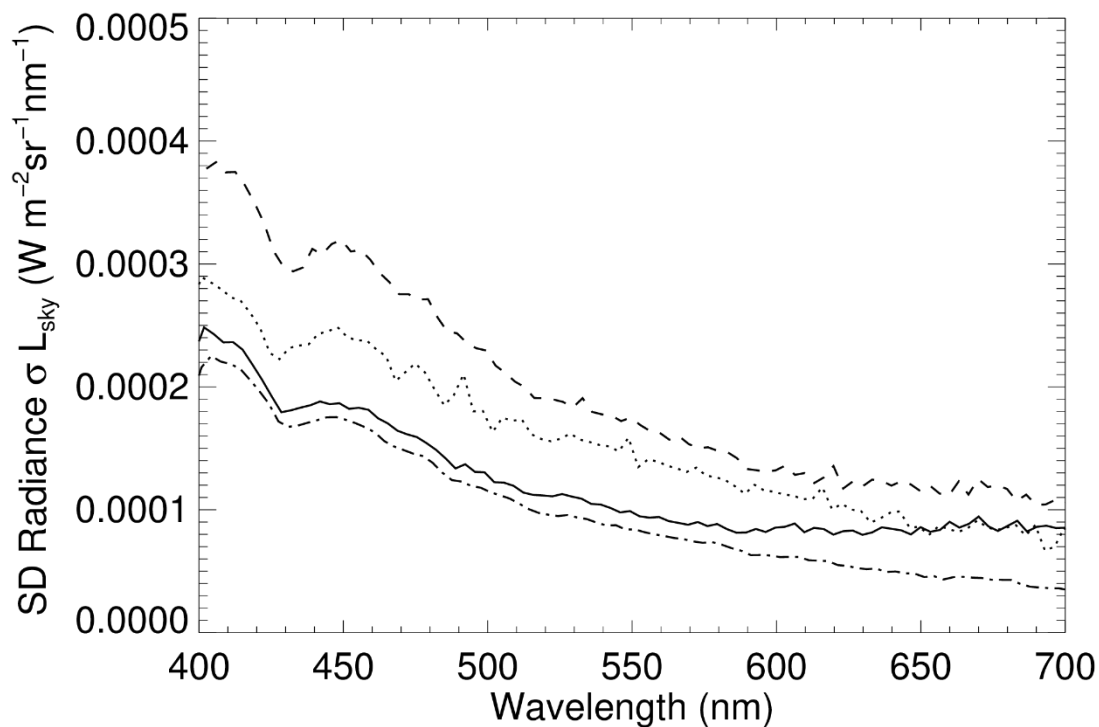


Figure 51: Normalised Standard Deviation (L_T) spectra from the data presented in Figure 30. The dashed line is IMOS DALEC (Corrected for pixel shift), the solid line is Hyper-OCR, the dotted line is Curtin DALEC showing spectral mismatch in the feature near 425nm and the dot-dashed line is the RAMSES.

Remote Sensing Reflectance

Background

A Remote Sensing Reflectance (R_{rs}) spectrum is determined by dividing the water-leaving radiance spectrum (L_w) by the downwelling irradiance spectrum (E_d). This normalises the spectrum so that the resultant information is less influenced by solar geometry and relatively more influenced by substances within the water:

$$R_{rs} = \frac{L_w}{E_d}$$

As discussed earlier, the measured sea-viewing radiance (L_t) depending on the sun and viewing geometry is contaminated by sun glint (ϵE_d), diffuse skylight reflection (ρL_{sky}) and potentially other surface features which may need to be removed (k) but are usually ignored or filtered by using the median Rrs or other statistical measures for a given measurement period (time window).

$$L_w = L_t - \rho L_{sky} - \epsilon E_d - k$$

The Remote Sensing Reflectance then becomes:

$$R_{rs} = \frac{L_t}{E_d} - \frac{\rho L_{sky}}{E_d} - \epsilon - \frac{k}{E_d}$$

Rho (ρ) has historically been presented as time-averaged, spectrally independent value equalling approximately 0.022 for calm sea state conditions up to 0.028 for optimal viewing conditions (Mobley, 1999). The Mobley 1999 paper described the dependence of ρ on sun-relative sensor azimuth, sun angle, sensor view angle, and wind speed, and geometry-specific calculations based on this paper have been used as the basis for corrections applied to SeaPRISM data (Zibordi, Hooker, F., & D'Alimonte, 2002), incorporated into their $S95_a$, $S95_m$, and $S00$ methodology.

Some researchers choose to model ρ as a function of wind speed for restricted sets of experimental geometries (Ruddick, 2006). Further spectrally-independent ρ values were calculated considering polarisation of the sea surface (Mobley, Polarized reflectance and transmittance properties of windblown sea surfaces, 2015), referred to as *M15*.

As the skylight reflection captured by a spectrometer (for one given sample) is dependent on a moving sea state, it is then also a function instrument FOV and integration time. Furthermore, as the spectral shape of L_{sky} varies with view angle, solar azimuth and solar zenith, it follows that so too must the spectral shape of ρ . Accordingly, a spectrally-dependent Hydrolight-based Look Up Table (LUT) was created which retrieves the spectral ρ factor for a variety of wind speeds, sun-relative sensor azimuths, solar zenith angles, and sensor view angles for clear sky conditions (Slivkoff, 2014). Additionally, a tropical (warm) water Near Infra-Red (NIR) similarity spectrum was calculated based on temperature-dependent water absorption measurements (Rottgers, McKee, & Utschig, 2014) combined with Great Barrier Reef (GBR) region specific backscattering spectra (Slivkoff, 2014, pp. 128-132). By spectrally fitting the similarity spectrum to the rho-corrected data in the NIR region using numerical optimisation technique, the residual sun glint ϵ can be determined without assuming $R_{rs}(NIR)=0$. This approach is referred to as *MS14*.

Some researchers prefer to use statistical means to reduce skylight and glint contamination. Whereas the $S95_a$ method uses averaged data from 3 repeat spectral measurements of L_t to produce what is referred to as L_{t_mean} , the $S95_m$ method uses the lowest value recorded for each wavelength based on a set of 3 spectral measurements, yielding L_{t_min} (Zibordi, Hooker, F., & D'Alimonte, 2002). This statistical approach in effect, reduces the $\frac{\rho L_{sky}}{E_d} - \epsilon - \frac{k}{E_d}$ terms, however it cannot remove the effects of invariant skylight reflection typical of high solar zenith angles, especially with larger FOV sensors, so is still combined with the skylight correction (Mobley, 1999) in the $S95_m$ method.

⁷This fact must also be acknowledged for other datasets when considering that a tilted DALEC or HyperSAS-style sensor can result in a large angular mismatches between the Nadir-relative view angle (L_u) and the required complementary zenith-relative view angle (L_{sky}).

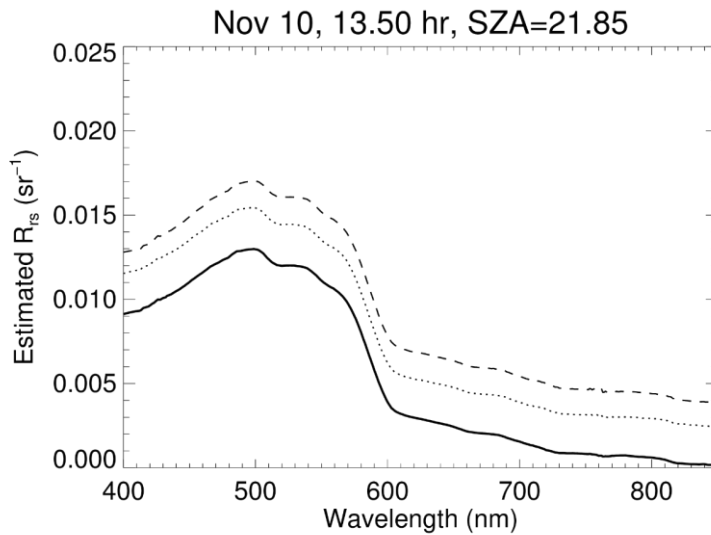


Figure 52: Estimated IMOS DALEC Rrs spectra with no skylight correction. Dashed line is based on the average L_t spectrum within the 5 minute period, the dotted line is based on the median and solid line is based on the mean of the lowest 10% of measurements.

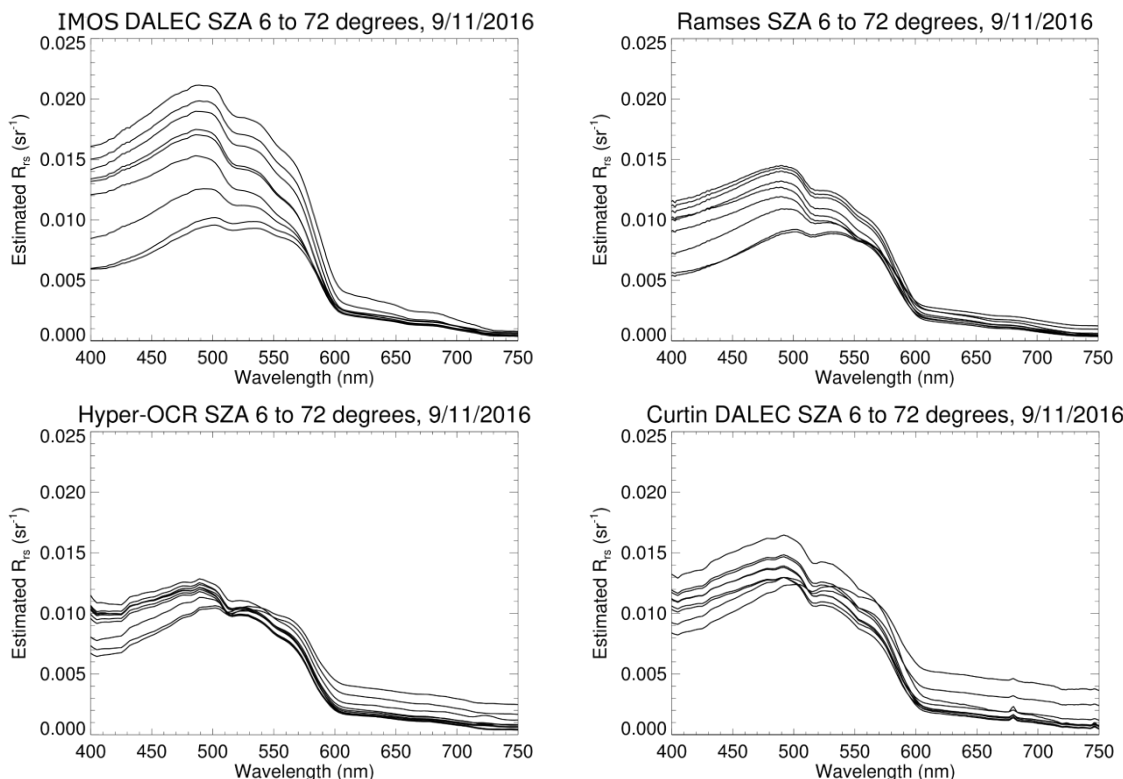


Figure 53: Estimated glint and skylight-uncorrected R_{rs} spectra for IMOS DALEC (top left), RAMSES (top right), Hyper-OCR (bottom left) and Curtin DALEC (bottom right) for the setting sun on Nov 9th, 2016. Each spectrum is an average of the lowest 10% reflectance spectra measured in a 5-minute period. Reflectance increased with solar zenith angle. The irradiance sensor of the Hyper-OCR has the cosine collector optimised for underwater use, so large errors are expected at high solar zenith angles.

Radiance-Comparison with SeaPRISM

Four SeaPRISM data products distributed by NASA-AERONET are of interest in this study; L_{t_mean} is the mean of 3 sea-viewing radiance measurements. L_{t_StdDev} is the standard deviation of these 3 measurements, L_{t_min} is the minimum of the 3 sea-viewing radiance measurements and L_w is the sky and glint corrected water-leaving radiance estimated with the $S95_m$ method (Zibordi, Hooker, F., & D'Alimonte, 2002).

During the course of the 5-minute measurement sequences made with the hyperspectral instruments described previously, the autonomous SeaPRISM captured data on approximately 30 min intervals. A few SeaPRISM

measurements were made close to the times when the hyperspectral radiometers were viewing the ocean surface (see Table 10), and this allowed comparison between the SeaPRISM and the hyperspectral equivalents.

The RTT Sea-viewing radiance dataset was processed with a series of different methods to quantify the differences between the aforementioned skylight reflection correction studies. The corrections were performed on mean L_t , median L_t and the mean of the lowest 10% of L_t data measured within 5 minutes. For each of these inputs, 4 different surface correction approaches were made. Each surface correction used the aforementioned GBR-tuned similarity spectrum approach MS14 to remove spectrally-constant sun glint, without having to assume $L_w(\text{NIR})=0$. The first method ignored sky reflection (Glint-only), the second correction was based on the spectrally-dependent ρ value with inputs for wind speed, sun-relative azimuth angle and solar zenith angle. Third, the latest spectrally constant ρ factors from Mobley 2015 were used, and then finally, the spectrally constant ρ factors from Mobley 1999 were used; consistent with the SeaPRISM skylight correction. This produced 12 sets of spectra for each sensor for comparison. Although the residual glint and skylight corrections are typically applied to R_{rs} , the corrections can also be applied to L_t to estimate L_w , and considering the errors in E_d , the effect of skylight reflection on the radiance product is treated separately.

Figure 54 compares the SeaPRISM $L_{t,\text{mean}}$ data products with the equivalent, 5 minute averaged, sun-glint only corrected L_t measurements from each spectrometer. Figure 55 compares the SeaPRISM $L_{t,\text{min}}$ data products with the equivalent, mean lowest 10% of data recorded in the 5-minute period, sun-glint only corrected L_t measurements from each spectrometer. Figure 56 compares the SeaPRISM L_w data products with the equivalent, mean lowest 10% of data recorded in the 5 minute period, and sky and sun-glint corrected (Slivkoff, 2014) L_w measurements from each spectrometer.

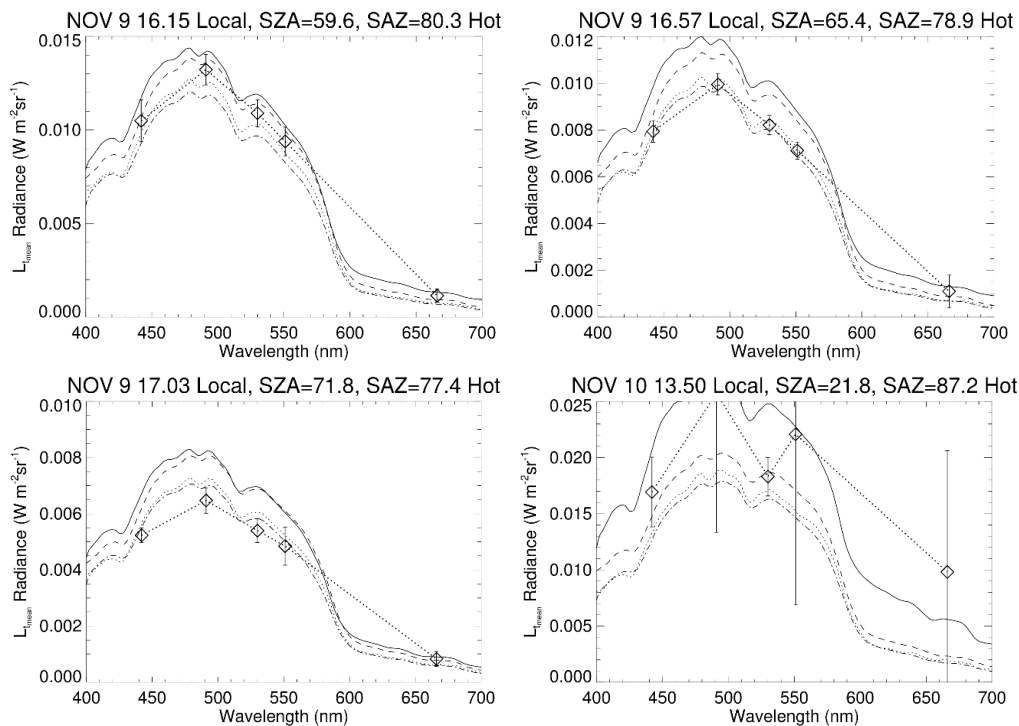


Figure 54 Near-coincident $L_{t,\text{mean}}$ Radiance products. The dashed line is IMOS DALEC (Corrected), the solid line is Hyper-OCR, the dotted line is Curtin DALEC and the dot-dashed line is the RAMSES. The “Hot” temperature calibrations were used. The diamond plot symbols show the SeaPRISM $L_{t,\text{mean}}$ data, with error bars equivalent to +/- one standard deviation of $L_{t,\text{mean}}$. Note, local times expressed in decimal hours. The hyperspectral data are the 5-minute mean data, corrected for glint only.

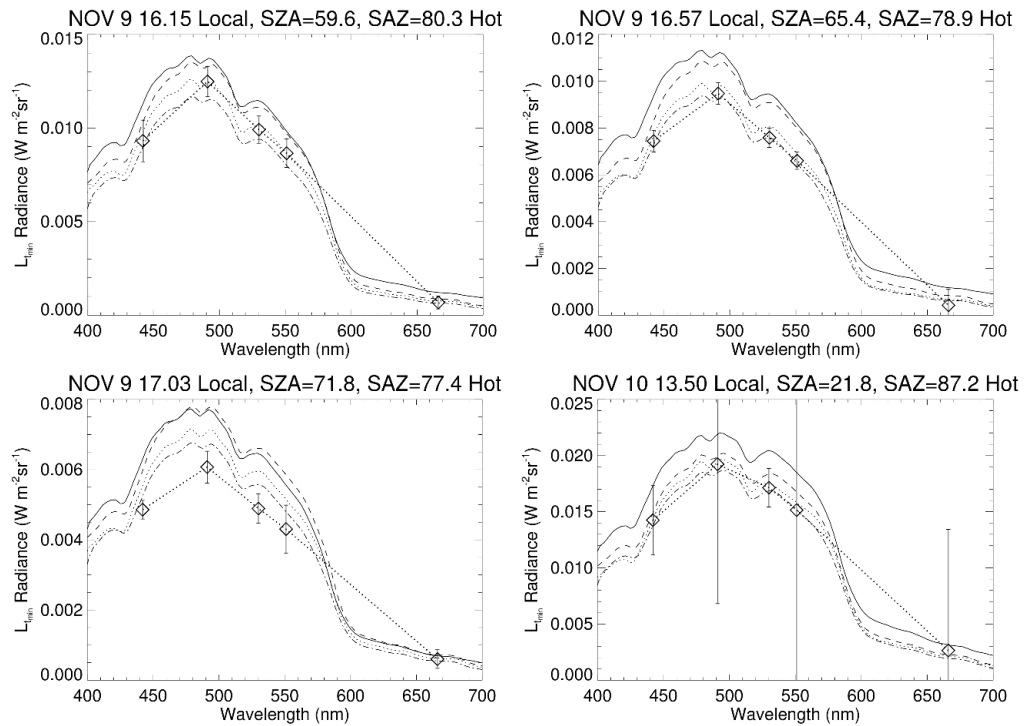


Figure 55. Near-coincident $L_{t\text{-min}}$ Radiance products. The dashed line is IMOS DALEC (Corrected), the solid line is Hyper-OCR, the dotted line is Curtin DALEC and the dot-dashed line is the RAMSES. The “Hot” temperature calibrations were used. The diamond plot symbols show the SeaPRISM $L_{t\text{-min}}$ data, with error bars equivalent to +/- one standard deviation of $L_{t\text{-mean}}$. Note, local times expressed in decimal hours. The hyperspectral data are the mean lowest 10%, and corrected for sun glint.

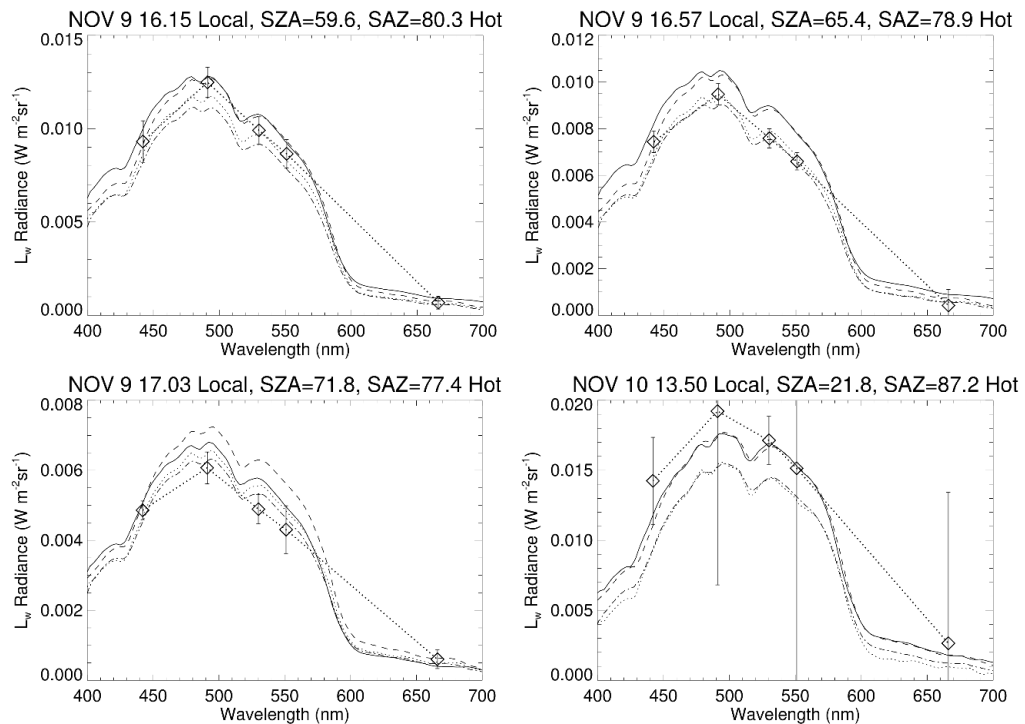


Figure 56. Near-coincident L_w . The dashed line is IMOS DALEC (Corrected), the solid line is Hyper-OCR, the dotted line is Curtin DALEC and the dot-dashed line is the RAMSES. The “Hot” temperature calibrations were used. The diamond plot symbols show the SeaPRISM L_w data, with error bars equivalent to +/- one standard deviation of $L_{t\text{-mean}}$. The hyperspectral data are the mean lowest 10%, and sky and sun-glint corrected (Slivkoff, 2014).

Generally, the radiance measurements for the mean, min and skylight corrected scenarios compared well with each other, considering the standard deviations experienced by the SeaPRISM, combined with issues with integration time, linearity, temperature effects (which have been minimised), sampling time mismatch and radiance sensor field of view differences between sensors. It is interesting to note the significant improvement in the SeaPRISM L_{t_min} product for the November 10, 13:30pm measurement compared with the L_{t_mean} equivalent. When observing the same measurement, the L_w equivalents compare less well between instruments, suggesting that these differences may result from variations in skylight correction procedures between the SeaPRISM and the hyperspectral products. This uncertainty needs to be explored further, with a more focused and comprehensive if SeaPRISM data is to be used to validate above water hyperspectral radiometer data.

With the limited dataset collected for these purposes, a brief qualitative comparison analysis was performed using the SeaPRISM L_w data. The last matchup where SZA = 21.8 was removed from the analysis due to high variability in the SeaPRISM L_w data. With the remaining 3 matchups (SZA 59.6, 65.4 and 71.8 degrees), the different hyperspectral sensor (4) L_w products produced with the different skylight correction methods (4) and input data (2) were compared. For selected wavelengths (442, 491, 530 and 551 nm), a slope and an offset (hyperspectral instrument *vs.* SeaPRISM) was fitted for each wavelength and each L_w product variant. This produced 128 different slopes and intercepts.

Generally, for all instruments and correction types, the slopes at 442 were between 3 and 20% higher than at longer wavelengths, indicating a spectral bias in all hyperspectral radiometers compared with the SeaPRISM, or spectral bias in all skylight correction approaches. To identify the least spectrally biased approach, the wavelength dependent slopes for a given sensor and approach were averaged and the standard deviation was calculated. The lowest spectrally averaged slope deviations occurred with the DALEC L_w products using average of the lowest 10% of the data. Of that group, the lowest spectral differences occurred where skylight correction was performed (as opposed to glint-only correction).

In terms of spectrally averaged slope, the HyperOCR L_w products (regardless of skylight correction or input type) compared better with the SeaPRISM than the Curtin DALEC and the RAMSES data, and similarly to the IMOS DALEC data, potentially suggesting that the overall radiometric accuracy of a spectrometer has a greater influence on the comparison with the SeaPRISM than the type of skylight correction approach used (see Figure 57). It is worth noting that the HyperOCR radiance meter software did not automatically collect the dark shutter measurements during deployment, so a manual dark offset had to be applied to the data. This may have had implications on the overall accuracy of the HyperOCR meter.

In terms of spectrally averaged offsets, all hyperspectral radiometers consistently exhibited offsets of between 0.0009 to 0.0027 $\text{Wm}^{-2}\text{sr}^{-1}$. This may be due to incomplete glint correction applied to all hyperspectral radiometers, however the theory behind the non-zero glint offset correction is sound.

Further work is needed on understanding the magnitude and spectral effects on skylight reflection contamination, however with this limited dataset, it appears as though instrument-specific variability on the radiometric calibration is a larger source of uncertainty than the type of skylight correction applied.

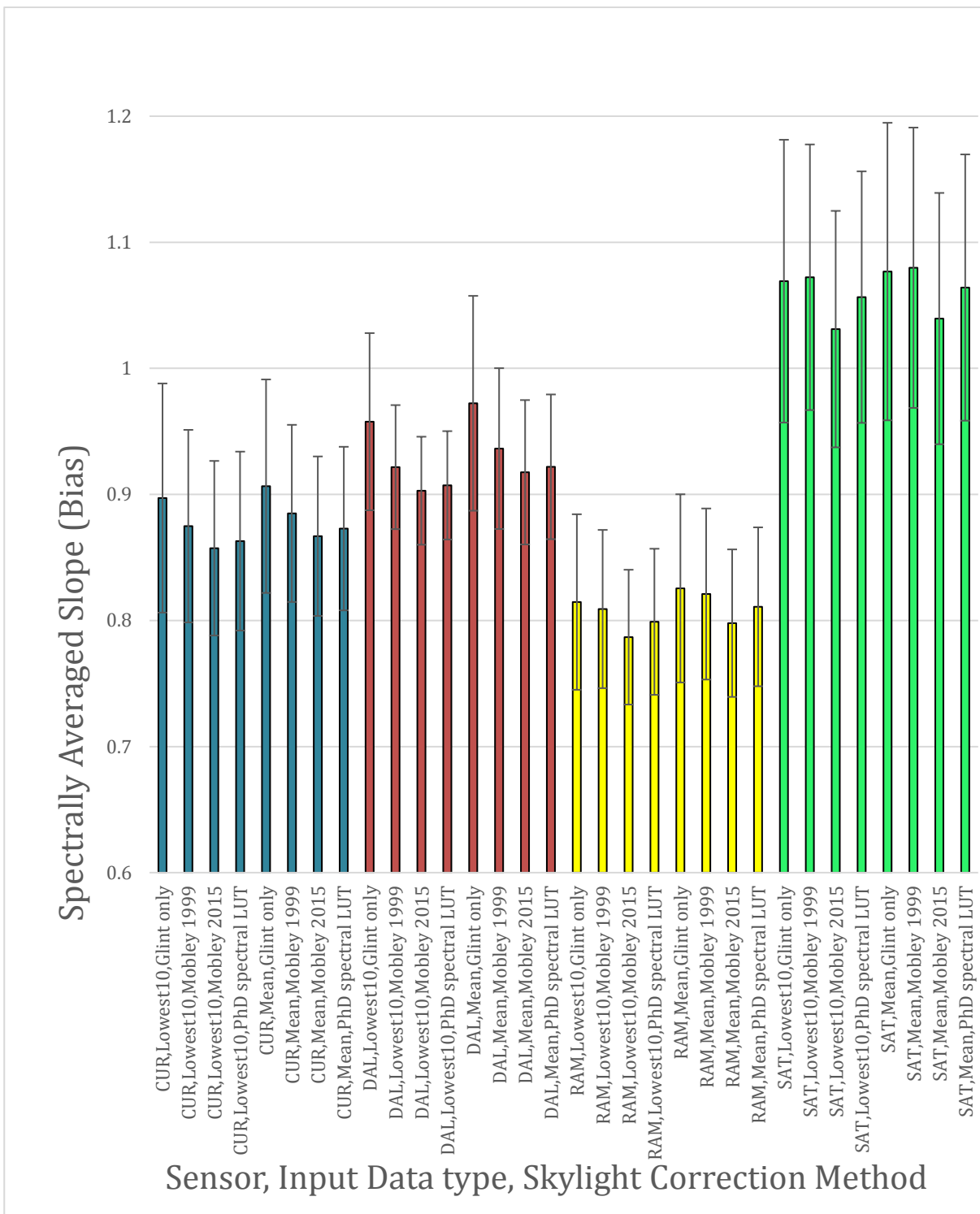


Figure 57: Spectrally Averaged Slope for different sensors and skylight correction methods compared to the SeaPRISM data (Error bars denote standard deviation of the spectrally-averaged slopes. The wavelengths used in average were 442, 491, 530 and 551nm). Hot calibrations were used. Note the Y-axis finished at a slope of 0.6.

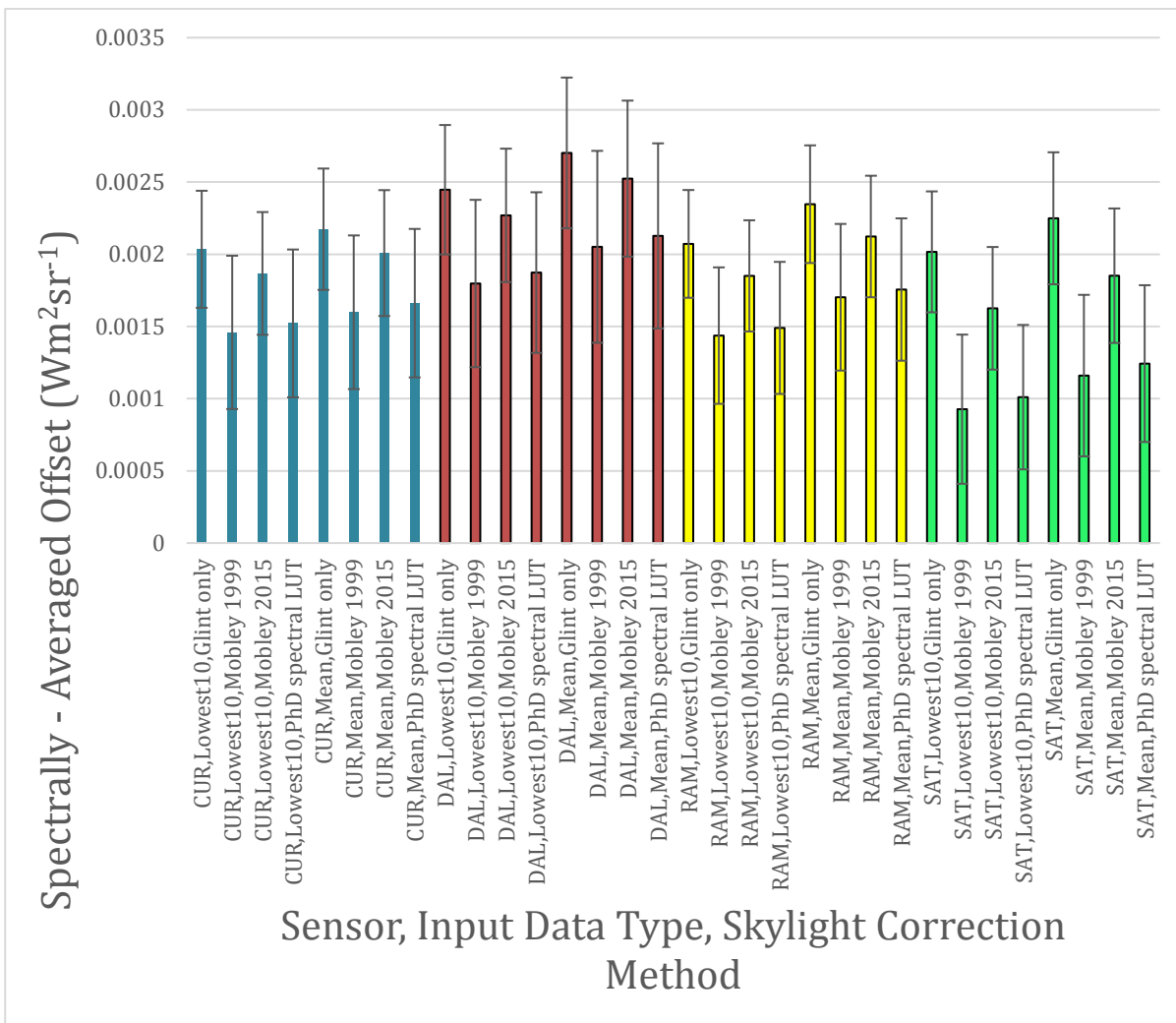


Figure 58: Spectrally Averaged Offset for different sensors and skylight correction methods compared to the SeaPRISM data (Error bars denote standard deviation of the spectrally-averaged offsets. The wavelengths used in average were 442, 491, 530 and 551nm). Hot calibrations were used.

Reflectance comparison with SeaPRISM

This section describes the inter-comparison of DALEC and AERONET-OC SeaPRISM derived above-water remote sensing reflectance, which in the framework of this study was considered as reference instrument. All other instrument configurations did not allow consistent computation of reflectance using concurrent triplicates of L_{sky} , L_{sea} and E_d measurements.

The SeaPRISM normalized water-leaving radiance data was obtained from NASA-AERONET in Level 1.5 cloud-screened quality and subsequently converted into remote sensing reflectance by normalizing to the Sun-Earth distance corrected extraterrestrial solar irradiance (Thuillier et al., 2003). The (DALEC) field observations could not be fully aligned in time with the SeaPRISM measurements (see Table 10), which follows an automated schedule of frequent atmospheric measurements followed by sea measurements at approximately 30 min intervals. The closest in time matching DALEC observations were selected for the radiometric comparison. A total number of 10 matching DALEC and SeaPRISM observations within a maximum time difference of 5 min were acquired on both days. Extending the maximum time difference between observations to 22 min resulted matching 13 spectra (Fig 56-58).

The DALEC data from both instruments was consistently processed by applying the hot calibration coefficients and the Mobley 2015 skylight correction, which is used as standard for processing the IMOS en-route data (Brando et al., 2016). The DALEC L_t data was not temporally averaged (as described in the previous radiance section) prior to the computation of the reflectance. Instead the instantaneous remote sensing reflectance was

computed from which the median remote sensing reflectance spectra were extracted and subsequently interpolated to the SeaPRISM bands.

The instantaneous DALEC spectral data presented in Figs. 56-58 show the temporal variability within each of the approximately 5 min measurement intervals. Some of the Curtin DALEC observations exhibit large variability (e.g. S03_1, Fig 43), which are possibly a result of a slow adjusting integration time. The median was still found a robust measure for determining the most representative spectrum within the 5-min measurement intervals even for the highly variable Curtin DALEC data, which for other applications (e.g. comparison with satellite data) would have been excluded.

The computed IMOS DALEC reflectance on 9 Nov for measurement sequences S07_1 to S12_2, correspond to solar zenith angles above 33 degrees and clearly show an overestimation compared to the SeaPRISM observations. This is likely a result of the poor cosine response of the irradiance sensor resulting in an underestimation the of the irradiance E_d as shown by the fractional error irradiance analysis (Figure 34-Figure 39).

Restricting the solar zenith to smaller angles (e.g. below 33 degree) result in a much better alignment of the IMOS DALEC with the SeaPRISM observations as shown by the scatter plots in Figs. 59 and 60 and reduces the spectrally averaged bias by a factor of 2 (see Tables 11 and 12) from 0.018 to 0.009 sr⁻¹. The Curtin DALEC in contrast shows a slightly negative bias of 0.009 sr⁻¹ and is underestimating the SeaPRISM observations on average. The spectrally averaged mean absolute percentage differences of IMOS and Curtin DALEC's with respect to the SeaPRISM are 52% and 45% respectively. The IMOS DALEC shows lowest percentage errors in the blue region of the solar spectrum at 412 nm, while the Curtin instrument performs best in the green spectral region at 491 nm (Table 12**Error! Reference source not found.**). DALEC measurements are highly correlated with the SeaPRISM observations ($R=0.96-0.99$) and shows similar spectrally averaged absolute errors (RMSE) of 0.012 sr⁻¹.

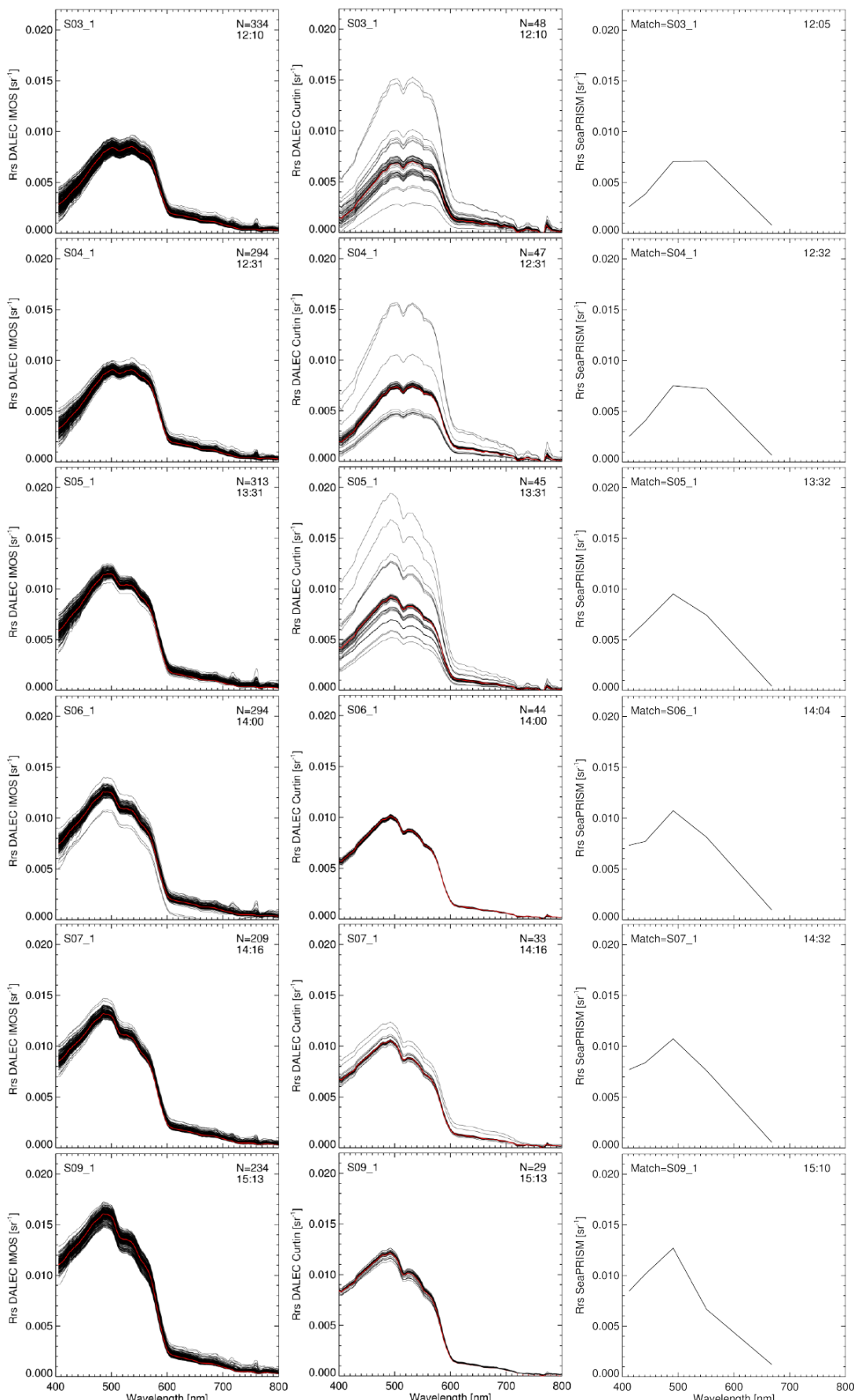


Figure 59: IMOS DALEC (left), the Curtin DALEC (centre) and SeaPRISM (right) reflectance spectra for 8 sequences on 9 Nov 2016 (see Tab. 3). DALEC sequence length approximately 5 minutes with median spectra shown in red.

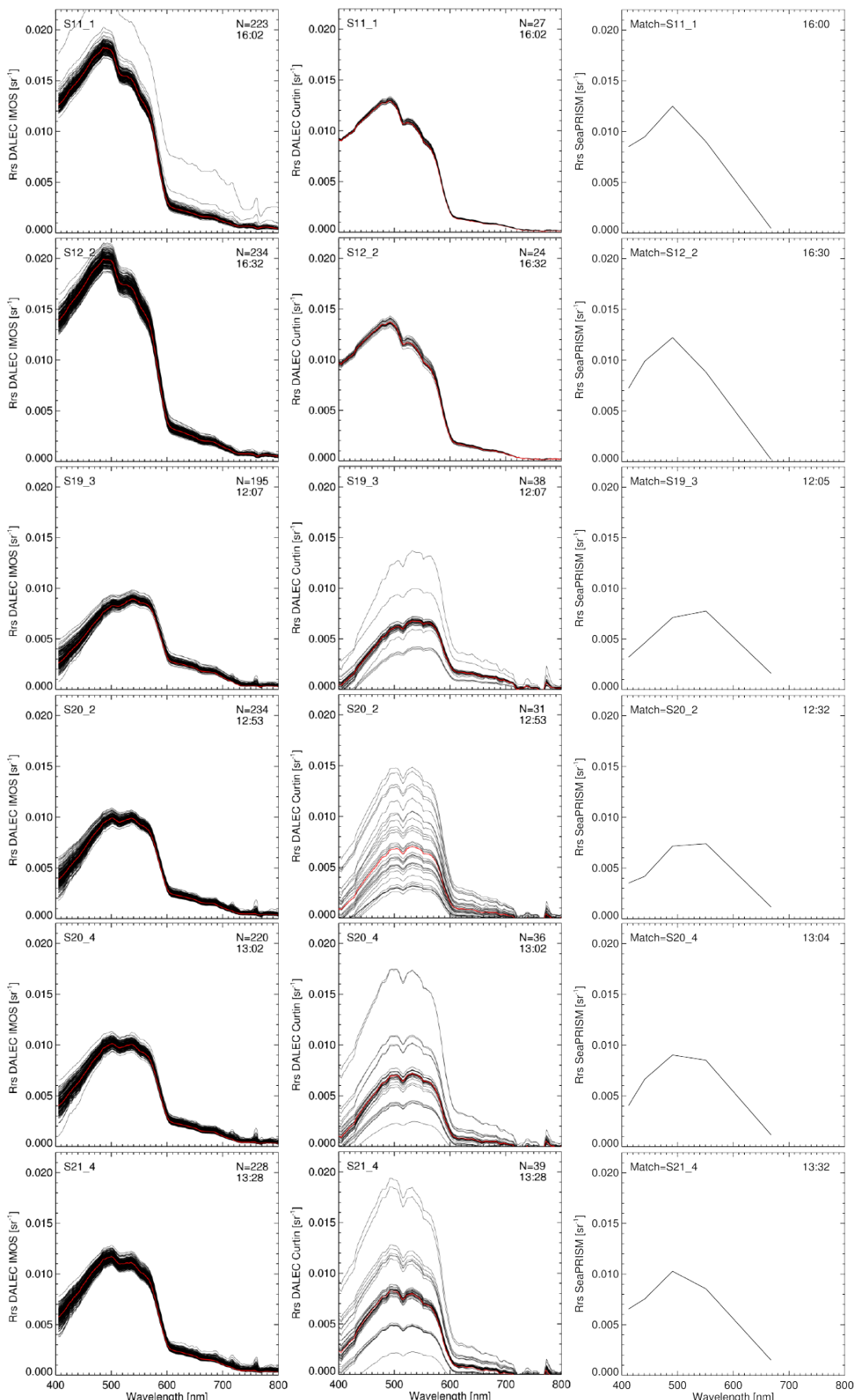


Figure 60: IMOS DALEC (left), the Curtin DALEC (centre) and SeaPRISM (right) reflectance spectra for 8 sequences on 9 and 10 Nov 2016 (see Tab. 3 and 4). DALEC sequence length approximately 5 minutes with median spectra shown in red.

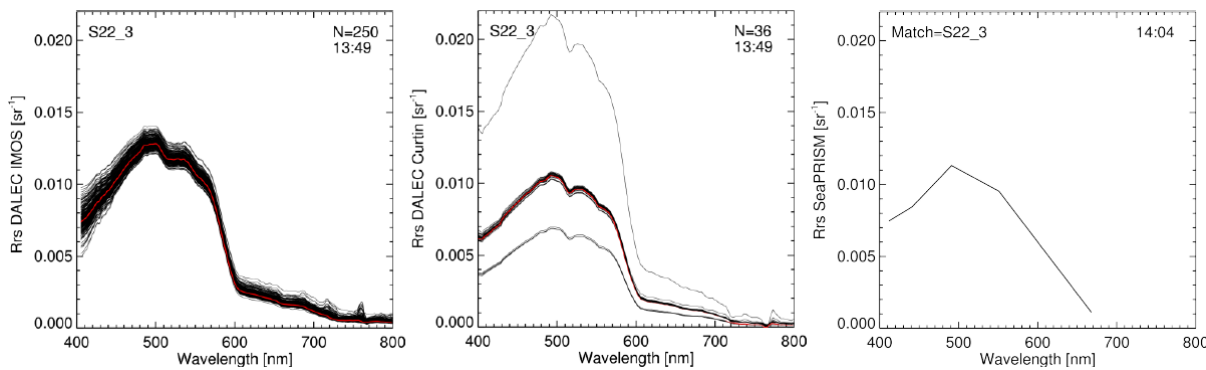


Figure 61: IMOS DALEC (left), the Curtin DALEC (centre) and SeaPRISM reflectance spectra for the final sequences acquired on 10 Nov 2016 (see Tab. 4). DALEC sequence length approximately 5 minutes with median spectra shown in red.

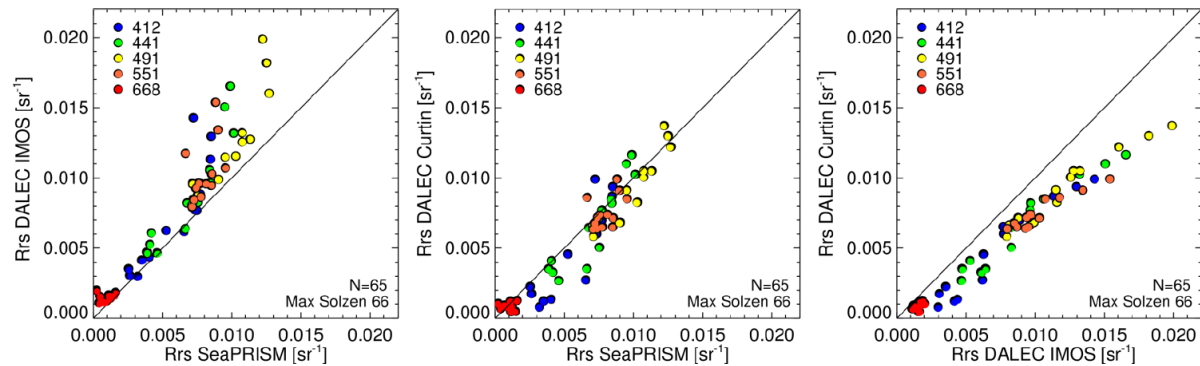


Figure 62: Scatter plots of IMOS DALEC versus SeaPRISM estimated reflectance (left), Curtin DALEC versus SeaPRISM (centre) and DALEC versus DALEC (right) measurements at five wavelengths and maximum solar zenith angles of 66 degrees.

Table 11: Spectral statistics of the IMOS and Curtin DALEC estimated reflectance with reference to the SeaPRISM observations shown in Fig. 59. Spectrally averaged results are listed in the last column.

Wavelength [nm]		412	441	491	551	668	412-668
MAPE [%]	DALEC IMOS	64	71	61	76	342	123
	DALEC Curtin	82	39	24	31	180	71
RMSE [10^{-3} sr $^{-1}$]	DALEC IMOS	2.5	2.8	3.2	2.9	0.7	2.4
	DALEC Curtin	1.9	1.4	1.1	1.1	0.4	1.2
BIAS [10^{-3} sr $^{-1}$]	DALEC IMOS	1.4	2.0	2.5	2.3	0.6	1.8
	DALEC Curtin	-0.9	-0.4	-0.6	-0.4	-0.1	-0.5
R	DALEC IMOS	0.87	0.92	0.92	0.50	0.21	0.94
	DALEC Curtin	0.87	0.92	0.94	0.48	-0.07	0.95

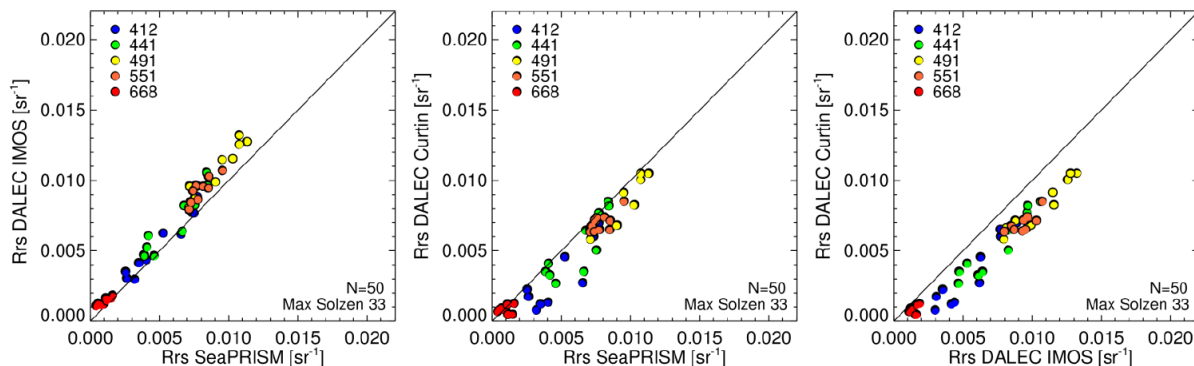


Figure 63: Scatter plots of IMOS DALEC versus SeaPRISM estimated reflectance (left), Curtin DALEC versus SeaPRISM (centre) and DALEC versus DALEC (right) measurements at five wavelengths and maximum solar zenith angles of 33 degrees.

Table 12: Spectral statistics of the IMOS and Curtin DALEC estimated reflectance with reference to the SeaPRISM observations shown in Figure 60. Spectrally averaged results are listed in the last column.

Wavelength [nm]		412	441	491	551	668	412-668
MAPE [%]	DALEC IMOS	27	40	34	36	121	52
	DALEC Curtin	72	32	20	22	79	45
RMSE [10 ⁻³ sr ⁻¹]	DALEC IMOS	0.7	1.4	1.6	1.5	0.5	1.2
	DALEC Curtin	1.9	1.4	1.1	1.0	0.5	1.2
BIAS [10 ⁻³ sr ⁻¹]	DALEC IMOS	0.5	1.1	1.5	1.4	0.4	0.9
	DALEC Curtin	-1.6	-0.9	-0.9	-0.9	-0.2	-0.9
R	DALEC IMOS	0.97	0.94	0.96	0.84	0.91	0.99
	DALEC Curtin	0.88	0.85	0.92	0.70	0.75	0.96

Conclusions

Through this RTT field exercise, two separate wavelength calibration issues were identified with each DALEC (IMOS and Curtin). These issues are easily avoided with the adoption of a wavelength calibration check during the routine (i.e. at least yearly) radiometric calibration. For the IMOS DALEC, this step will improve the accuracy of each individual DALEC sensor by approximately 6% at 400nm, however this calibration issue has an insignificant impact for the Rrs product, because the errors from each spectrometer tend to cancel each other out when forming the ratio Lt/Ed.

The IMOS DALEC irradiance cosine response was also shown to have larger errors than the other irradiance spectrometers. It is recommended that the IMOS DALEC cosine collector be upgraded to the same design used in the USSIMO, and this will improve the accuracy of the irradiance and resultant Rrs products by up to approximately 20% at solar zenith angles of 70 degrees, and at red wavelengths.

By looking at the irradiance curves vs solar zenith angle collected on 2 different days (ascending and descending sun) temperature effects are observed in the data as the internal temperature of the sensors varies. For the IMOS DALEC, a temperature-specific correction will improve the accuracy of the data by up to 5% at certain wavelengths (i.e. see differences between bold and normal plot symbols in Figure 41). For sensors that record internal temperature, a post-processing scheme is feasible, however this is not currently implemented in any commercial instrument's processing workflow. As a result, further engagement with instrument manufacturers is required and/or advanced radiometric post-processing codes should be implemented.

A more comprehensive inter-comparison between the IMOS DALEC and the SeaPRISM instruments can be achieved, at radiance and reflectance level, by using the routinely collected data at LJCO. This analysis then

should incorporate additional uncertainties of the environmental data used as input to the different skylight correction methods such as the wind speed, as well as the solar and viewing geometry. Platform perturbations may also impact on the quality of the radiometric measurements and could be investigated through a modelling approach. Radiometric measurements performed by Hooker et al. (2003) showed that larger solar zenith angles produce larger reflections off the platform superstructure and thus can have a significant impact on data quality. These radiometric contaminations depend on the size and structure of the platform as well as on the geometry between the sun and the platform, which is a function of the time of the day (Hooker et al., 2003)

References

- Gregg, W., & Carder, K. L. (1990). A simple solar irradiance model for cloudless maritime atmospheres. *Limnology and Oceanography*, 1657-1675.
- Hooker, S., Zibordi, G., Berthon, J.-F., D'Alimonte, D., van der Linde, D., and Brown, J. W., (2003), SeaWiFS Postlaunch Technical Series, Vol. 23, Tower-Perturbation Measurements in Above-Water Radiometry, NASA/TM-2003-206892.
- In-situ Marine Optics Pty. Ltd. (2016). IMOS Radiometry Task Team Absolute Calibration Report. Bibra Lake.
- Mobley, C. (1999). Estimation of the remote-sensing reflectance from above-surface measurements. *Applied Optics*, 7442-7455.
- Mobley, C. (2015). Polarized reflectance and transmittance properties of windblown sea surfaces. *Applied Optics*, 4828 - 4849.
- Rottgers, R., McKee, D., & Utschig, C. (2014). Temperature and salinity correction coefficients for light absorption by water in the visible to infrared spectral region . *Applied Optics*, 25093-25108.
- Ruddick, K. (2006). Seaborne measurements of near infrared water-leaving reflectance: The similarity. *Limnology and Oceanography*, 1167-1179.
- Slivkoff, M. (2014). Ocean Colour Remote Sensing of the Great Barrier Reef Waters. PhD dissertation. Curtin University. URL: <https://espace.curtin.edu.au/handle/20.500.11937/798>
- Thuillier, G., Hersé, M., Labs, D., Foujols, T., Peetermans, W., Gillotay, D., . . . Mandel, H. (2003). The Solar Spectral Irradiance from 200 to 2400 nm as Measured by the SOLSPEC Spectrometer from the Atlas and Eureca Missions. *Solar Physics*, 1-22 .
- Zibordi, G., Hooker, S. B., F., B.J., & D'Alimonte, D. (2002). Autonomous Above-Water Radiance Measurements from an Offshore Platform: A Field Assessment Experiment. *Journal of Atmospheric and Oceanic Technology*, 808-819.

13 Appendix 4: participants lists

The full list of participants to the RTT is provided on the cover page of this report

The laboratory calibrations were conducted and involved:

- Matthew Slivkoff, Curtin University
- Wojciech Klonowski, In situ Marine Optics
- David Boddle, CSIRO
- Kevin Davies, UTS
- David Antoine, Curtin University

The data processing also involved:

- Elizabeth Botha, CSIRO
- Charlotte Robinson, UTS and then Curtin University

The field work at LJCO included:

- David Antoine, Curtin University
- Thomas Schroeder, CSIRO
- Matthew Slivkoff, Curtin University
- Brett Baker, CSIRO
- David Boddle, CSIRO
- Martina Dobbin ,UTS
- Jenny Lovell, CSIRO

The related data processing also included, in addition to those listed above:

- Elizabeth Botha, CSIRO
- Charlotte Robinson, UTS and then Curtin University

14 Appendix 5. What's “System Vicarious Calibration” (SVC), and the need for it

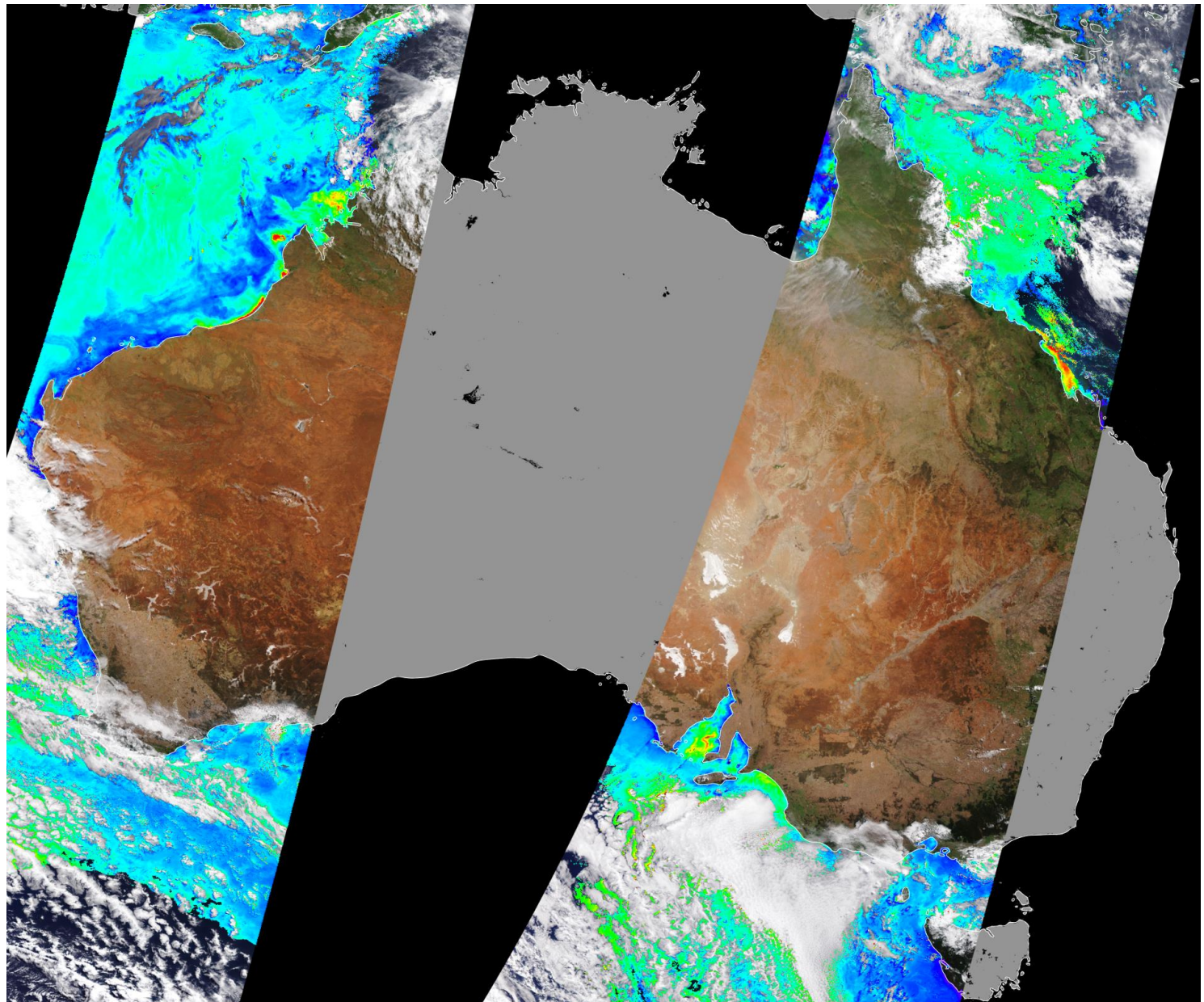
This is a piece of text adapted from the recommendations of the INSITU-OCR⁸ white paper: Absolute calibration uncertainty of satellite ocean colour sensors has been targeted at 0.5% at the top-of-atmosphere level (TOA). This stringent requirement is meant to appropriately serve the use of satellite ocean colour products in climate research in particular. This level of accuracy can be achieved with so-called “system vicarious calibration” (SVC), which consists in adjusting the pre-launch calibration coefficients using TOA radiances predicted from in situ measurements and modelling of the radiative transfer in the atmosphere. By this way, combined uncertainties resulting from satellite absolute pre-launch calibration and from the specific models/algorithms applied for determining primary radiometric products (e.g., normalized water-leaving radiance spectra) from TOA radiance can be minimized. SVC must use high-quality in situ radiometry measurements with full traceability to SI standards. SVC sites should be selected in regions where variability and complexity of the atmospheric and oceanic optical properties are low.

The recommendation by the INSITU-OCR white paper is to maintain at least one long-term vicarious calibration site with SI traceable radiometry pursuing the objective of producing and delivering highly accurate measurements collected under ideal measurement condition (e.g., spatial homogeneity, known aerosol and marine optical properties) in a region representative of global ocean observations. Multiple sites are encouraged, however. They may offer additional information and alternative sources of data, provided that they are appropriately characterized in terms of measurement accuracy, traceability and observation conditions.

⁸ International Network for Sensor Inter-comparison and Uncertainty assessment for Ocean Colour Radiometry, developed as part of the CEOS “Ocean Colour Radiometry Virtual Constellation” (OCR-VC)



Integrated Marine Observing System



© ESA/EUMETSAT, NOAA OCview

Back cover illustration:

**Normalized water-leaving radiance at 443 nm from several overpasses of the
ESA's Sentinel-3-OLCI sensor, covering Australia's surrounding seas**